Probing the Mechanisms of Aldehyde Decarbonylation Using Radical Clock Substrate Analogues

by

Benjamin Rex Ellington

A dissertation submitted in partial fulfillment
of the requirements for the degree of
Doctor of Philosophy
(Biological Chemistry)
in the University of Michigan
2016

Doctoral Committee:

Professor E. Neil G. Marsh, Chair
Professor Carol A. Fierke
Associate Professor Nicolai Lehnert
Associate Professor Bruce A. Palfey
Professor Stephen W. Ragsdale

Dedication

I would like to dedicate this body of work to my parents, Dixie and Rex Ellington, for constantly encouraging and supporting me in all my pursuits, and to my sister Bailey Ellington for always pushing me to better myself.

Acknowledgements

Above all others, I would like to express my deep appreciation of the wealth of knowledge I have gained from my research advisor, Professor E. Neil G. Marsh. Not only was his instruction in the scientific method, manuscript preparation, and overall mechanistic thinking invaluable in preparing me as a scientist, but without my acceptance into his research group I doubt that I would have made it to this stage in my education. I would additionally like to thank my committee members Prof. Carol Fierke, Prof. Stephen Ragsdale, Prof. Bruce Palfey, and Prof. Nicolai Lehnert for their collective patience and valuable guidance in my research. I would also like to thank Prof. Paul Zimmerman and Mr. Andrew Vitek for their computational work and insights into transition-metal catalyzed decarbonylation. I would like to thank Dr. Debasis Das and Dr. Bishwajit Paul for their incredible patience in mentoring me upon my induction into the Marsh Laboratory, and for all the work they did in the many projects we collaborated on. I would also like to thank all present and past Marsh group members, including Dr. Benjamin Buer, Dr. Fengming Lin, Dr. Gabriel Roman, Dr. Tad Ogorzalek, Dr. Aaron Sciore, Dr. Caitlyn Makins, McKenna Schroeder, and Kyle Ferguson for their advice, suggestions, collaborations, distractions and antics that together made graduate school an enjoyable experience. I would especially like to thank Dr. Matthew Waugh for his endless support, advice, mead, and, above all else, friendship, without which I would likely have been lost.

Table of Contents

List of Figures

List of Appendices

List of Abbreviations

CoA	Coenzyme A
NADH	Nicotinamide Adenine Dinucleotide, Reduced
NADPH	Nicotinamide Adenine Dinucleotide Phosphate, Reduced
P450	Cytochrome P450
cADO	Cyanobacterial Aldehyde Deformylating Oxygenase
GMO	Genetically Modified Organism
UV	Ultraviolet
RNA	Ribonucleic Acid
ACP	Acyl Carrier Protein
PMS	Phenazine Methosulfate
EPR	Electron Paramagnetic Resonance
SIE	Solvent Isotope Effect
LC-MS	Liquid Chromatography-Mass Spectrometry
MALDI-TOF	Matrix-Assisted Laster Desorption/Ionization
HppE	(S)-2-hydroxypropylphosphonic acid epoxidase
HEPES	4-(2-hydroxyethyl)-1-piperazineethanesulfonic acid
DMSO	Dimethyl Sulfoxide
LTQ	Linear Trap Quadropole
TBDMS	*tert*-butyldimethylsilyl
TBAF	Tetra-n-butylammonium fluoride
TEMPO	(2,2,6,6-Tetramethylpiperidin-1-yl)oxyl
GC-MS	Gas Chromatography-Mass Spectrometry
HPLC	High Performance Liquid Chromatography
DTT	Dithiothreitol
NMR	Nuclear Magnetic Resonance
ESI	Electrospray Ionization
CHES	*N*-Cyclohexyl-2-aminoethanesulfonic acid
HRMS	High Resolution Mass Spectrometry

Abstract

Global warming has led to increasing research into environmentally-friendly energy sources. One of the greatest sources of greenhouse gases is consumption of fossil fuels to power modern transportation. In this context, the recent discovery of a soluble, stable enzyme that generates alkanes, cyanobacterial aldehyde deformylating oxygenase (cADO), has garnered considerable interest for its potential use in biofuel production. Biological alkane formation in biology is chemically challenging and the mechanisms of the enzymes that catalyzes alkane formation poorly understood. The mechanistic characterization of aldehyde decarbonylation through the use of radical clock substrate analogues is the subject of this dissertation.

A β-cyclopropyl aldehyde was used as a “radical clock” to probe the mechanism of cADO. Reaction with the enzyme yielded only ring-opened product, providing evidence of homolytic scission of the aldehyde formyl group. The minimum lifetime of the intermediate cyclopropylcarbinyl radical formed was calculated to be ≥10 ns. The compound also acted as a mechanism-based inhibitor of cADO, and was found to form a covalent adduct after deformylation.

The subsequent use of an α-oxiranyl aldehyde as a slow radical clock, allowed the lifetime of the radical formed after C-C bond homolysis to be more accurately estimated to be between 10 and 100 μs. Using isotopically labeled α-oxiranyl aldehydes also

revealed the stereorandom nature of electron-proton transfer reaction that constitutes the final step in formation of the alkane product.

A reaction that mimics the aldehyde decarbonylation catalyzed by the insect enzyme, CYP4G1, was uncovered through studies of an α-cyclopropyl aldehyde. This molecule was found to undergo nonenzymatic decarbonylation in the presence of O_2 and Fe^{2+} salts. The reaction produced CO_2 as a byproduct, and exhibited retention of the carbonyl hydrogen in the alkane product. The simplicity of this model system allowed computational simulations to be performed, which identified an energetically feasible mechanism to explain the experimental findings. The simulations indicated that control over the electrophilicity of the carbonyl carbon was key in directing the aldehyde towards decarbonylation.

Chapter 1

Introduction

1.1 Global Carbon Cycle and Industrial Emissions

The constant spread of the industrialized world has resulted in motorized vehicles becoming commonplace, and despite its finite resource pool, an ever-increasing consumption of fossil fuel. A number of issues have arisen from this, the most pressing of which are the eventual (and increasingly nigh) depletion of fossil fuel reserves and the steadily increasing release by humans of previously sequestered carbon into the atmosphere. In a healthy ecosystem, atmospheric carbon in the form of CO_2 is absorbed by photosynthetic organisms and used in the biosynthesis of sugars, proteins, fats and other organic molecules. These molecules are consumed by animals and broken down into constituents, releasing CO_2 back into the atmosphere through respiration (Figure 1.1). Though fluctuations in CO_2 levels occur over geological timescales, the atmospheric concentration of CO_2 remains constant in the short term. By combusting sequestered carbon, we release massive quantities of greenhouse gases into the atmosphere and overburden the standard carbon cycle, resulting in sharply increasing greenhouse gas concentrations (Figure 1.2), acidification of the ocean, and a global temperature increase of approximately 1º C in the last century alone.[1] As the population continues to grow and industrialized life becomes a more widespread standard, our effect on the climate will continue to accelerate.

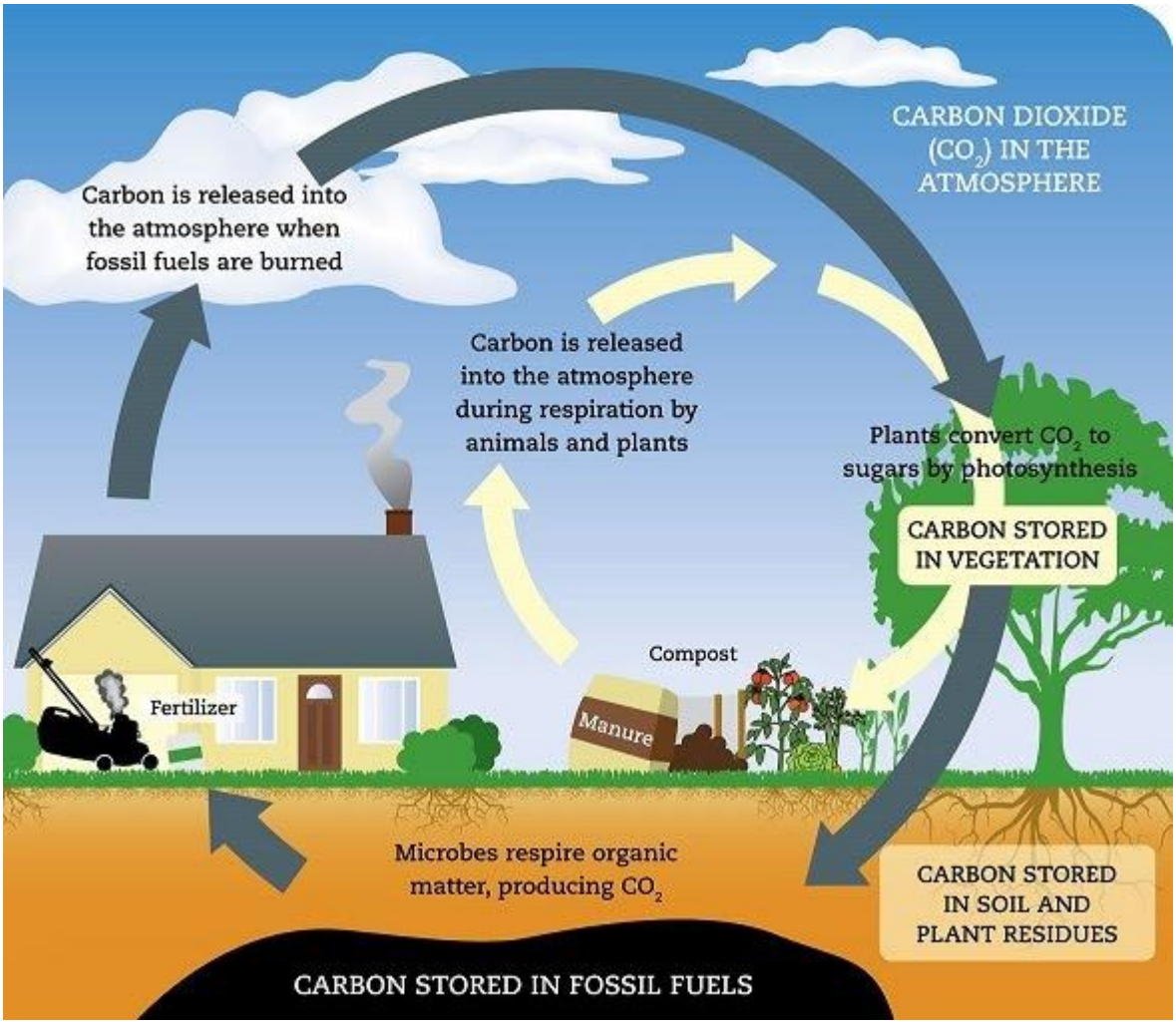

Figure 1.1. The global carbon cycle.[2]

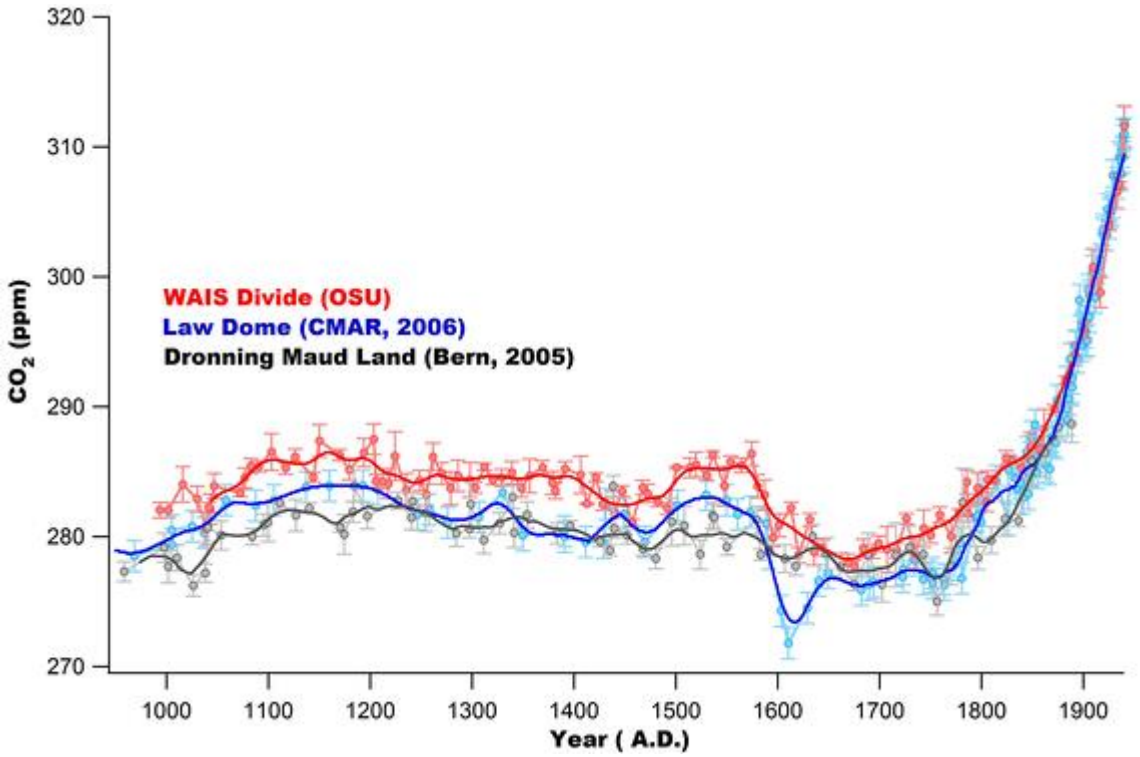

Figure 1.2. Atmospheric CO_2 over the last 1000 years.[1b]

In an attempt to curb our detrimental effect on the atmosphere, significant research into and implementation of renewable energy sources has occurred. Solar, wind, nuclear and hydroelectric power all admirably serve to reduce our reliance on combustion-based electricity. Transportation, however, remains massively reliant on fossil fuels. In order to truly address mankind's profound effect on atmospheric pollution, personal transportation needs either be drastically altered, or an efficient and renewable method for fuel production developed and standardized.

1.2 Biofuels

Because the production of fossil fuels requires hundreds of millions of years to occur, chemical and biological alternatives to efficiently produce combustible molecules

from biomass (plant matter) have been of great interest in recent years. As research in the field has expanded, four distinct generations of biofuels have evolved.

1.2.1 Biofuel Varieties

The first generation of biofuels are so-classified due to their derivation from food crops rich in available sugar and oil, and include both bioethanol (from the fermentation of available sugars) and biodiesel (from transesterification of oils extracted from said food crops).[3] Bioethanol is currently the most heavily utilized biofuel in the world, with the United States alone having produced an estimated 14.3 billion gallons of bioethanol in 2014, a figure that will only increase in coming years as governmental restrictions on greenhouse gas emissions tighten.[4] The second generation of biofuels involve production of bioethanol from lignocellulose, which accounts for the majority of dry plant biomass.[5] A significant advantage of second generation biofuels is the availability of both agricultural waste (stalks and leaves of corn, wheat, and other plants) and fast-growing plants such as grasses as feedstocks.[5]

Unlike the production of bioethanol, the third generation of biofuels come in the form of oils directly produced by green algae, which can be grown in areas unusable for agriculture and can produce significant quantities of oil.[6] The most recent area of interest is the “next generation” of biofuels, in which long-chain hydrocarbons, rather than alcohols or esters, are produced to act as drop-in biofuels.[7] These molecules mimic petroleum-based fuels, are entirely compatible with the current fuel infrastructure, and can theoretically be produced directly from photosynthetic carbon fixation.[7]

1.2.2 Associated Challenges

Multiple factors currently limit the usefulness and feasibility of biofuels. Although it accounts for nearly 75% of the biofuel market, bioethanol is plagued by numerous flaws.[3] Significant derivation from edible crops (first generation) would require a large allocation of agricultural effort, diminishing food production. Production of fermentable sugars from lignocellulose (second generation) would be ideal, and current research focuses heavily on efficiently breaking down cellulose, but the inherent stability of cellulose remains a significant roadblock for the efficient production of bioethanol from non-food crops.[8] Even were bioethanol easily produced, its hydrophilic nature would be too corrosive for the current design of internal combustion engines, and would require a major overhaul in engine design. Although biodiesel is energetically dense and well-produced by algae, it is currently not as economically viable a solution as other fuel alternatives, primarily due to the high operating costs associated with growth and harvest, as well as the cost of infrastructure development.[6] The biological hydrocarbon production of the next generation biofuels addresses a number of issues inhibiting the usefulness of previous generation biofuels, but the mechanism by which these are produced remains an active area of study. In order to develop this new generation, a deeper understanding of the enzymatic mechanisms and biosynthetic pathways involved is required.

1.3 Biosynthesis of Hydrocarbons

The production of hydrocarbons is quite common in Nature, and can be found in plants, animals and a variety of microbial organisms.[9] In plants, these molecules function

as waxy, hydrophobic exterior coatings to aid in waterproofing and defend against dessication.[9c] Multiple species of insects and birds similarly employ hydrocarbons. The waxy molecules are secreted and used to waterproof bird feathers, allowing flight and insulation regardless of inclement weather.[9a] Insects also produce a plethora of hydrocarbon molecules, which function both as contact pheromones regulating social interactions and cuticular linings to aid in water retention and defend against dessication.[9b, 10] Algae synthesize a large quantity of long-chain alkanes (up to 30% of dry mass) naturally, and store them as a reserve energy source to be utilized in lieu of photosynthesis.[11]

Despite the prevalence of alkanes in Nature, their synthesis is difficult and was, until recently, poorly understood.[12] The most common source of long, aliphatic chains is fatty acid biosynthesis, and indeed early research showed that the abovementioned hydrocarbons were derived from them.[13] Though other possibilities exist, such as the direct decarboxylation of fatty acids to produce n-1 alkenes by the enzyme OleTJE, most biological alkane production is accomplished via a fatty aldehyde intermediate species. Alkane production is catalyzed by an unusual and mechanistically intriguing class of metalloenzyme; aldehyde decarbonylases.

1.4 Aldehyde Decarbonylases

The enzymes known to catalyze alkane formation reaction, loosely termed aldehyde decarbonylases, include phylogenetically distinct enzymes from plants and green/blue algae, animals, and cyanobacteria. Production of the fatty aldehyde substrate in all cases is mediated by fatty acyl-CoA reductases, which employ NAD(P)H to remove

the CoA functional group and release the corresponding aldehydes (Figure 1.3).[14] Each decarbonylase evolved to accomplish the removal of the carbonyl moiety from fatty-acid derived aldehyde substrates, yet they are distinct in structure, catalytic mechanism, and the nature of the carbonyl group released. Past research has indicated that the insect cytochrome P450 (CYP4G1), the cyanobacterial Aldehyde Deformylating Oxygenase (cADO), and the plant aldehyde decarbonylase (Cer1) release the carbonyl moiety as CO_2, HCO_2^-, and CO, respectively (Figure 1.3).[9c, 11, 15] Improving our understanding of how these enzymes evolved to catalyze this specific type of reaction is key to developing efficient, environmentally sound sources of combustible fuel.

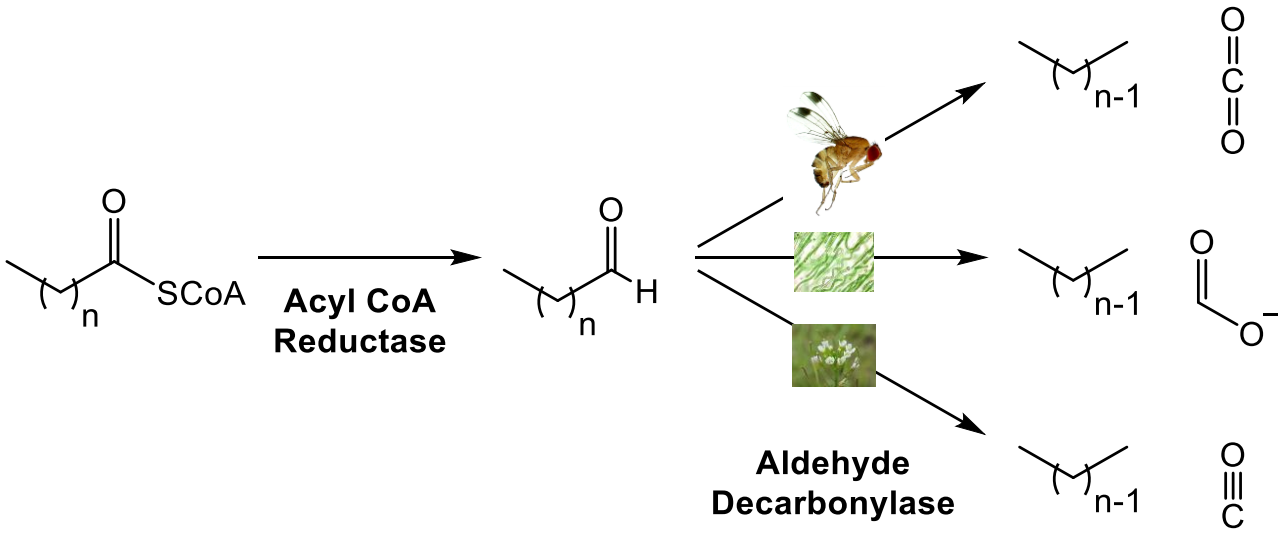

Figure 1.3. Fatty aldehyde decarbonylation in insects (top), cyanobacteria (middle), and plants (bottom). Fatty aldehydes are produced from fatty acyl-CoA esters by Acyl-CoA Reductases in all cases.

1.4.1 Plant

Despite being the first aldehyde decarbonylases studied, the plant and algal decarbonylase enzymes continue to elude characterization. Of interest both for biofuel production and agricultural GMO development, the plant aldehyde decarbonylases are responsible for very-long chain alkane production. These very-long chain alkanes compose the waxy residue covering the surface of exposed plant organs, and are necessary to protect organisms from dessication in arid conditions as well as damage from UV radiation.[15g, 16]

Early studies of heavy particulate preparations of *Pisum sativum* in the Kolattukudy laboratory revealed isolated microsomal fractions that catalyzed the conversion of octadecanal ($CH_3(CH_2)_{16}CHO$) to heptadecane ($CH_3(CH_2)_{15}CH_3$) with a specific activity of up to 25 nmol min^{-1} per mg of protein.[15g] Further studies with this fraction identified aldehyde, rather than fatty acid, as the substrate, and the use of isotopic labels (^3H and ^{14}C) on the C1 and C2 positions, resulted in the identification of CO as the primary byproduct as well as significant retention of the carbonyl hydrogen in the heptadecane produced.[15g] Inhibition of catalysis by metal chelators indicated that a metalloenzyme was most likely responsible for the decarbonylation,[15g] and the partial purification of a decarbonylase from the green algae *Botyrococcus braunii* allowed for limited characterization.[11] The enzyme was estimated to have a molecular mass of 66 kDa and was, again, membrane-bound, but was shown to have measurable decarbonylation activity.[11]

Due to the difficulty of purifying integral membrane proteins, the structure of the plant/algal aldehyde decarbonylase remains a mystery. Recent genetic studies of

Arabidopsis thaliana have identified the gene coding for the enzyme, *cer1*, and have allowed for limited characterization of the protein.[17] The 630-residue protein seems most closely related to the stearoyl-CoA desaturase/hydroxylase family of integral membrane non-heme iron enzymes, and contains the family's conserved 8-His motif.[17-18] This, along with the findings that all other all other aldehyde decarbonylases are iron-dependant enzymes, implies that Cer1 is an iron enzyme, despite earlier indications that the enzyme was Co-dependant.[19]

A more recent study performed in the Joubès Laboratory managed to reconstitute plant alkane biosynthesis in *Saccharomyces cerevisiae*, and expand on our understanding of the system.[20] Though the importance of Cer1 in alkane biosynthesis was implied from genetic studies, it was previously shown to be insufficient for decarbonlyation in heterologous expression systems.[21] In order to identify other enzymes necessary for alkane biosynthesis in plants, yeast 2-hybrid screens were set up and performed based on previous genetic analyses of *A. thaliana* Cer1 studies,[22] and found Cer1 to physically interact with Cer3 (another 8-His motif-containing enzyme with high sequence homology to Cer1) and multiple cytochrome b_5 proteins, which most commonly mediate electron transfer to non-heme iron enzymes.[20] Activity assays in a yeast strain engineered to produce very-long chain fatty acids showed that while Cer1 and Cer3 were independently insufficient to stimulate alkane production, Cer1 and Cer3 together were sufficient to support nonacosane production. The addition of $Cytb_5$ to the system significantly increased nonacosane production, implicating redox chemistry as integral to the system.[20] Mutagenesis of the conserved His-clusters in Cer1 was also carried out, and showed all 3 His-rich domains to be necessary for alkane formation. The same

mutations were produced in the Cer3 protein, but alkane formation was not impacted. This indicated that the 8-His motif is key to the catalysis of the decarbonlyation reaction in Cer1, and provided a model for the production of hydrocarbons in plants (Figure 1.4).[20] In this model, very-long chain acyl CoAs are first reduced to aldehydes (putatively by Cer3), and then decarbonylated by Cer1 with the redox support of $Cytb_5$ proteins. Despite the great interest in Cer1 and its many applications, its recalcitrant nature has made mechanistic characterization highly problematic.

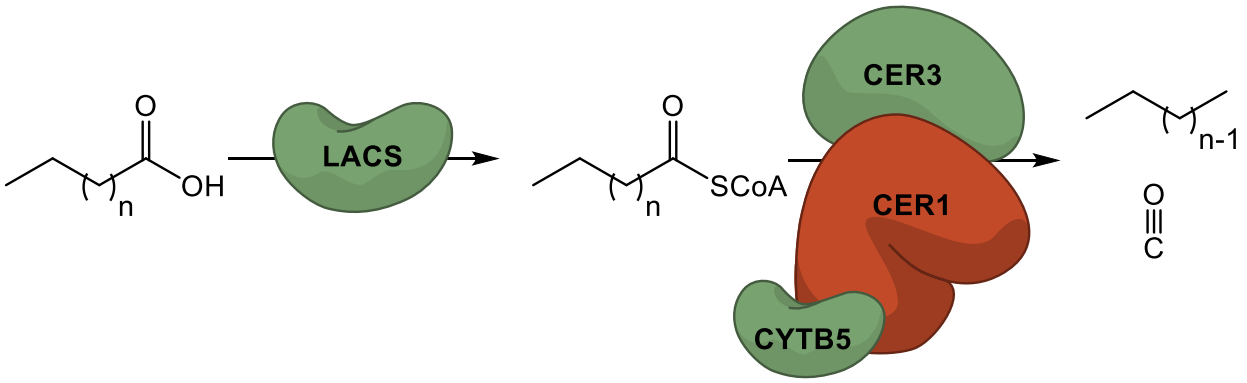

Figure 1.4. Basic mechanism of the Cer1/Cer3 plant aldehyde decarbonylase system. CER3 is implicated in NADPH-mediated reduction of Very Long Chain Acyl-CoA to aldehyde, while CER1 catalyzes decarbonylation with redox support from $CYTB_5$.

1.4.2 Insect

Hydrocarbons serve a variety of roles in insects, including hydrophobic cuticular linings, chemical communication, and water retention.[9a, b, 10] Such insect species as *Musca domestica* and *Drosophila melanogaster* have been demonstrated to biosynthesize a complex mixture of long-chain alkanes and alkenes to fill the aforementioned roles.[23] Initial investigations of the biosynthetic route to the important female house fly sex pheromone (Z)-9-tricosene by the Blomquist laboratory were able

to preliminarily characterize the mechanism of aldehyde decarbonylation using *M. domestica* microsomal preparations.[15b] Incubation of isotopically labelled tetracosanoic acid with microsomal preparations yielded stoichiometric (1:1) quantities of labelled (Z)-9-tricosene and, unexpectedly, CO_2.[15b] Further studies identified NADPH and O_2 as necessary for the production of tricosenes from the corresponding aldehyde, and demonstrated that whilst insect hydrocarbon production proceeded along a similar pathway to plant and algal systems, the mechanism by which the decarbonylation was accomplished was inherently different.[15b, 24] Initial use of insect cytochrome P450 reductase inhibitors in the microsomal preparations did inhibit tricosene production; however, it was not until later, when CYP6A1 (a specific insect P450 enzyme) antibodies were shown to similarly inhibit tricosene production, that the enzyme responsible for aldehyde decarbonylation in *M. domestica* was identified as a cytochrome P450.[24] Initial mechanistic characterization of the reaction was carried out using deuterated [1-^{2}H]tetracosenal, demonstrating the retention of the aldehyde deuterium atom in the tricosene product.[24] Additionally, use of the oxidants H_2O_2, cumene hydroperoxide, and iodosobenzene in lieu of O_2 and NADPH effectively supported aldehyde decarbonylation, allowing for a mechanistic proposal in which the initial iron-peroxy species underwent heterolytic O-O cleavage and abstracted an electron from the substrate carbonyl group.[24] Formation of an iron-hemiacetal diradical is proceeded by radical fragmentation to yield an alkyl radical which then abstracts the hydrogen from the formyl radical to yield tricosene and CO_2 (Figure 1.5). The ability to investigate the mechanism by which insects catalyzed aldehyde decarbonylation was a significant step from the early plant and algal

studies, as was the finding that two completely separate classes of enzymes evolved to support aldehyde decarbonylation in plants and insects.

Identification of the specific P450 responsible for the reaction in insects came in 2012, when the *Cyp4g1* gene in *Drosophila melanogaster* was identified through genomic sequencing and microarray analysis to be both highly expressed and conserved through multiple insect species.[15a] Using RNAi suppression, CYP4G1 was found to have a significant impact on hydrocarbon production in fly cuticles, resulting in drastic decreases in organism viability and survival. Insect cytochrome P450 reductase (CPR) was similarly shown to be necessary for insect viability and hydrocarbon production, and heterologous expression of a CYP4G2-CPR fusion in *Saccharomyces cerevisiae* was sufficient to support the time- and NADPH-dependent decarbonylation of octadecanal to heptadecane with the concomitant release of CO_2.[15a] CYP4G2 is the *M. domestica* ortholog of *D. melanogaster* CYP4G1 previously studied. Despite the advances made in the investigation of enzymatic aldehyde decarbonylation, the membrane-bound nature of both plant and insect proteins remained a significant roadblock to a deep, mechanistic understanding of biological hydrocarbon production. A soluble form was needed.

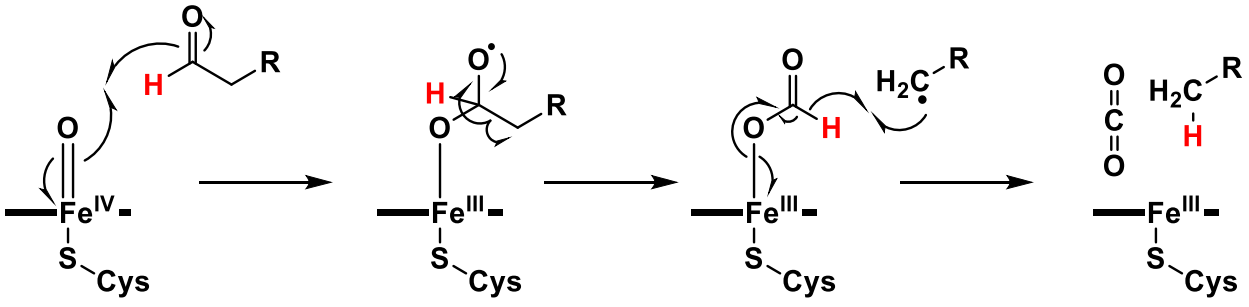

Figure 1.5. Aldehyde decarbonylation by the Insect P450, CYP4G1. The initial high-valent iron-oxo heme species is proposed to decarbonylate aldehydes as shown. The red hydrogen atom depicts conservation of the aldehyde hydrogen in the alkane product as determined by labelling studies. Figure adopted from reference 24.

1.4.3 Cyanobacteria

Though alkane biosynthesis has been detected in a variety of microbial organisms, it was in cyanobacteria that the pathway and genes responsible for hydrocarbon production were first identified.[15c] In 2010, Schirmer et al tested 11 cyanobacterial strains for hydrocarbon production, and identified 10 of the 11 strains as positive for alkane biosynthesis. Using genomic subtraction, the conserved genes for decarbonylation and fatty acyl-ACP reduction were identified, revealing a pathway for the conversion of fatty acids into aldehydes, and the corresponding decarbonylation to alkanes.[15c] While the purpose of hydrocarbon production in cyanobacteria was unknown, the study of it had begun in earnest. Heterologous expression in *Escherichia coli* of the aforementioned genes from *Synechococcus elongates* was sufficient to support hydrocarbon biosynthesis, and revealed aldehydes as the most likely intermediate species.[15c] Unlike the aldehyde decarbonylases studied from plants and animals, the corresponding cyanobacterial enzyme was soluble, allowing for a much more detailed approach to enzyme characterization.

The soluble nature of the cyanobacterial enzyme allowed for the first chance to examine the structure of an aldehyde decarbonylase, and the crystal structure of the *Prochlorococcus marinus* ortholog had been solved previously, though no known enzyme function had yet been assigned.[25] Both the sequence and the crystal structure revealed cyanobacterial aldehyde deformylating oxygenase (cADO) to be ~29 kDa member of the non-heme diiron oxygenase family, which included such well-characterized enzymes as class I ribonucleotide reductases, methane monooxygenase (MMO), and fatty-acyl-ACP desaturase.[26] The core of the enzyme consists of an antiparallel 4-helix bundle, within

which is housed the diiron active site at the terminus of a long, hydrophobic substrate binding channel (Figure 1.6).[25] More recent structures have revealed alternative, nonproductive binding modes within cADO, and identified the most likely route by which oxygen accesses the diiron active site.[27] The cADO monomer is notably smaller than MMO (251 kDa), lacking the subunits necessary for reduction found in its larger family member.[26a, 28] Instead, cADO requires an external reducing system for activity, though the "native" system has of yet not been identified.

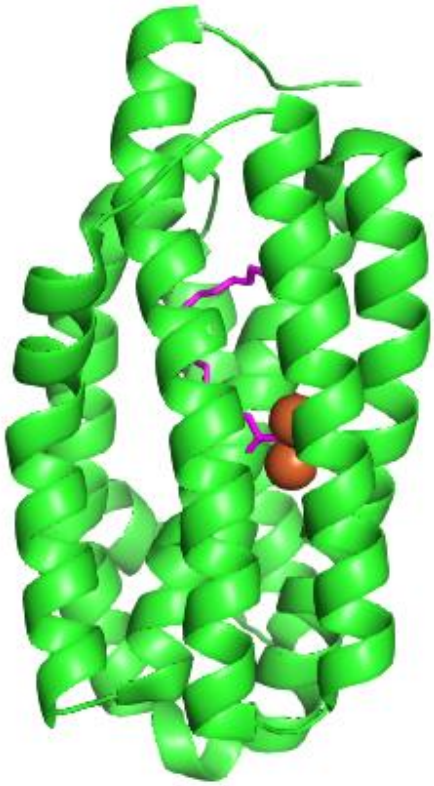

Figure 1.6. Structure of cADO as determined by X-Ray crystallography. Structure exhibits a 4-helix bundle surrounding the diiron active site (in orange) with octadecanal (purple) bound.

Because it is the only soluble aldehyde decarbonylase yet identified, cADO has been the most fully characterized. Decarbonylation requires the input of 4 electrons per turnover, and results in the redox-neutral conversion of substrate aldehydes to n-1 alkanes and, unlike either the insect (CO_2) or plant (CO), formate (HCO_2-).[29] The reduction of the diiron center of cADO can be accomplished both by biological systems, including spinach and cyanobacterial ferredoxin/ferredoxin reductase, and chemically using phenazine methosulfate (PMS) and NADH.[15f, 29] Isotopic labelling has been key in elucidating the mechanism by which this chemically unusual conversion occurs. Using $^{18}O_2$, Li et al demonstrated that one of the oxygen atoms in the product formate derives directly from molecular oxygen, suggesting the other atom is reduced to water.[30] Additionally, deuterium labelling of the aldehyde hydrogen was used to probe for retention of said hydrogen in the alkane product as per insect and plant studies, but instead demonstrated retention of the deuterium atom in formate.[30] Such findings indicated that aldehyde decarbonylation in cyanobacteria proceeds via a mechanism widely differing from that in either insects or plants.

Kinetic analysis of cADO revealed the enzyme to be unusually slow, with a maximum reported steady-state turnover rate of 1 min^{-1}.[31] Based on the observed products, electron requirements, structural similarities to other well-characterized non-heme diiron oxygenase enzymes, a basic mechanism has been proposed for cADO (Figure 1.7). Initial reduction of the resting diferric enzyme to the active diferrous form is accomplished with an external reducing system.[15f, 29] Aldehyde substrate access to the active site and oxygen binding by the diferrous center then occurs, and an intermediate peroxy-hemiacetal is formed. Support for this structure was provided by the Bollinger

group using U.V.-Vis and Mössbauer spectroscopy, and it was shown to be quite stable, with a $t_{1/2}$ of ~400s.[32] Addition of reduced PMS resulted in the rapid decay of this species and production of n-1 alkane and formate to a diferric enzyme unique, by Mössbauer spectroscopy, from both the peroxy intermediate and the initial diferric enzyme, likely indicating the product-bound state.[32] Solvent isotope effect studies by Waugh et al indicated that the most likely source of the proton donor for the alkyl species resulting from homolytic C-C bond cleavage was an iron-bound water molecule.[33] Product release and reduction back to the diferrous form begins the catalytic cycle anew.

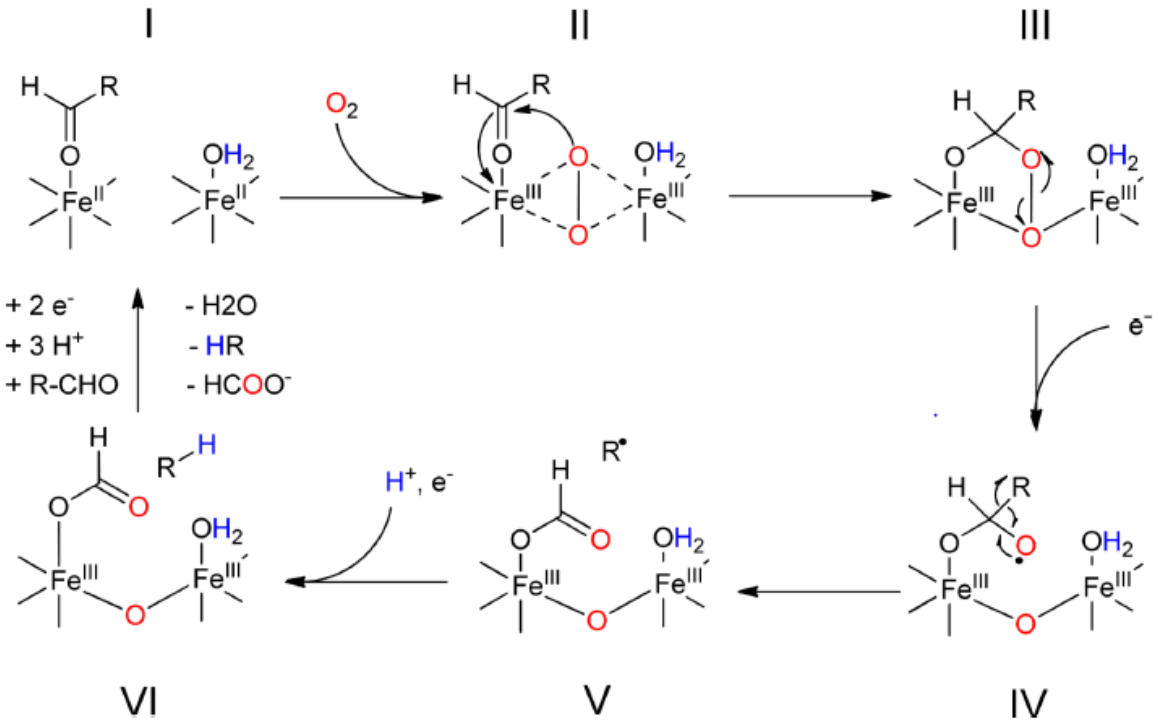

Figure 1.7. Proposed mechanism of aldehyde decarbonylation by cADO.

Despite the characterization accomplished thus far, numerous questions remain. Though many causes have been proposed, the sluggish nature of the enzyme continues to elude understanding. In order to efficiently produce hydrocarbon-based biofuels, the

catalysis of decarbonylation must be well-understood and methods by which activity can be maximized developed. Of particular interest is the nature of the reaction –whether it occurs via a radical or charged intermediate- and the rate constants of individual steps. Though initial EPR studies indicated the presence of a radical intermediate, a more recent study invoked a heterolytic C-C bond cleavage to produce formate and an alkyl carbanion.[15f] In order to address this disparity, and investigate rate constants within the reaction, we turned to the numerous insights provided by radical clock mechanistic probes.

1.5 Mechanistic Probes

1.5.1 Radical Clocks

Radical chemistry is a highly pertinent area of study, as multiple reactions, both biological and not, proceed via radical intermediate species. Radical kinetics are important both in planning chemical syntheses and investigating enzyme catalysis, and the corresponding rate constant can be measured using a variety of methods. Direct measurements of radical rate constants typically involve UV-visible spectroscopy and pulse irradiation methods, while indirect measurements are accomplished by product analysis of competition reactions using more simple chromatographic or spectroscopic techniques.[34] Due to the short lifespans and low concentrations of radicals in most reactions, the indirect method of radical rate constant measurement is most commonly used in mechanistic enzymology, wherein the ratio of the standard enzyme-catalyzed reaction product to the intramolecular reaction of the substrate analogue (often in the form of bond rearrangements) is measured, and thence is derived the rate constant of the

radical step in the reaction.[34] Radical clock reactions are unimolecular, and include such conversions as cyclizations,[35] ring openings,[36] and radical migrations.[36] Alkyl radical clocks have been widely studied, and alkyl radical clocks with rate constants ranging from 300 s^{-1} to $5x10^{11}$ s^{-1} have been developed to probe a wide range of enzyme reactions.[36-37] The use of carbon radical clocks to indirectly measure the rate constant of the radical step in a given reaction generally requires the use of a small library of designed substrates over a range of rate constants, and the design of such substrates depends on a variety of criteria. In particular, the radical clock must be able to access the active site and initiate reaction, contain a functional probe in the vicinity of the (suspected) formed radical, and exist long enough to compete with the standard reaction catalyzed.

1.6 Aims of This Work

While the membrane-bound nature of the insect and plant aldehyde decarbonylases rendered them recalcitrant to detailed characterization, the discovery of the soluble cyanobacterial aldehyde deformylating oxygenase stimulated a wave of studies attempting to characterize it and better understand biological decarbonylation reactions. Such studies identified the necessity of molecular oxygen and reducing equivalents to catalyze the redox-neutral deformylation of aldehyde substrates with an upper rate limit of 1 min^{-1},[29, 31] showed the incorporation of molecular oxygen in product formate,[15e] and identified the intermediate peroxyhemiacetal species as highly stable ($t_{1/2}$ ~400s).[32] The source of alkyl protonation was identified as an iron-bound water molecule by SIE studies,[33] and a radical species implicated in the mechanism.[15f] Despite this, multiple facets of catalysis remain unexplored, including concrete identification of the

nature of the C-C bond scission (whether a radical or a carbocation is produced), rate constants of the associated steps in the reaction, and how other, structurally dissimilar enzymes, such as CYP4G1, catalyze related decarbonylation reactions. A deeper understanding of the methods by which enzymes catalyze decarbonylation is needed ere these systems can be applied to address our growing need for fossil fuel alternatives.

The research documented herein focuses on addressing these issues and providing valuable insight into biological aldehyde decarbonylation. Chapter 2 describes the use of a β-cyclopropyl aldehyde substrate analogue to investigate the nature and associated rate constant of the C-C bond scission. Despite acting as an unexpected mechanistic inhibitor, homolytic C-C bond scission was identified and a minimum rate constant for quenching of the alkyl radical generated. The mechanism by which cADO was inactivated by β-cyclopropyl was also identified, and a substrate-binding channel phenylalanine identified as the site of covalent modification of the enzyme. In chapter 3, we developed an α-oxiranyl-aldehyde substrate analogue to more accurately measure the rate constant for C-C bond scission, as well as study the stereochemistry of the reaction. We thus determined that the rate constant for the proton + electron transfer step was 10^4-10^5 s^{-1}, and that proton transfer was stereorandom. The final chapter describes an α-cyclopropyl substrate analogue that acts as a nonenzymatic model of CYP4G1 activity. High resolution mass spectrometry was used to identify CO_2 as the carbonyl product, and deuterium labeling showed that the aldehyde proton was retained in the alkane product. Mechanistic simulations identified an energetically plausible mechanism, aiding in our understanding of the otherwise difficult to study mechanism by which a P450 enzyme catalyzes aldehyde decarbonylation. Taken together, this work

significantly advances our understanding of enzyme-mediated aldehyde decarbonylation, and will help to inform and direct future studies on industrialization of aldehyde decarbonylation as a source of biofuel production.

1.7 References

1. (a) Meehl, G. A., T.F. Stocker, W.D. Collins, P. Friedlingstein, A.T. Gaye, J.M.; Gregory, A. K., R. Knutti, J.M. Murphy, A. Noda, S.C.B. Raper,; I.G.; Watterson, A. J. W. a. Z.-C. Z., Global Climate Projections in Climate Change 2007: The Physical Science Basis. Contribution of Working Group I to the Fourth Assessment Report of the Intergovernmental Panel on Climate Change. 2007; (b) Ahn, J.; Brook, E. J.; Mitchell, L.; Rosen, J.; McConnell, J. R.; Taylor, K.; Etheridge, D.; Rubino, M., Atmospheric CO2 over the last 1000 years: A high-resolution record from the West Antarctic Ice Sheet (WAIS) Divide ice core. *Global Biogeochemical Cycles* 2012, *26* (2), n/a-n/a.

2. Biologist, T. A.-L., Nutrient Cycles. http://www.thealevelbiologist.co.uk/_/rsrc/1383673881844/nutrient-cycles/carbon.jpg, Ed.

3. (a) Farrell, A. E.; Plevin, R. J.; Turner, B. T.; Jones, A. D.; O'Hare, M.; Kammen, D. M., Ethanol Can Contribute to Energy and Environmental Goals. *Science* 2006, *311* (5760), 506-508; (b) Somerville, C., Biofuels. *Current Biology* 2007, *17* (4), R115-R119.

4. Falling Walls & Rising Tides. *2014 Ethanol Industry Outlook* 2014.

5. Kumar, R.; Singh, S.; Singh, O., Bioconversion of lignocellulosic biomass: biochemical and molecular perspectives. *J Ind Microbiol Biotechnol* 2008, *35* (5), 377-391.

6. Rosenberg, J. N.; Oyler, G. A.; Wilkinson, L.; Betenbaugh, M. J., A green light for engineered algae: redirecting metabolism to fuel a biotechnology revolution. *Current Opinion in Biotechnology* 2008, *19* (5), 430-436.

7. Peralta-Yahya, P. P.; Zhang, F.; del Cardayre, S. B.; Keasling, J. D., Microbial engineering for the production of advanced biofuels. *Nature* 2012, *488* (7411), 320-328.

8. Bokinsky, G.; Peralta-Yahya, P. P.; George, A.; Holmes, B. M.; Steen, E. J.; Dietrich, J.; Soon Lee, T.; Tullman-Ercek, D.; Voigt, C. A.; Simmons, B. A.; Keasling, J. D., Synthesis of three advanced biofuels from ionic liquid-pretreated switchgrass using engineered Escherichia coli. *Proceedings of the National Academy of Sciences* 2011, *108* (50), 19949-19954.

9. (a) Cheesbrough, T. M.; Kolattukudy, P. E., Microsomal preparation from an animal tissue catalyzes release of carbon monoxide from a fatty aldehyde to generate an alkane. *Journal of Biological Chemistry* 1988, *263* (6), 2738-2743; (b) Howard, R. W.; Blomquist, G. J., ECOLOGICAL, BEHAVIORAL, AND BIOCHEMICAL ASPECTS OF INSECT HYDROCARBONS. *Annual Review of Entomology* 2005, *50* (1), 371-393; (c) Bernard, A.; Joubès, J., Arabidopsis cuticular waxes: Advances in synthesis, export and regulation. *Progress in Lipid Research* 2013, *52* (1), 110-129; (d) Ladygina, N.; Dedyukhina, E. G.;

Vainshtein, M. B., A review on microbial synthesis of hydrocarbons. *Process Biochemistry* 2006, *41* (5), 1001-1014.

10. Yoder, J. A.; Denlinger, D. L.; Dennis, M. W.; Kolattukudy, P. E., Enhancement of diapausing flesh fly puparia with additional hydrocarbons and evidence for alkane biosynthesis by a decarbonylation mechanism. *Insect Biochemistry and Molecular Biology 22*.

11. Dennis, M. W. M., Alkane biosynthesis by decarbonylation of aldehyde catalyzed by a microsomal preparation from Botryococcus braunii. *Archives of biochemistry and biophysics* 1991, *287* (2), 268-275.

12. Buist, P. H.; Adeney, R. A., Synthesis of a new family of chiral fluorinated synthons: (R)- and (S)-4-fluoro-1-alkynes. *The Journal of Organic Chemistry* 1991, *56* (10), 3449-3452.

13. Kolattukudy, P. E., Plant waxes. *Lipids* 1970, *5* (2), 259-275.

14. (a) Vioque, J.; Kolattukudy, P. E., Resolution and Purification of an Aldehyde-Generating and an Alcohol-Generating Fatty Acyl-CoA Reductase from Pea Leaves (Pisum sativumL.). *Archives of biochemistry and biophysics* 1997, *340* (1), 64-72; (b) Wang, X.; Kolattukudy, P. E., Solubilization and purification of aldehyde-generating fatty acyl-CoA reductase from green alga Botryococcus braunii. *FEBS Letters* 1995, *370* (1–2), 15-18; (c) Wang, X.; Kolattukudy, P. E., Solubilization, Purification and Characterization of Fatty Acyl-CoA Reductase from Duck Uropygial Gland. *Biochemical and Biophysical Research Communications* 1995, *208* (1), 210-215.

15. (a) Qiu, Y.; Tittiger, C.; Wicker-Thomas, C.; Le Goff, G.; Young, S.; Wajnberg, E.; Fricaux, T.; Taquet, N.; Blomquist, G. J.; Feyereisen, R., An insect-specific P450 oxidative decarbonylase for cuticular hydrocarbon biosynthesis. *Proceedings of the National Academy of Sciences* 2012, *109* (37), 14858-14863; (b) Reed, J. R.; Vanderwel, D.; Choi, S.; Pomonis, J. G.; Reitz, R. C.; Blomquist, G. J., Unusual mechanism of hydrocarbon formation in the housefly: cytochrome P450 converts aldehyde to the sex pheromone component (Z)-9-tricosene and CO2. *Proceedings of the National Academy of Sciences of the United States of America* 1994, *91* (21), 10000-10004; (c) Schirmer, A.; Rude, M. A.; Li, X.; Popova, E.; del Cardayre, S. B., Microbial Biosynthesis of Alkanes. *Science* 2010, *329* (5991), 559-562; (d) Aarts, M. G.; Keijzer, C. J.; Stiekema, W. J.; Pereira, A., Molecular characterization of the CER1 gene of arabidopsis involved in epicuticular wax biosynthesis and pollen fertility. *The Plant Cell* 1995, *7* (12), 2115-27; (e) Warui, D. M.; Li, N.; Nørgaard, H.; Krebs, C.; Bollinger, J. M.; Booker, S. J., Detection of Formate, Rather than Carbon Monoxide, As the Stoichiometric Coproduct in Conversion of Fatty Aldehydes to Alkanes by a Cyanobacterial Aldehyde Decarbonylase. *Journal of the American Chemical Society* 2011, *133* (10), 3316-3319; (f) Das, D.; Eser, B. E.; Sciore, A.; Marsh, E. N. G.; Han, J., Oxygen-independent decarbonylation of aldehydes by cyano-bacterial aldehyde decarbonylase: a new reaction of di-iron enzymes. *Angewandte Chemie (International Ed. in English)* 2011, *50* (31), 7148-7152; (g) Cheesbrough, T. M.;

Kolattukudy, P. E., Alkane biosynthesis by decarbonylation of aldehydes catalyzed by a particulate preparation from Pisum sativum. *Proceedings of the National Academy of Sciences of the United States of America* 1984, *81* (21), 6613-6617.

16. Kerstiens, G., Plant Cuticles; an Integrated Functional Approach. *Journal of Experimental Botany* 1996, *47*, 50-60.

17. Aarts, M. G.; Keijzer, C. J.; Stiekema, W. J.; Pereira, A., Molecular characterization of the CER1 gene of arabidopsis involved in epicuticular wax biosynthesis and pollen fertility. *The Plant Cell* 1995, *7* (12), 2115-2127.

18. Shanklin, J.; Whittle, E.; Fox, B. G., Eight Histidine Residues Are Catalytically Essential in a Membrane-Associated Iron Enzyme, Stearoyl-CoA Desaturase, and Are Conserved in Alkane Hydroxylase and Xylene Monooxygenase. *Biochemistry* 1994, *33* (43), 12787-12794.

19. Dennis, M.; Kolattukudy, P. E., A cobalt-porphyrin enzyme converts a fatty aldehyde to a hydrocarbon and CO. *Proceedings of the National Academy of Sciences of the United States of America* 1992, *89* (12), 5306-5310.

20. Bernard, A.; Domergue, F.; Pascal, S.; Jetter, R.; Renne, C.; Faure, J.-D.; Haslam, R. P.; Napier, J. A.; Lessire, R.; Joubès, J., Reconstitution of Plant Alkane Biosynthesis in Yeast Demonstrates That Arabidopsis ECERIFERUM1 and ECERIFERUM3 Are Core Components of a Very-Long-Chain Alkane Synthesis Complex. *The Plant Cell* 2012, *24* (7), 3106-3118.

21. Bourdenx, B.; Bernard, A.; Domergue, F.; Pascal, S.; Léger, A.; Roby, D.; Pervent, M.; Vile, D.; Haslam, R. P.; Napier, J. A.; Lessire, R.; Joubès, J., Overexpression of Arabidopsis ECERIFERUM1 Promotes Wax Very-Long-Chain Alkane Biosynthesis and Influences Plant Response to Biotic and Abiotic Stresses. *Plant Physiology* 2011, *156* (1), 29-45.

22. Samuels, L.; Kunst, L.; Jetter, R., Sealing Plant Surfaces: Cuticular Wax Formation by Epidermal Cells. *Annual Review of Plant Biology* 2008, *59* (1), 683-707.

23. Souda, P.; Ryan, C. M.; Cramer, W. A.; Whitelegge, J., Profiling of integral membrane proteins and their post translational modifications using high-resolution mass spectrometry. *Methods (San Diego, Calif.)* 2011, *55* (4), 330-336.

24. Reed, J. R.; Quilici, D. R.; Blomquist, G. J.; Reitz, R. C., Proposed mechanism for the cytochrome P 450-catalyzed conversion of aldehydes to hydrocarbons in the house fly, Musca domestica. *Biochemistry* 1995, *34* (49), 16221-16227.

25. Khara, B.; Menon, N.; Levy, C.; Mansell, D.; Das, D.; Marsh, E. N. G.; Leys, D.; Scrutton, N. S., Production of Propane and Other Short-Chain Alkanes by Structure-

Based Engineering of Ligand Specificity in Aldehyde-Deformylating Oxygenase. *Chembiochem* 2013, *14* (10), 1204-1208.

26. (a) Wallar, B. J.; Lipscomb, J. D., Dioxygen Activation by Enzymes Containing Binuclear Non-Heme Iron Clusters. *Chemical Reviews* 1996, *96* (7), 2625-2658; (b) Krebs, C.; Bollinger, J. M.; Booker, S. J., Cyanobacterial alkane biosynthesis further expands the catalytic repertoire of the ferritin-like “di-iron-carboxylate” proteins. *Current opinion in chemical biology* 2011, *15* (2), 291-303.

27. Buer, B. C.; Paul, B.; Das, D.; Stuckey, J. A.; Marsh, E. N. G., Insights into Substrate and Metal Binding from the Crystal Structure of Cyanobacterial Aldehyde Deformylating Oxygenase with Substrate Bound. *ACS Chemical Biology* 2014, *9* (11), 2584-2593.

28. Blazyk, J. L.; Gassner, G. T.; Lippard, S. J., Intermolecular Electron-Transfer Reactions in Soluble Methane Monooxygenase: A Role for Hysteresis in Protein Function. *Journal of the American Chemical Society* 2005, *127* (49), 17364-17376.

29. Li, N.; Nørgaard, H.; Warui, D. M.; Booker, S. J.; Krebs, C.; Bollinger, J. M., Conversion of Fatty Aldehydes to Alka(e)nes and Formate by a Cyanobacterial Aldehyde Decarbonylase: Cryptic Redox by an Unusual Di-metal Oxygenase. *Journal of the American Chemical Society* 2011, *133* (16), 6158-6161.

30. Warui, D. M.; Li, N.; Nørgaard, H.; Krebs, C.; Bollinger, J. M.; Booker, S. J., Detection of formate, rather than carbon monoxide, as the stoichiometric co-product in conversion of fatty aldehydes to alkanes by a cyanobacterial aldehyde decarbonylase. *Journal of the American Chemical Society* 2011, *133* (10), 3316-3319.

31. Eser, B. E.; Das, D.; Han, J.; Jones, P. R.; Marsh, E. N. G., Oxygen Independent Alkane Formation by Non-Heme Iron-Dependent Cyanobacterial Aldehyde Decarbonylase: Investigation of Kinetics and Requirement for an External Electron Donor(). *Biochemistry* 2011, *50* (49), 10743-10750.

32. Pandelia, M. E.; Li, N.; Nørgaard, H.; Warui, D. M.; Rajakovich, L. J.; Chang, W.-c.; Booker, S. J.; Krebs, C.; Bollinger, J. M., Substrate-Triggered Addition of Dioxygen to the Diferrous Cofactor of Aldehyde-Deformylating Oxygenase to form a Diferric-Peroxide Intermediate(). *Journal of the American Chemical Society* 2013, *135* (42), 10.1021/ja405047b.

33. Waugh, M. W.; Marsh, E. N. G., Solvent Isotope Effects on Alkane Formation by Cyanobacterial Aldehyde Deformylating Oxygenase and Their Mechanistic Implications. *Biochemistry* 2014, *53* (34), 5537-5543.

34. Newcomb, M., Radical Kinetics and Clocks. In *Encyclopedia of Radicals in Chemistry, Biology and Materials*, John Wiley & Sons, Ltd: 2012.

35. Chatgilialoglu, C.; Ingold, K. U.; Scaiano, J. C., Rate constants and Arrhenius parameters for the reactions of primary, secondary, and tertiary alkyl radicals with tri-n-butyltin hydride. *Journal of the American Chemical Society* 1981, *103* (26), 7739-7742.

36. Walton, J. C., Non-perfect synchronisation of [small beta]-scission with product stabilisation in radical ring-opening reactions. *Journal of the Chemical Society, Perkin Transactions 2* 1989, (2), 173-177.

37. Newcomb, M.; Johnson, C. C.; Manek, M. B.; Varick, T. R., Picosecond radical kinetics. Ring openings of phenyl-substituted cyclopropylcarbinyl radicals. *Journal of the American Chemical Society* 1992, *114* (27), 10915-10921.

Chapter 2

Probing the Mechanism of Cyanobacterial Aldehyde Decarbonylase Using a Cyclopropyl Aldehyde

The work described in this chapter was performed in collaboration with Dr. Debasis Das, who analyzed the formate byproduct and assisted in LC-MS and Proteomics work, and Dr. Bishwajit Paul, who synthesized the substrate and its derivatives. Additionally, MALDI-TOF analysis was carried out by Dr. Benjamin C. Buer, and MS analysis was performed by Dr. V. Basrur. It has been published in the *Journal of the American Chemical Society* **2013**, *135* (14), 5234-5237.

2.1 Introduction

The biosynthesis of long-chain aliphatic hydrocarbons is widely distributed in Nature, occurring in plants,[1] animals[2] and microbes,[3] and is typified by the production of alkanes with an odd number of carbon atoms.[4] These are derived from fatty acid biosynthesis in a two-step pathway in which fatty-acyl-CoA reductase reduces long-chain fatty-acyl-CoA esters to the corresponding fatty aldehydes.[5] In the second step, aldehyde decarbonylase (AD) removes the formyl (HCO) group from fatty aldehydes to yield the long-chain aliphatic hydrocarbons.[6] Recently, these biosynthetic processes have garnered increasing interest because of the potential for such pathways to be harnessed for the production of biofuels.[7]

The reaction catalyzed by aldehyde decarbonylase is unusual because it represents a rare biological case in which a completely unfunctionalized product is formed.[8] Recently, it has become apparent that there are three different classes of aldehyde decarbonylases. In insects, the enzyme is a membrane-associated cytochrome P450 system and the aldehyde carbon is converted to CO_2.[2b, 9] In plants and algae, the enzyme is also membrane bound and is most likely iron dependent; however, in this case the aldehyde carbon is converted to CO.[5a, 6, 10] The most recently discovered cyanobacterial aldehyde deformylating oxygenase[3a] (cADO) is a soluble protein, whose crystal structure[11] reveals it to share the same non-heme di-iron metal site as enzymes such as methane monoxygenase, class I ribonucleotide reductase and ferritin.[12]

Dr. Debasis Das recently demonstrated that in the cADO-catalyzed reaction the aldehyde carbon is converted to formate. Isotope-labeling studies established that the aldehyde C-H bond remains intact during the reaction and that the proton in the newly formed methyl group of the alkane derives from solvent (or a solvent-exchangeable group on the enzyme);[13] findings that were independently arrived at by Warui *et al*.[14]

Other di-iron enzymes that are structurally related to cADO utilize molecular oxygen, and although the substrate is not formally oxidized in the decarbonylation reaction, support for the involvement of molecular oxygen derives from labeling experiments in which ^{18}O from $^{18}O_2$ was found to be incorporated into formate.[15] This implies that, in addition to the two electrons needed to reduce the diferric enzyme to the oxygen-reactive diferrous state, two further electrons, (supplied by the external reducing system) are required for the reaction, so that overall O_2 is fully reduced to water (Figure 2.1).

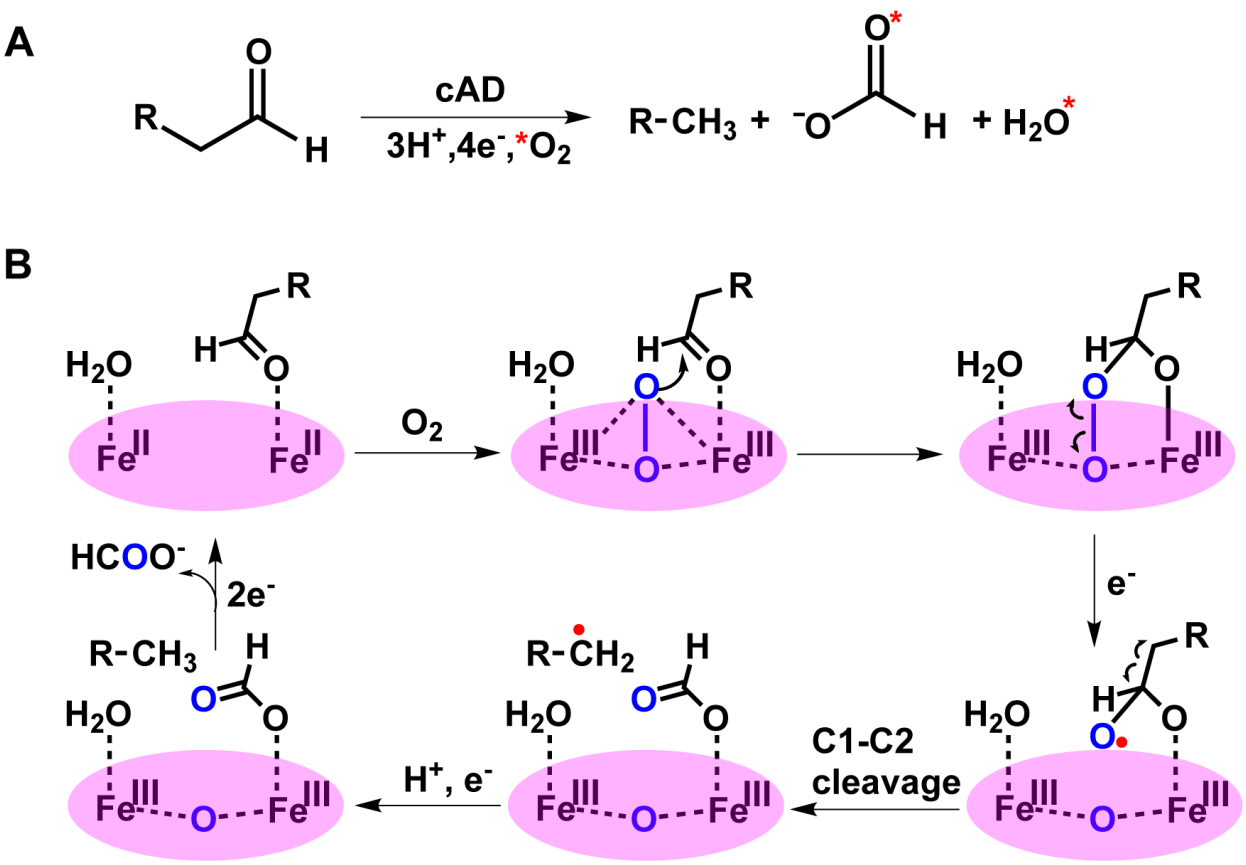

Figure 2.1. A) Reaction Catalyzed by cADO B) Proposed Mechanism for cADO

A central mechanistic question, which remains to be answered for all classes of aldehyde decarbonylase, is how the bond between aldehyde carbon (C1) and the α-carbon (C2) is cleaved. One plausible mechanism[15a] is shown in Figure 2.1 B. This involves initial formation of a reactive iron-peroxo species that attacks the aldehyde carbon. A 1-electron reduction leads to the formation of a hemiacetal radical followed by scission of the C1-C2 bond. A subsequent proton-coupled electron transfer step reduces the alkyl radical to the alkane. Tentative evidence that the reaction may involve radicals comes from spin-trapping experiments performed on cADO incubated with substrates in

the absence of a reducing system.[13] Therefore, to gain insights into the C1-C2 bond scission step I have investigated the reaction of cADO with a substrate that incorporates a strategically placed cyclopropyl group that can act as a “radical clock”.

Cyclopropylcarbinyl radicals, formed when radicals are generated adjacent to the cyclopropyl ring, undergo rapid and very well characterized ring-opening reactions.[16] Cyclopropyl compounds have been extensively employed to investigate the mechanisms of cytochrome P450 enzymes[16-17] and non-heme iron enzymes including methane monooxygenase,[18] isopenicillin N synthase[19] and, most recently, HppE that catalyzes epoxide formation in the biosynthesis of fosfomycin.[20] Depending upon the lifetime of the postulated alkyl radical intermediate, one would expect to observe either retention of the cyclopropyl ring in the product, if either the radical is very short lived or the reaction is concerted, or ring-opening if the radical intermediate is relatively long-lived.

2.2 Materials and Methods

2.2.1 Materials

Octadecanal, pentadecanal, tetradecane, heptadecane, 1-octadecene, phenazine methosulfate (PMS), ferrous ammonium sulfate and NADH were obtained from Acros Organics. Potassium chloride, HEPES were from Fisher chemicals. D_2O (99.9%) and DMSO-d_6 (99.9%) were from Cambridge Isotope Laboratories, Inc. Desalting of protein samples was accomplished using Zeba Spin Desalting Columns (2 mL) from Thermo Scientific, and sequence grade trypsin and Glu-C were purchased from Promega (USA) for MALDI-TOF and LTQ mass analysis. All other reagents were of the purest grade commercially available and used without further purification.

2.2.2 Synthesis of 2-(2-tetradecylcyclopropyl)acetaldehyde (6)

As a potential radical clock substrate, we synthesized the cyclopropyl analog of octadecanal, 2-(2-tetradecylcyclopropyl)-acetaldehyde **6**, in which the cyclopropyl group is positioned β-to the carbonyl group, as outlined in Figure 2.2 and detailed more thoroughly in Appendix A. Briefly, a Wittig reaction between pentadecanal, **1**, and 3-hydroxypropyl-triphenylphosphonium bromide was employed to form octadec-3-ene-1-ol, **2**, as the (*E*) stereoisomer.[21] After protection of the alcohol as its TBDMS silyl ether, the double bond was converted to a cyclopropyl group using diethylzinc and diiodomethane, to give the *trans* stereoisomer, **4**, as major product.[22] Finally, deprotection of TBDMS group by TBAF, followed by oxidation of the alcohol with TEMPO yielded the cyclopropyl aldehyde, **6**.[23]

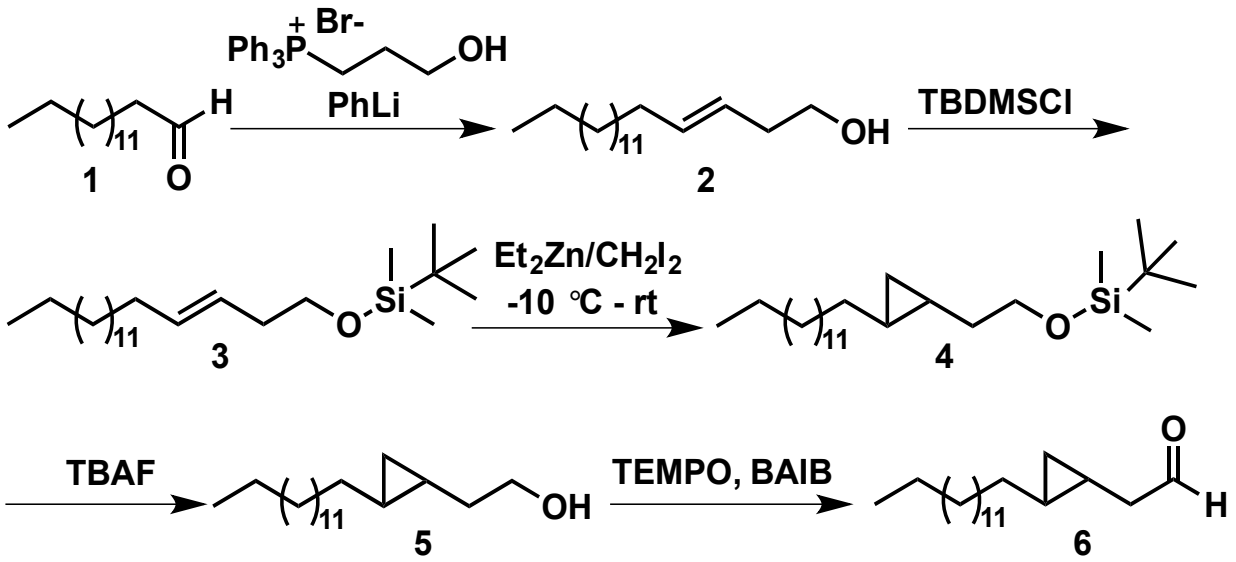

Figure 2.2. Synthesis of Cyclopropyl aldehyde **6**.

2.2.3 Enzyme Assays

Assays were performed in 100 mM HEPES buffer, pH 7.2, containing 100 mM KCl and 10% glycerol. Aldehydes substrates were made up to a stock solution in DMSO. A

typical assay contained 10 µM cADO, 20 µM ferrous ammonium sulfate, 400 µM aldehyde substrate, 100 µM phenazine methosulfate (PMS) and 1 mM NADH in a total volume of 500 µL. Assays were shaken for 1 hr at 37 ºC at 200 rpm. Reactions were quenched by addition of 500 µL ethyl acetate and vortexed well to extract hydrocarbon products and un-reacted substrate. The ethyl acetate layer was separated and 8 µL sample of the ethyl acetate layer was injected into GC-MS for analysis. Enzymatic production 1-octadecene was quantified using a calibration plot of 1-octadecene.

Gas chromatography analysis was performed using a Shimadzu QP2010S GC-MS instrument equipped a quadrupole mass detector. A DB-5 column (Restek, 30m x 0.25 mm x 0.25 µm) was used for elution. The flow rate of the helium carrier gas was kept constant at 1 mL/min and the inlet temperature was maintained at 200 °C. The interface temperature was maintained at 250 °C. Injections were made in splitless mode. Oven temperature was held initially at 70 °C for 2 min and then gradually increased to 300 °C at 20 °C/min and finally maintained at 300 °C for 5 min. Data analysis was performed by GC-MS PostRun analysis software.

2.2.4 Formate Assays

The detection of formate as a co-product in cADO assay was confirmed by derivatizing the products of the enzyme reaction with 2-nitrophenylhydrazine (2-NPH) followed by reverse phase HPLC. 400 µl of the products of the enzyme reaction was mixed with 40 µl of 120 mM 2-NPH solution (aqueous solution in 0.25 M HCl) and 40 µl of EDC working solution (300 mM EDC in 1:1 pyridine:HCl). After vortexing for ~30 s, the reaction mixtures were incubated at 60 °C for 30 min. The samples were then centrifuged to remove precipitated protein and insoluble reaction products. 400 µl of the clear

supernatant was subjected to chromatography on a Nucleosil C18 RP HPLC column (250 mm x 4 mm, 5 µM, 120 Å). The column was equilibrated in 50 % water, (acidified with 0.05% AcOH) and 50 % methanol (acidified with 0.05% AcOH) and compounds were eluted with a gradient of 30% methanol to 90% methanol over 45 min at 0.7 mL/min.

2.2.5 LC-ESI-MS Analysis

Covalent modifications on cADO were analyzed by LC-MS using an Agilent 6520 LC - accurate-mass Q-TOF MS system. After incubation with either cyclopropyl substrate **6** or with octadecanal, the protein was recovered, desalted and reconstituted with 0.1% formic acid. 5 µl of the sample was injected into a Poroshell 300SB-C8 column equilibrated with 0.1% formic acid and 5% acetonitrile. Proteins were eluted for 5 min with 95% water: 5% acetonitrile followed by an increase in gradient to 100% acetonitrile over 7 min at a constant flow rate of 0.5 ml/min. Eluting proteins were detected at 280 nm; cADO eluted with a retention time of 8.6-9.5 min. Mass data were obtained using intact protein mode and analyzed using Agilent MassHunter Qualitative Analysis software. The raw data was deconvoluted with respect to maximum entropy.

2.2.6 MALDI-TOF Analysis

To determine the location of the covalent modification, samples of the inactivated and unmodified enzyme were subjected to proteolytic digestion with either trypsin or Glu-C and studied by MALDI-TOF (Micromass TofSpec2E). α-cyano-4-hydroxycinnamic acid was used as a matrix. The instrument was calibrated using an external reference of five standard peptide of known mass. Proteins were denatured with 8 M urea and reduced with 10 mM DTT prior to alkylation of cysteine residues using 50 mM iodoacetamide. The resulting alkylated protein was diluted to reduce the urea concentration to 1.5 M and

treated with sequencing grade modified trypsin (Promega) and Glu-C separately overnight at 37 °C. The proteolytic fragments were analyzed by MALDI-TOF mass spectrometry and the spectra of the modified and unmodified enzyme digests compared.

2.2.7 LC-Tandem Mass Analysis

Tandem mass analysis was performed by ion-trap mass spectrometer (LTQ-XL, ThermoFisher). Proteins were digested as described before for MALDI-TOF analysis. The samples were further acidified with trifluoroacetic acid and peptides were purified using SepPak C18 cartridge (Waters). The resulting sample was injected into a C18 reverse phase column (Aquasil) equilibrated with 5% acetonitrile/1% acetic acid and peptides eluted with a linear gradient of increasing acetonitrile from 5 % to 60% over 40 min at a flow rate of 300 nl/min. The eluting peptides were directly introduced into ion-trap mass spectrometer (LTQ-XL) equipped with a nano-spray source. A full MS scan (m/z 400-2000) was acquired and the most abundant 6 ions were studied by MS/MS mode (relative collision energy ~ 35%). Raw files were searched against an E. coli database appended with the Np cADO sequence and a decoy database using X!Tandem (www.thegpm.org). The modification of phenylalanine, tyrosine, histidine, or glutamic acid, by a mass increment of 250.4 Da, together with methionine oxidation (+ 16 Da) and carbamidomethylation of cysteine (+ 57 Da) were considered as variables. The mass tolerance limit was set at 1 Da for precursor peptides and 0.5 Da for fragmented peptides. Results were further analyzed by Trans-Proteomic Pipeline (TPP) analysis, including PeptideProphet and ProteinProphet.

2.2.8 Preparation of di-Deuterated 6

6 (final concentration 10 mM) was dissolved in 90% DMSO-d_6, 10% in D_2O, buffered with 10 mM HEPES at pD 8.4. The solution was shaken for 12 h at 37 °C after which time GC-MS analysis revealed that the α-protons were greater than 95 % exchanged (Figure 2.3). The stock solution was stored frozen at -80 °C for further use in deuterium incorporation assays.

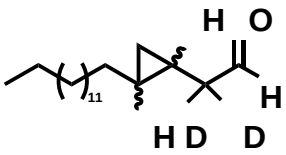

Di-deuterated 6

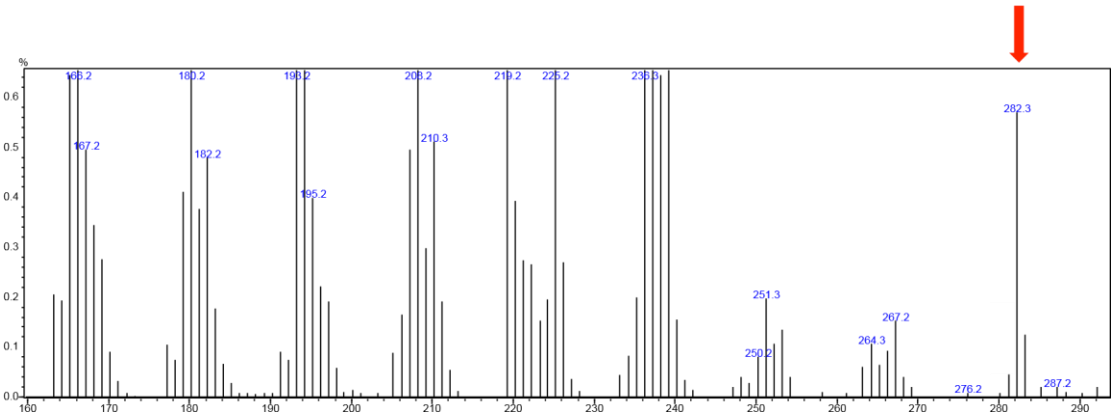

Figure 2.3. A section of mass spectrum of di-deuterated cyclopropyl substrate **6** showing molecular ion peak of *m/z* 282.3.

2.3 Results and Discussion

2.3.1 Reaction of Cyclopropyl Analog with cADO Yields 1-Octadecene and Formate

We investigated the reaction of **6** with cADO from *Nostoc punctiformes*, which was recombinantly over-expressed in *E. coli* and purified as previously described.[24] Assays were performed at 37 °C and typically contained 400 μM **6**, 10 μM cADO, 1 mM NADH and 100 μM phenazine methosulfate (PMS) in 100 mM HEPES buffer, 100 mM KCl, 10

% glycerol, pH 7.2 and 4 % DMSO to improve substrate solubility. The reaction products were extracted with ethyl acetate and analyzed by GC-MS.[13, 24] The chromatograph revealed a new peak at 9.84 min, which co-chromatographed with an authentic standard of 1-octadecene and was characterized by a molecular ion of *m/z* = 252.3, confirming its identity (Figures 2.4 and 2.5).

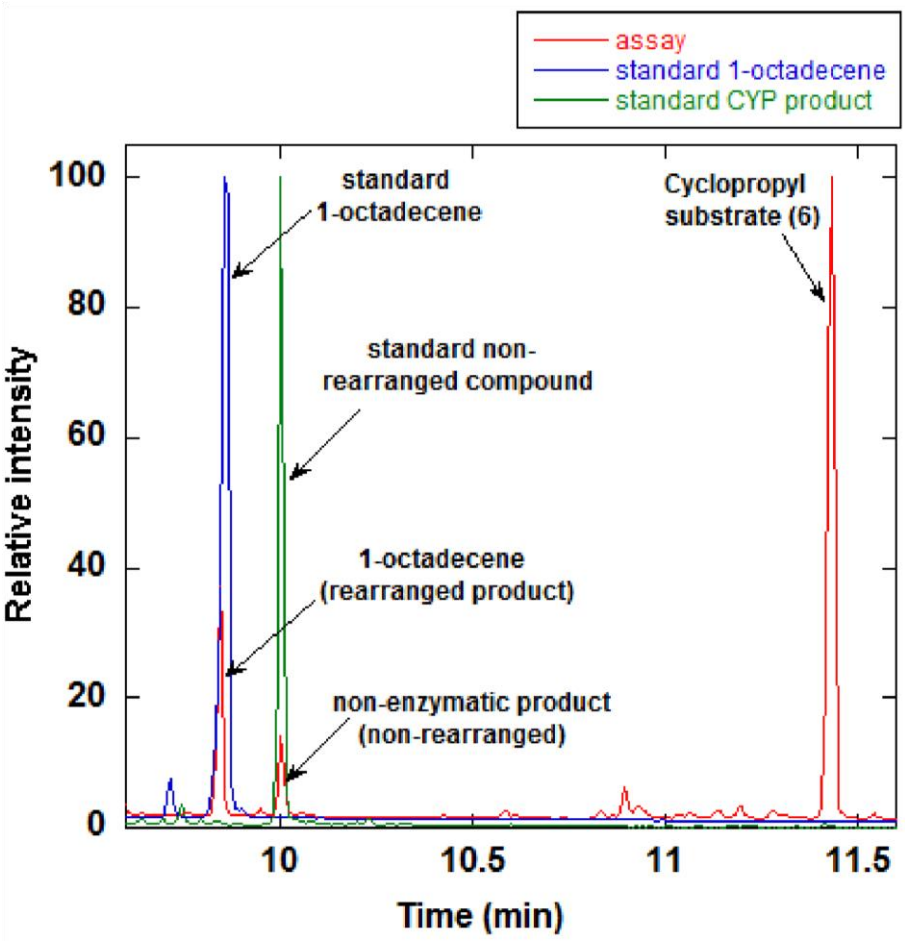

Figure 2.4. Gas chromatographs of 1-octadecene formed from **6** by *Np* cADO (in red), an authentic standard 1-octadecene (in blue) and an authentic standard of 1-methyl-2-tetradecylcyclopropane, formed non-enzymatically (in green). Retention times of 1-octadecene and 1-methyl-2-tetradecylcyclopropane products are at 9.84 min and 10 min, respectively.

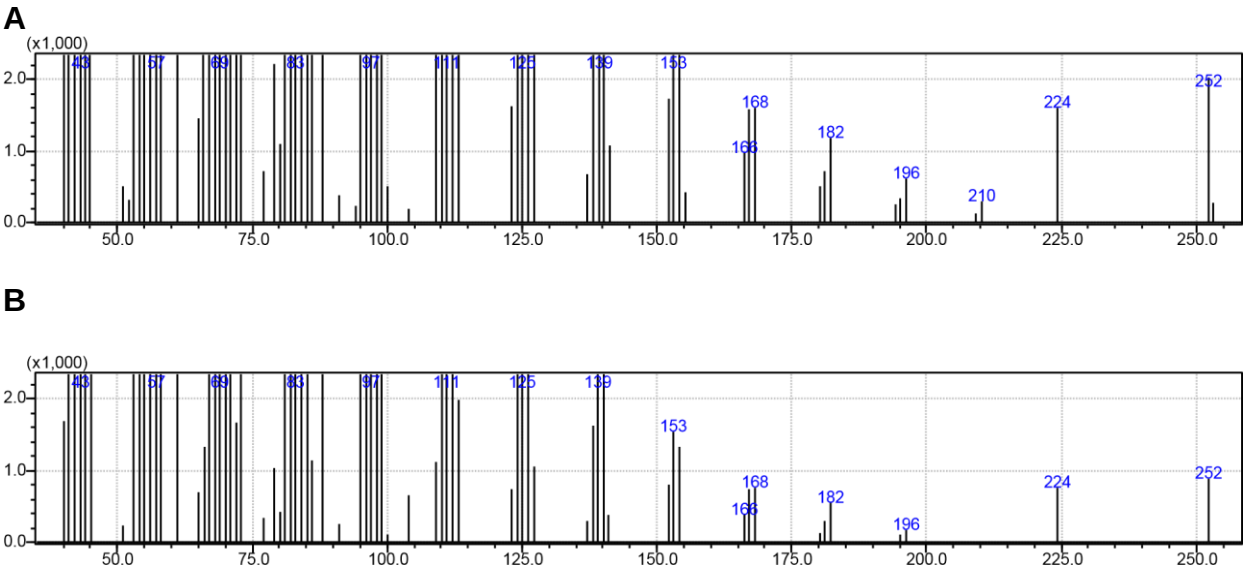

Figure 2.5. Electron Impact mass spectral analysis of authentic standard 1-octadecene (A) and enzymatically obtained 1-octadecene (B). Molecular ion peak of *m/z* = 252 is characteristic of 1-octadecene.

The formation of 1-octadecene was strictly dependent on the presence of PMS, NADH and molecular oxygen. Prolonged incubation of the assay mixture under rigorously anaerobic conditions (pO_2 < 0.5 ppm) gave no reaction products (Figure 2.6). This observation supports a radical mechanism for C-C bond scission, in which the cyclopropylcarbinyl radical rearranges to the octadecenyl radical, leading to the formation of 1-octadecene as the product, as shown in Figure 2.7. The rate constant for ring opening of cyclopropylcarbinyl radicals is known; $k = 8.6 \times 10^7\ s^{-1}$ at 298 K.[25] This implies that the radical generated at the α-carbon of **6** has lifetime ≥ 10 ns. The hydrazide derivative of formate was eluted at ~28 min and detected at 230 nm (Figure 2.8). The presence of formate in the derivatized assay samples was confirmed by comparison with the retention time of an authentic standard. Analysis of this peak by UV-visible and mass spectrometry further confirmed the identity of the compound as the 2-NPH derivative of formate.

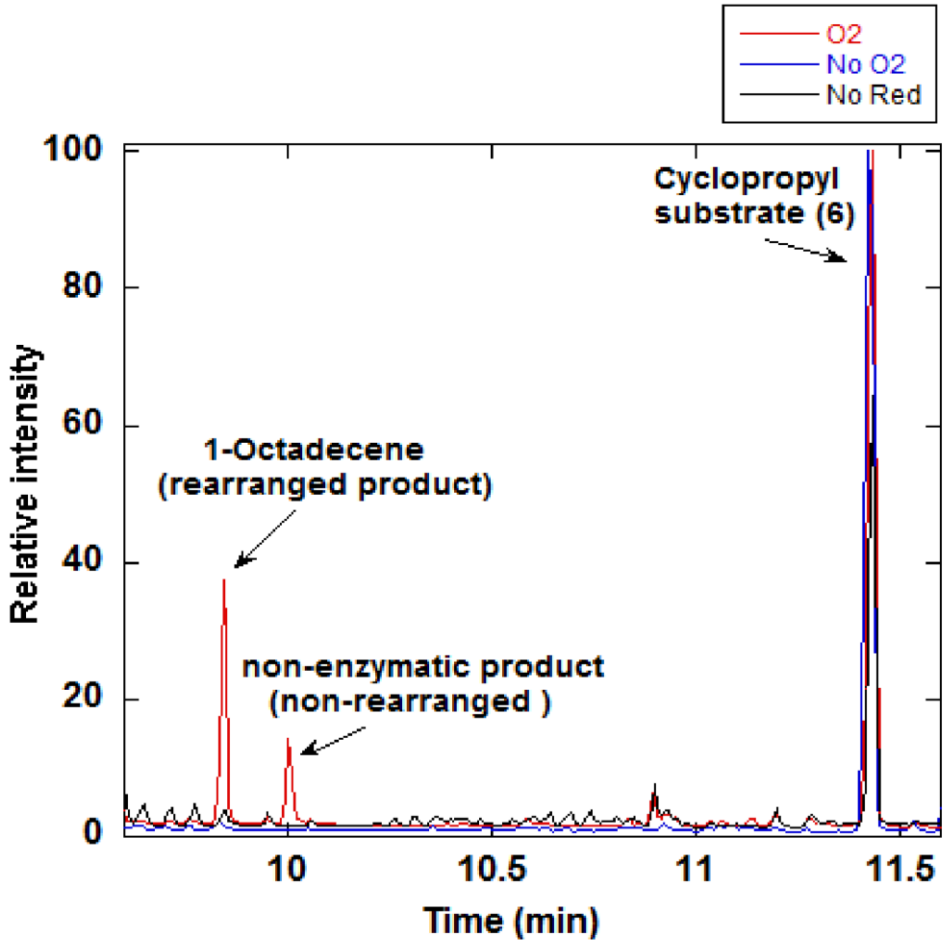

Figure 2.6. Overlaid chromatographs showing the formation of 1-octadecene and the non-enzymatically formed cyclopropyl alkane product in the presence of cADO, O_2 and PMS/NADH (red trace). In the absence of O_2 (blue trace) or in the absence of reducing system PMS/NADH (black trace), neither 1-octadecene nor the cyclopropyl alkane product is observed.

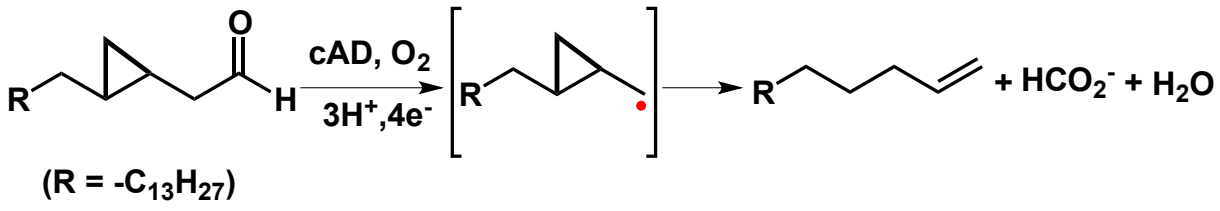

Figure 2.7. Reaction of Cyclopropyl Substrate **6** with *Np* cADO.

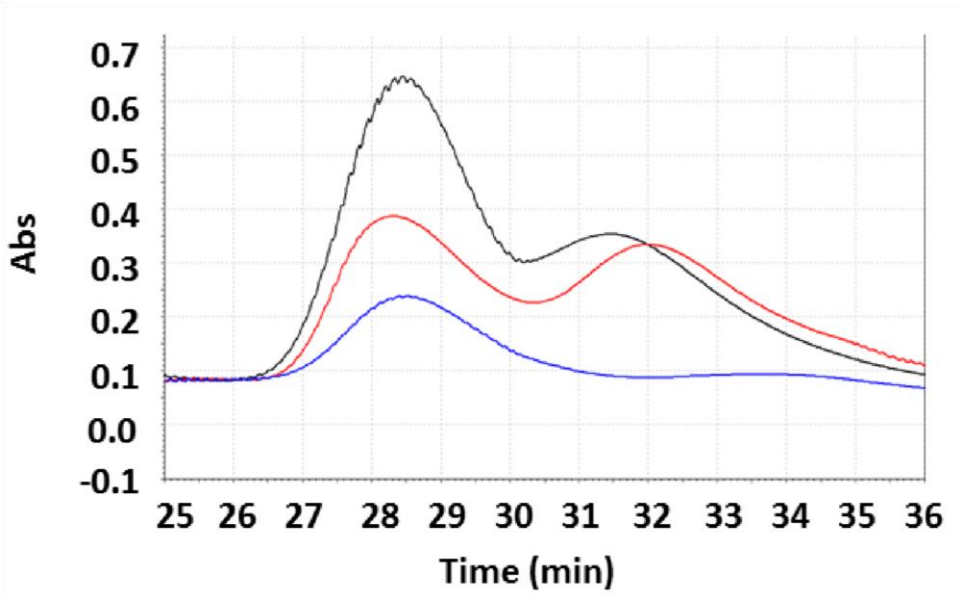

Figure 2.8. Overlaid HPLC traces of 2-NPH derivatives of authentic formate (in blue), *Np* cADO reaction product with cyclopropyl compound **6** (red) and *Np* cADO reaction product with octadecanal (black) at 230 nm. 2-NPH-formate derivative elutes at retention time of ~ 28 min. Fractions were collected and studied by ESI-MS (negative mode). Identity of each formate derivative was confirmed by obtained mass of *m/z* = 180.1.

Interestingly, a minor peak at 10.0 min with *m/z* = 252.3 was also evident that co-chromatographed with an authentic standard of 1-methyl-2-tetradecylcyclopropane, the non-rearranged product from the decarbonylation of **6** (Figure 2.4). However, this compound was also present in similar amounts in control experiments in which the enzyme was omitted and thus must arise from non-enzymatic decarbonylation of the cyclopropyl aldehyde (Figure 2.9). The non-enzymatic reaction requires the presence of NADH, PMS and O_2: no non-rearranged product was observed if any of these reagents were omitted (Figure 2.6). Nor was the non-rearranged product formed if a “biological” reducing system comprising NADPH, ferredoxin, and ferredoxin reductase was substituted for NADH and PMS. The mechanism for this unusual side reaction remains unclear.

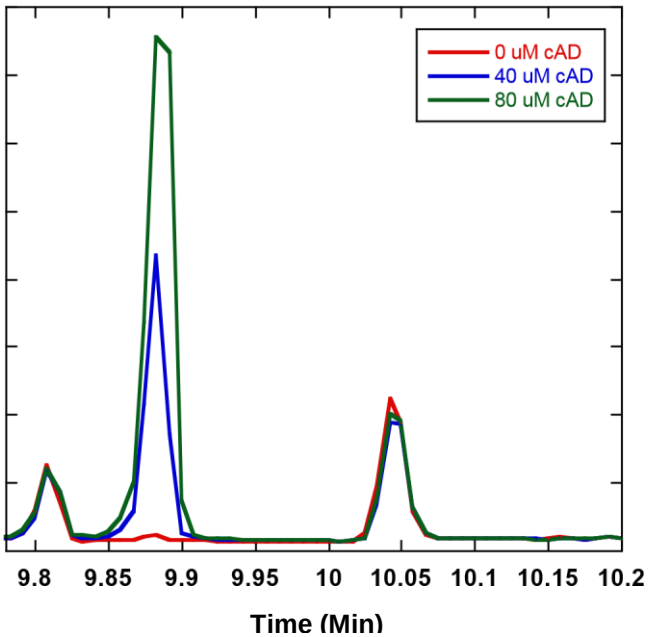

Figure 2.9. Formation of 1-methyl-2-tetradecylcyclopropane (retention time = 10.05 min) from **6** is independent of cADO. The formation of octadecene increases linearly with enzyme concentration (blue and green traces); in the absence of cADO no octadecene is formed (red trace), whereas the amount of 1-methyl-2-tetradecylcyclopropane formed is constant.

2.3.2 Cyclopropyl Analog Inhibits cADO

Despite varying the concentrations of reagents and the length of assay, no more than about one equivalent of 1-octadecene was observed in the reaction of **6** with cADO (Figure 2.10). This observation suggested that **6** may partition between turn-over and acting as an irreversible inhibitor of the enzyme. Inactivation of cADO was confirmed by incubating cAD with **6** (400 μM) in assay buffer containing PMS, NADH and O_2 for 1 hour. The activity of the enzyme was then assayed using octadecanal (400 μM) as the substrate. Essentially no activity remained, as shown in Figure 2.11 (I). In contrast, if the alternate substrate, pentadecanal (400 μM), was substituted for **6** a significant amount of enzyme activity remained after 1 hour when the enzyme was assayed with octadecanal (Figure 2.11 (II)). The formation of 1-octadecene appeared to be described by first order

kinetics. The partitioning of substrate between turnover and enzyme inactivation is described by the equation below:

$$\frac{P_t}{E} = \frac{k_{cat}}{k_{in}}(1 - e^{-k_{in}t}) \quad (1)$$

In which P_t is the concentration of product at time t; E is enzyme concentration and k_{in} is the rate constant for inactivation. Fitting the data Equation 1, $k_{cat} \approx k_{in}$ = 0.088 ± 0.011 min^{-1}; for comparison k_{cat} = ~ 0.4 min^{-1} with octadecanal as the substrate.[13]

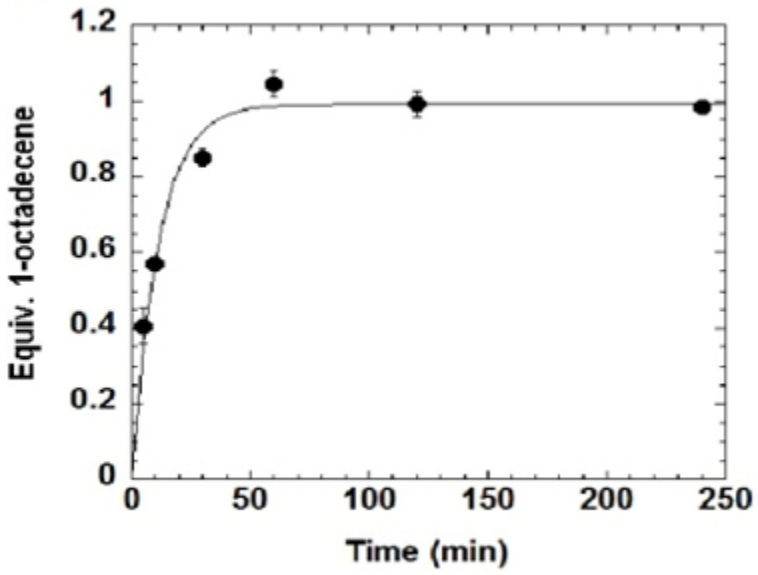

Figure 2.10. Time course for formation 1-octadecene by cADO.

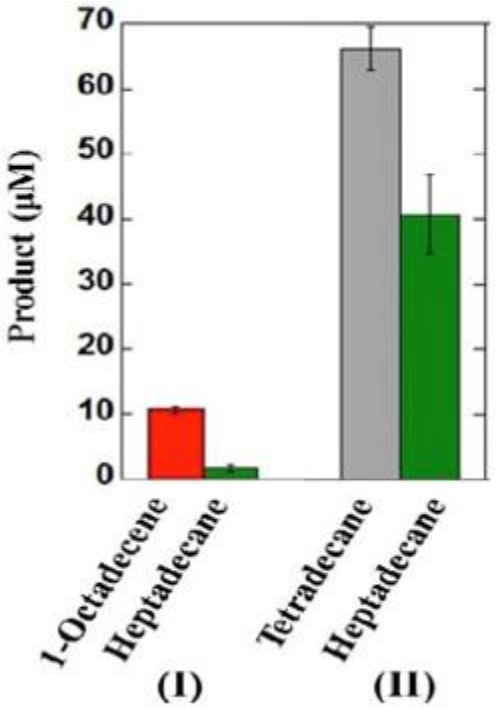

Figure 2.11. Inactivation of cADO by **6**. (I) Reaction of cADO with **6** for 1 h followed by addition of octadecanal results in negligible heptadecane being formed; (II) as a control, reaction of cADO with pentadecanal for 1 h followed by addition of octadecanal demonstrates that significant enzyme activity remains.

2.3.3 Mechanistic Inhibition of cADO Through Formation of a Covalent Adduct

To gain further insight into the mechanism of inactivation, we analyzed the inactivated cADO by LC-ES-MS. The mass of the cADO prior to reaction with **6** was determined as 28911 ± 0.5 Da (Figure 2.12), in excellent agreement with the calculated molecular weight. Reaction of cADO with octadecanal resulted in no change in M_r (Figure 2.13A). However, reaction of cADO with **6** resulted in between 60 - 80 % of the recovered enzyme eluting from the column as a species characterized by a slightly longer retention time and a molecular weight of 29162 ± 0.5 Da (Figure 2.13B). The increase in molecular weight of 251 ± 0.5 Da is consistent with the formation of a covalent adduct between

decarbonylated **6** and cADO. Covalent modification of cADO by **6** provides a plausible mechanism for inactivation.

A

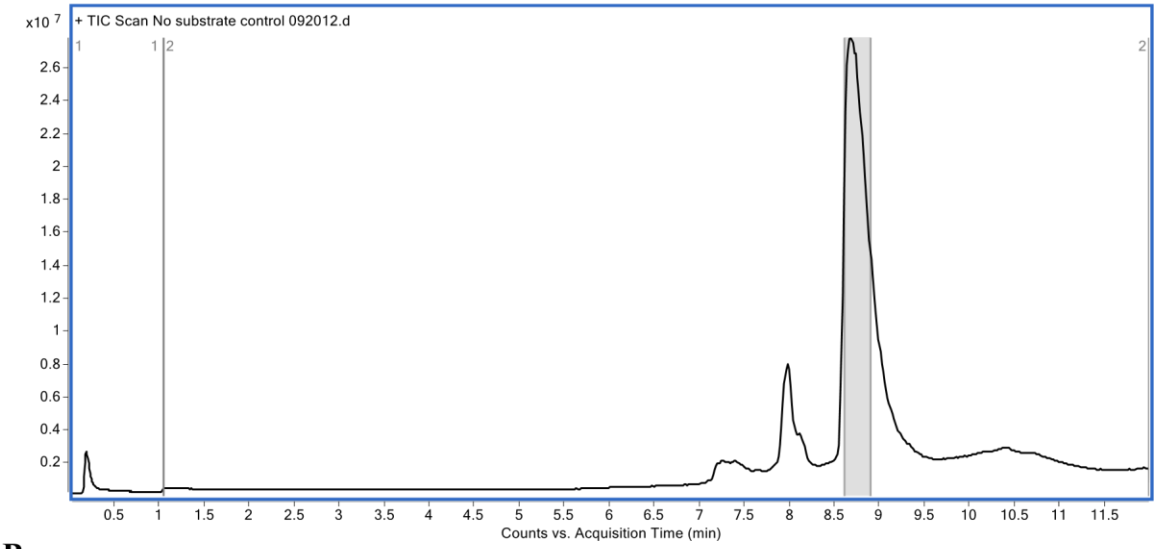

B.

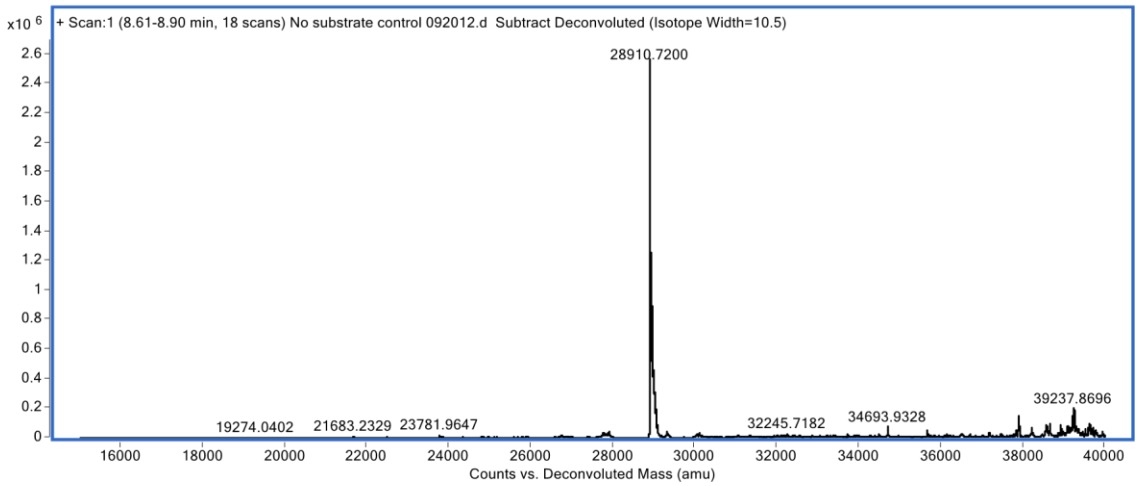

Figure 2.12. Reverse phase liquid chromatogram and mass spectral analysis of *Np* cADO. A. Total ion chromatogram (TIC) B. Deconvoluted mass spectrum of as isolated *Np* cADO. Highlighted region of A was extracted for mass spectral analysis. *Np* cADO elutes as a single peak with retention time 8.6 to 9.2 min. Mass of *Np* cADO is 28911 ± 0.5 Da.

Reaction of cADO with octadecanal resulted in no change in M_r (Figure 2.13A). However, reaction of cADO with **6** resulted in between 60 - 80 % of the recovered enzyme

eluting from the column as a species characterized by a slightly longer retention time and a molecular weight of 29162 ± 0.5 Da (Figure 2.13B). The increase in molecular weight of 251 ± 0.5 Da is consistent with the formation of a covalent adduct between decarbonylated **6** and cADO. Covalent modification of cADO by **6** provides a plausible mechanism for inactivation.

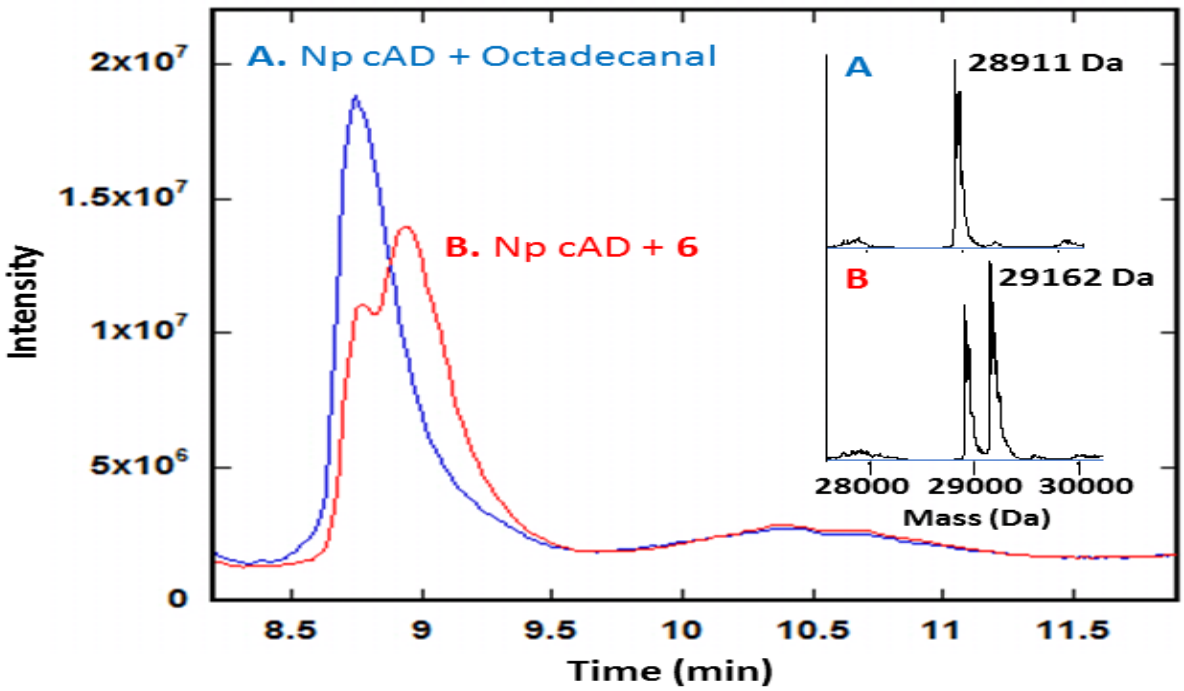

Figure 2.13. LC-MS of cADO. A: No modification occurs after reaction of cADO with octadecanal (blue); M_r of cADO = 28911 Da; B: reaction of cADO with **6** results in covalently modified protein (red), M_r = 29162 Da.

2.3.4 Determining the Site of the Covalent Modification

To determine the location of the covalent modification, samples of the inactivated and unmodified enzyme were subjected to proteolytic digestion with either trypsin or Glu-C. The proteolytic fragments were analyzed by MALDI-TOF mass spectrometry and the spectra of the modified and unmodified enzyme digests compared (Figures 2.14 and

2.15). Analysis of the spectra identified two peptides, one Glu-C-derived, the other trypsin-derived, which were absent from the spectra of the covalently modified enzyme. Significantly, the peptides overlapped in sequence and encompass a 20-residue segment, CFAIAAYNIYIPVADDFARK, that forms part of the hydrophobic substrate-binding channel of cADO.

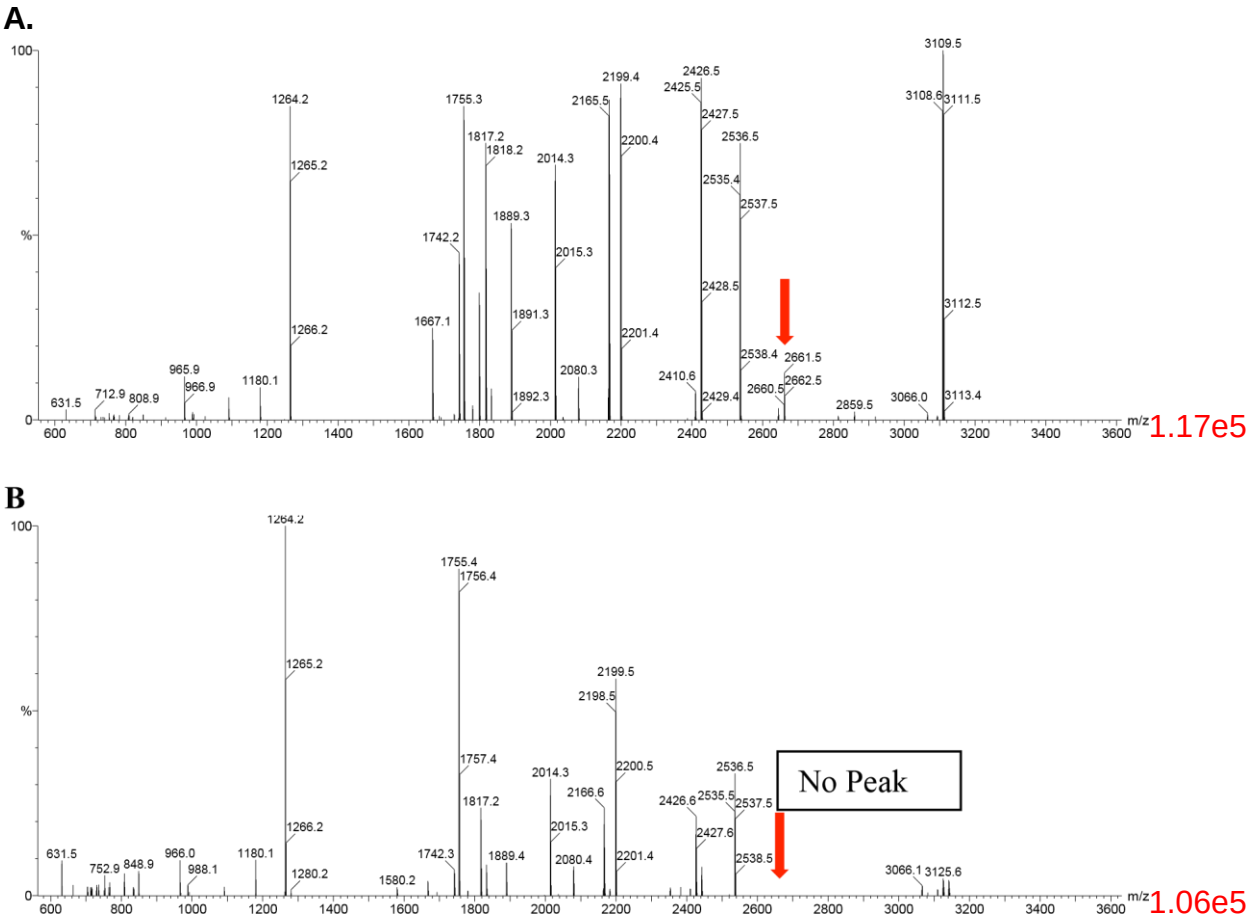

Figure 2.14. MALDI spectrum of GluC digests of *Np* cADO (A) and **6** treated *Np* cADO (B). Red arrow on spectrum **A** shows the peak of interest with mass 2661.5 Da that represents carbamidomethylated CFAIAAYNIYIPVADDFARKIT peptide fragment that is absent in spectrum **B**.

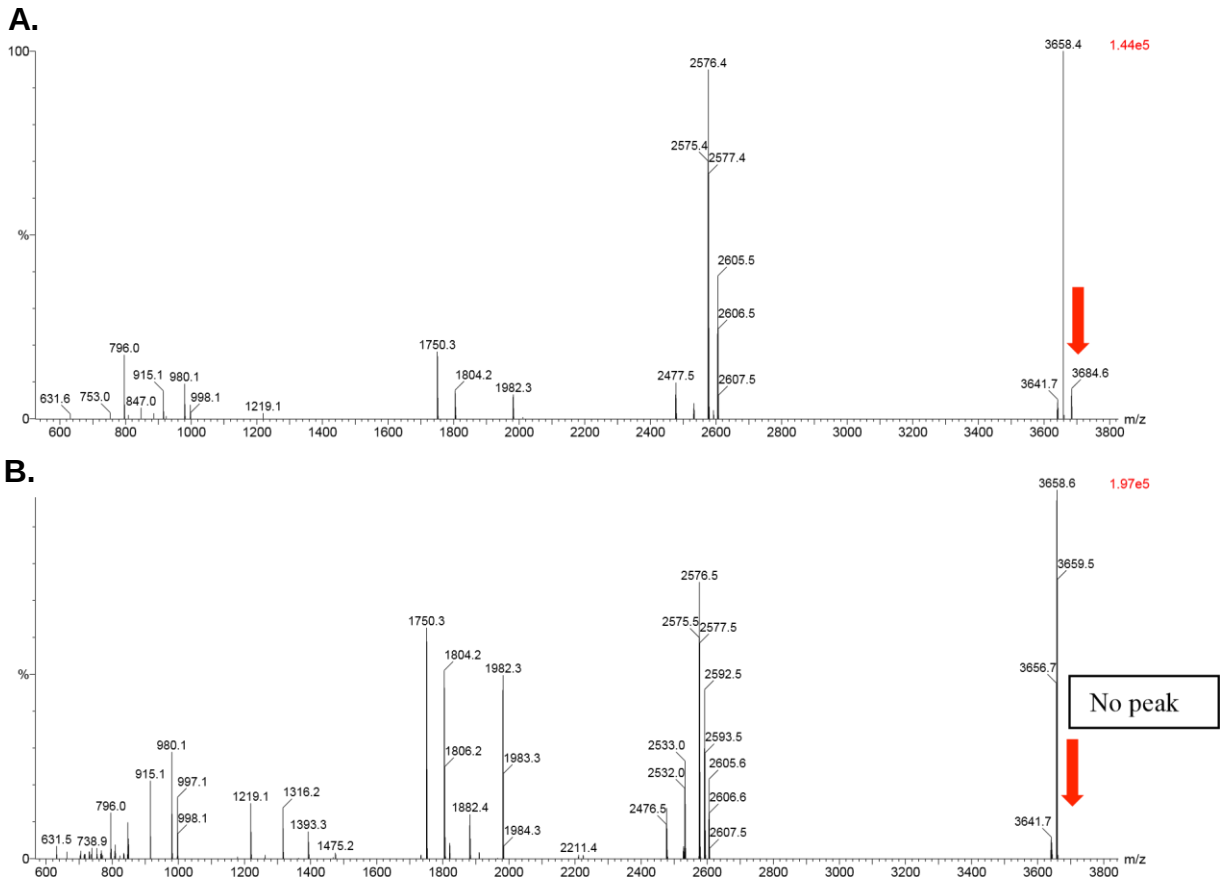

Figure 2.15. MALDI spectrum of trypsin digests of *Np* cADO (A) and **6** treated *Np* cADO (B). Red arrow on spectrum **A** shows the peak of interest with mass 3684.6 Da that represents VVTCLLIQSLIIECFAIAAYNIYIPVADDFARK peptide fragment that is absent in spectrum **B**.

Unfortunately, we were unable to detect the alkylated peptides directly by MALDI-TOF mass spectrometry. However, it is commonly observed that hydrophobic peptides are under-represented or absent in “bottom up” proteomic analyses of proteins.[26] This may be attributed to loss of hydrophobic peptides during sample preparation steps prior to MS analysis; there is also the potential for the modification to interfere with the proteolytic digestion of the peptide, and/or adversely affect its ability to ionize in the mass spectrometer.

The proteolytic digests of covalently modified cADO were subjected to more extensive analysis using ES-MS-MS. Samples were analyzed using an ion-trap mass spectrometer (LTQ-XL, ThermoFisher) equipped with a nano-spray ion source; the resulting mass spectra were analyzed using Trans-Proteomic Pipeline (TPP) software including PeptideProphet and ProteinProphet.[27] This analysis succeeded in identifying one covalently modified peptide, present in low-abundance, in the tryptic digest. The secondary ion mass spectrum of this peptide displayed a fragmentation pattern that was consistent with F107 being modified by an additional mass of 251 ± 0.5 Da (Figure 2.16). F107 forms part of the hydrophobic substrate channel of cADO (Figure 2.17) and would be within ~ 5 Å of the putative alkyl radical formed by the opening of the cyclopropyl ring of **6**. These results suggest that the reaction of the product alkyl radical with the phenylalanine ring results in the covalent attachment of the alkyl fragment to the protein, thereby inactivating the enzyme (Figure 2.18, pathway II).

A

IECFAIAAYNIYIPVADDFAR, MH+ 2933.2853, m/z 978.4333

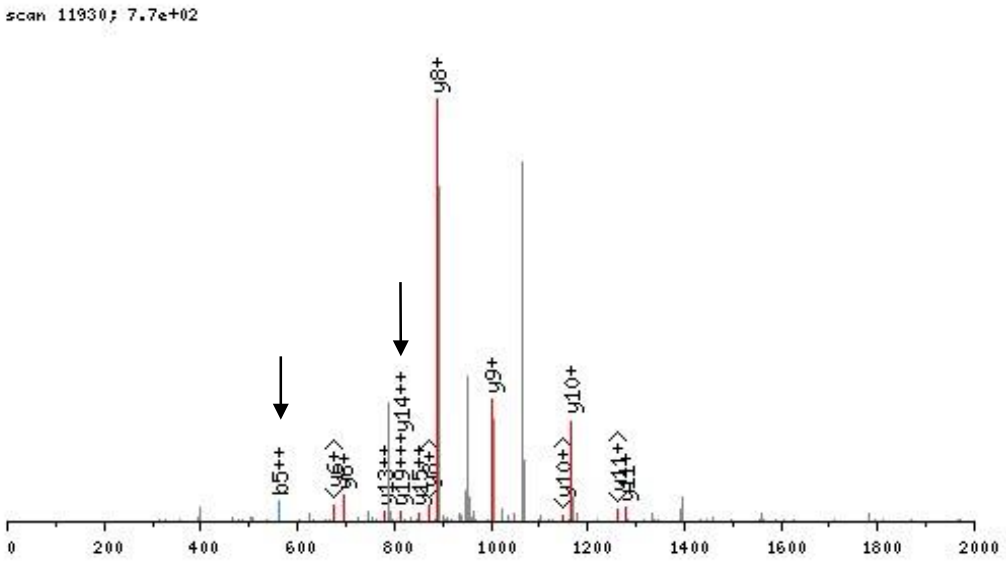

B

b^+	b2+	#	AA	#	y^+	y2+	y3+
114.0913	57.5496	**1**	**I**	**21**			
493.6068	247.3073	**2**	**E**	**20**	2820.2007	1410.6043	940.7388
653.7456	327.3767	**3**	**C**	**19**	2440.6852	1220.8465	**814.2336**
1051.3222	526.1650	**4**	**F**	**18**	2280.5464	1140.7771	760.8540
1122.3594	**561.6836**	**5**	**A**	**17**	1882.9698	941.9888	628.3285
1235.4434	618.2256	**6**	**I**	**16**	1811.9327	906.4702	604.6494
1306.4805	653.7442	**7**	**A**	**15**	1698.8486	**849.9282**	566.9547
1377.5176	689.2627	**8**	**A**	**14**	1627.8115	**814.4097**	543.2757
1540.5810	770.7944	**9**	**Y**	**13**	1556.7744	**778.8911**	519.5967
1654.6239	827.8159	**10**	**N**	**12**	1393.7110	697.3594	465.2422
1767.7080	884.3579	**11**	**I**	**11**	**1279.6681**	640.3380	427.2279
1930.7713	965.8896	**12**	**Y**	**10**	**1166.5841**	583.7959	389.5332
2043.8554	1022.4316	**13**	**I**	**9**	**1003.5207**	502.2643	335.1788
2140.9081	1070.9580	**14**	**P**	**8**	**890.4367**	445.7222	297.4841
2239.9765	1120.4922	**15**	**V**	**7**	793.3839	397.1959	265.1332
2311.0137	1156.0107	**16**	**A**	**6**	**694.3155**	347.6617	232.1104
2426.0406	1213.5242	**17**	**D**	**5**	623.2784	312.1431	208.4313
2541.0675	1271.0377	**18**	**D**	**4**	508.2514	254.6296	170.0890
2688.1360	1344.5719	**19**	**F**	**3**	393.2245	197.1162	131.7467
2759.1731	1380.0904	**20**	**A**	**2**	246.1561	123.5819	82.7239
		21	**R**	**1**	175.1190	88.0634	59.0449

Figure 2.16. Linear trap quadrupole (LTQ) mass spectral analysis of trypsin digests of *Np* cADO after reaction with **6**. **A**. Mass spectrum of the peptide fragment IECFAIAAYNIYIPVADDFAR. **B**. Peptide ions with different charges. Presence of b5++ and y19+++ ions is consistent with F107 residue of *Np* cAD modified with the hydrocarbon chain.

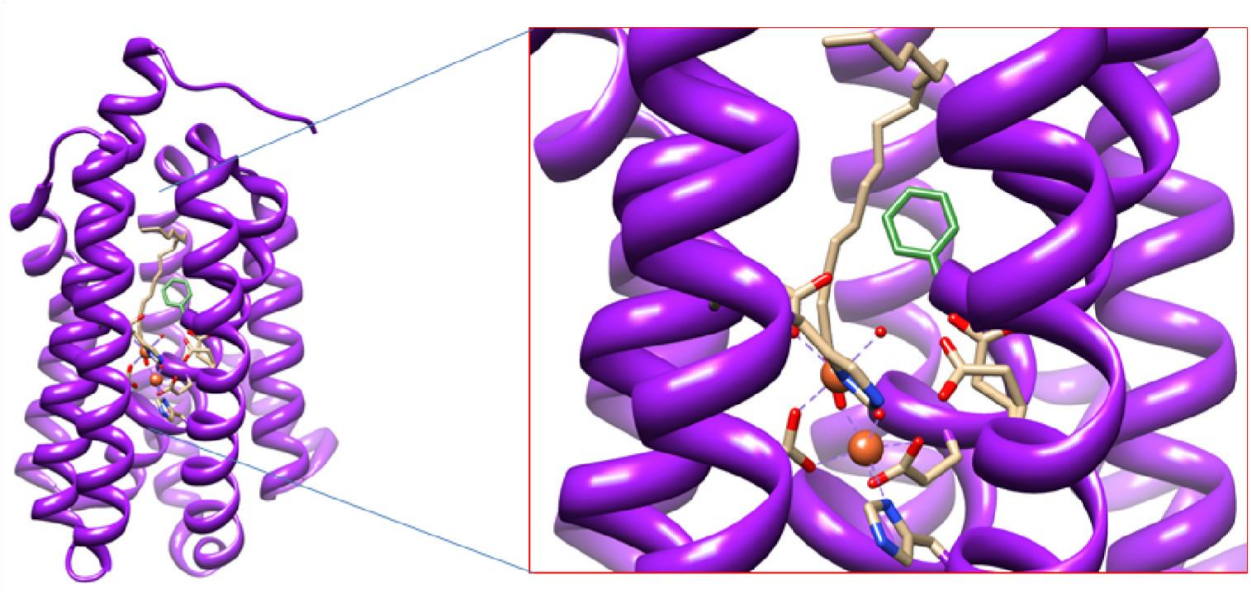

Figure 2.17. Crystal structure of cADO from *Prochlorococcus marinus* MIT9313 (PDB ID 2OC5A) showing di-iron active site and co-crystalized long chain fatty acid. The phenylalanine residue as shown in green most likely undergoes covalent modification after incubation of cADO with cyclopropyl aldehyde **6**.

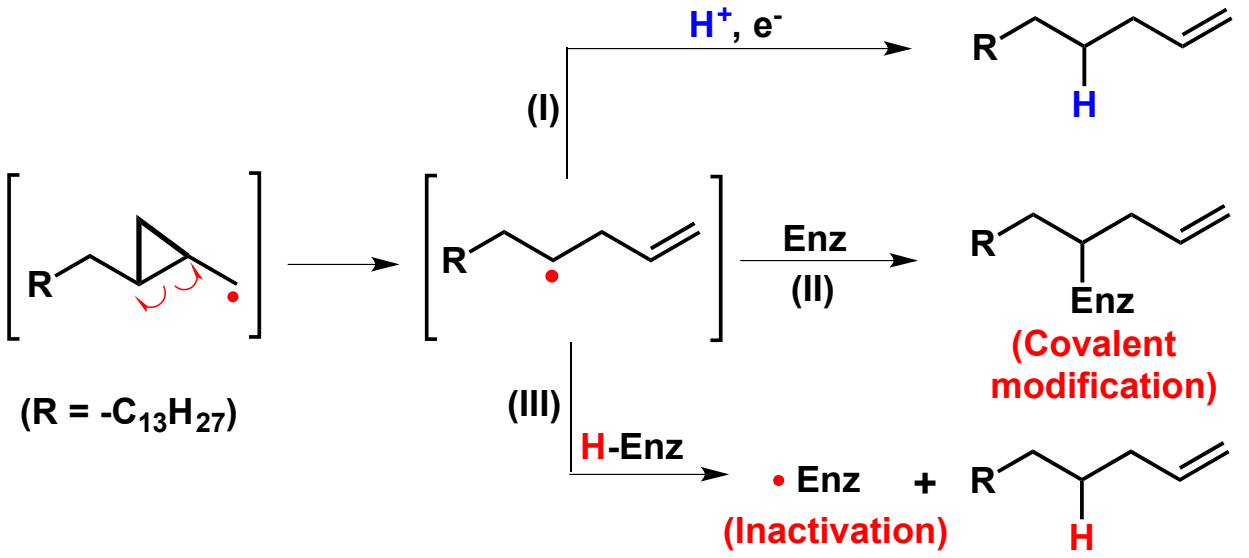

Figure 2.18. Alternate pathways for reaction of 6 with cADO. Pathway I details formation of soluble 1-octadecene. Pathway II shows inactivation of cADO by covalent modification, while pathway III shows a possible explanation for inactive enzyme lacking a covalent modification.

2.3.5 Proposed Mechanism of Inactivation

Although **6** completely inactivated cADO, a significant fraction of the protein escaped covalent modification by **6** (Figure 2.13B), suggesting that another inactivation mechanism might be operating. Further insights into the mechanism of inactivation came from deuterium labeling experiments. We previously determined that for the decarbonylation of octadecanal, the proton in heptadecane is derived from the solvent.[13] However, the rearrangement of the cyclopropylcarbinyl radical derived from **6** would place the presumed radical intermediate at C-4, rather than at C-1, of the product (Figure 2.18). We were therefore interested to know whether the new hydrogen in 1-octadecene was derived from the solvent or some other source. To avoid complications arising from exchange of aldehyde proton during the deuterium labeling experiment, we prepared **6** in which the α-carbon was di-deuterated. When di-deuterated **6** was reacted with cADO in deuterated buffer the predominant molecular ion for 1-octadecene had *m/z* = 255.3 (Figure 2.19), corresponding to tri-deuterated 1-octadecene. This is consistent with the proton coming from the solvent or a solvent-exchangeable group on the enzyme.

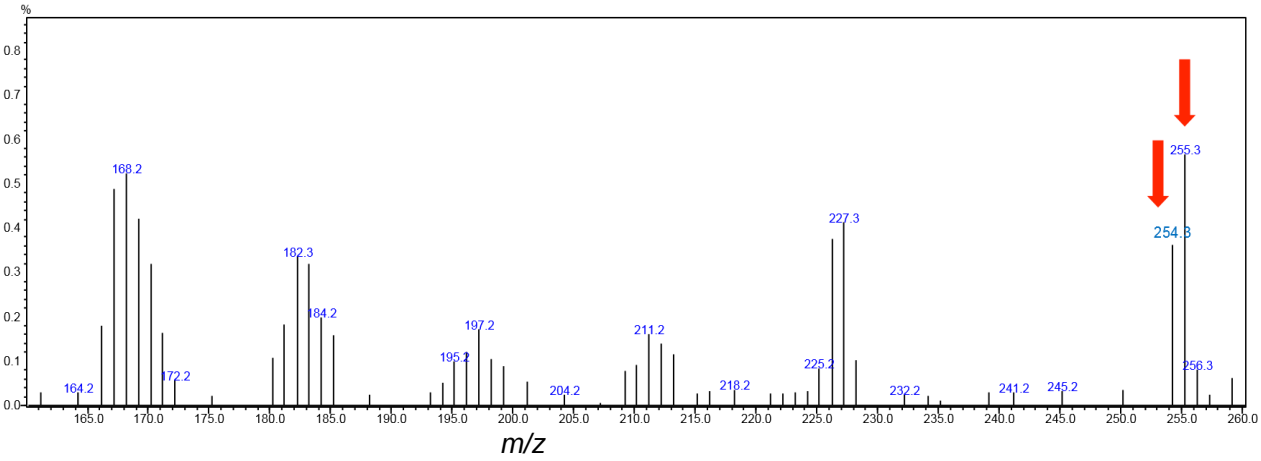

Figure 2.19. A section of mass spectrum of enzymatically obtained product from dideuterated **6** in deuterated buffer, showing a more intense tri-deuterated 1-octadecene molecular ion peak of *m/z* 255.3 and a less intense peak of di-deuterated 1-octadecene of molecular ion peak of *m/z* 254.3. The peak of *m/z* = 254.3 was derived from nonexchangeable protons presumably from the side chains of the protein.

However, a less abundant but still significant peak at *m/z* = 254.3 was also observed, corresponding to di-deuterated 1-octadecene (Figure 2.19). This suggests that some protons may derive from a non-exchangeable position on the protein. (Some protium may also come from the 1 – 2 % of protium remaining in the buffer, but it seems unlikely that this would account for all the di-deuterated product). Abstraction of hydrogen from a non-acidic side-chain by the alkyl radical derived from **6** would certainly be energetically feasible. Such oxidative damage might plausibly result in inactivation of the enzyme. This may provide an alternative pathway for the inactivation of cADO by **6** that does not involve in the formation of a covalent adduct between the protein and substrate (Figure 2.18, pathway III).

2.4 Conclusions

In conclusion, these experiments provide support for a radical mechanism for C-C bond scission in the unusual decarbonylation reaction catalyzed by cADO. In order to

investigate the nature of the C1-C2 bond scission catalyzed by cADO, a radical clock substrate analogue containing a β-cyclopropyl functionality was synthesized and reacted with the enzyme. Incubation of the substrate with cADO resulted in the formation of 1-octadecene as the sole enzyme-mediated product. Based on the well-documented lifetimes for the ring-opening of cyclopropylcarbinyl radicals, the reaction of cADO with **6** supports the formation of a relatively long-lived radical, i.e. one with a lifetime greater than 10 ns, on the α-carbon during the reaction. Unexpectedly, the reaction seemed to be limited to a single turnover.

Investigation of the reaction using sequential incubation with the cyclopropyl substrate or a pentadecanal control, followed by octadecanal, revealed the inhibitory nature of **6**. Further studies elucidated that the complete loss of enzymatic activity was accompanied by the covalent modification of 60-80% of the enzyme by a ~251 Da adduct, corresponding to decarbonylated **6**. In order to identify the site of modification, cADO (purified and modified) was digested with trypsin and Glu-C and analyzed by MALDI-TOF. The loss of a peptide fragment in the modified enzyme samples was noted, corresponding to a portion of the 4-helix bundle forming the hydrophobic substrate binding channel of cADO.

In an attempt to narrow down the specific residue modified by the cyclopropyl substrate, the aforementioned digests were submitted for proteomics analysis by tandem mass spectrometry. This work identified Phe107 as the likely site of modification by decarbonylated **6**. To further understand the mechanism of cADO inactivation by **6**, di-deuterated substrate was prepared and reacted in deuterated buffer. The primary product thereof was tri-deuterated alkane, though some di-deuterated product remained. This

indicated that while most product resulted from abstraction of a deuterium from solvent or a solvent-exchangeable sidechain, some product resulted from abstraction of hydrogrens from non-exchangeable sites in the enzyme, likely leading to the mechanism of inactivation proposed in Figure 2.18. The opening of the cyclopropyl ring results in the migration of the radical initially generated at C-1 of the product to C-4. The shift in the position of the radical appears to cause the reaction to partition between completing the catalytic cycle, i.e. producing 1-octadecene as product, and reacting with the protein to inactivate cADO.

2.5 References

1. Aarts, M. G. M.; Keijzer, C. J.; Stiekema, W. J.; Pereira, A., Molecular characterization of the CER1 gene of arabidopsis involved in epicuticular wax biosynthesis and pollen fertility. *Plant Cell* **1995,** *7* (12), 2115-2127.

2. (a) Cheesbrough, T. M.; Kolattukudy, P. E., Microsomal preparation from an animal tissue catalyzes release of carbon monoxide from a fatty aldehyde to generate an alkane. *J. Biol. Chem.* **1988,** *263* (6), 2738-43; (b) Reed, J. R.; Vanderwel, D.; Choi, S. W.; Pomonis, J. G.; Reitz, R. C.; Blomquist, G. J., Unusual mechanism of hydrocarbon formation in the housefly -cytochrome-P450 converts aldehyde to the sex-pheromone component (Z)-9-tricosene and CO_2. *Proc. Natl. Acad. Sci. U. S. A.* **1994,** *91* (21), 10000-10004.

3. (a) Schirmer, A.; Rude, M. A.; Li, X. Z.; Popova, E.; del Cardayre, S. B., Microbial Biosynthesis of Alkanes. *Science* **2010,** *329* (5991), 559-562; (b) Ladygina, N.; Dedyukhina, E. G.; Vainshtein, M. B., A review on microbial synthesis of hydrocarbons. *Process Biochem. (Amsterdam, Neth.)* **2006,** *41* (5), 1001-1014.

4. Kunst, L.; Samuels, A. L., Biosynthesis and secretion of plant cuticular wax. *Prog. Lipid Res.* **2003,** *42* (1), 51-80.

5. (a) Bourdenx, B.; Bernard, A.; Domergue, F.; Pascal, S.; Leger, A.; Roby, D.; Pervent, M.; Vile, D.; Haslam, R. P.; Napier, J. A.; Lessire, R.; Joubes, J., Overexpression of Arabidopsis ECERIFERUM1 Promotes Wax Very-Long-Chain Alkane Biosynthesis and Influences Plant Response to Biotic and Abiotic Stresses. *Plant Physiol.* **2011,** *156* (1), 29-45; (b) Rowland, O.; Zheng, H. Q.; Hepworth, S. R.; Lam, P.; Jetter, R.; Kunst, L., CER4 encodes an alcohol-forming fatty acyl-coenzyme A reductase involved in cuticular wax production in Arabidopsis. *Plant Physiol.* **2006,** *142* (3), 866-877; (c) Wang, X.; Kolattukudy, P. E., Solubilization and purification of aldehyde-generating fatty acyl-CoA reductase from green alga Botryococcus braunii. *FEBS Lett.* **1995,** *370* (1), 15-18.

6. Cheesbrough, T. M.; Kolattukudy, P. E., Alkane biosynthesis by decarbonylation of aldehydes catalyzed by a particulate preparation from Pisum sativum. *Proc. Natl. Acad. Sci. U. S. A.* **1984,** *81* (21), 6613-6617.

7. (a) Ghim, C. M.; Kim, T.; Mitchell, R. J.; Lee, S. K., Synthetic Biology for Biofuels: Building Designer Microbes from the Scratch. *Biotechnol. Bioprocess Eng.* **2010,** *15* (1), 11-21; (b) Somerville, C.; Youngs, H.; Taylor, C.; Davis, S. C.; Long, S. P., Feedstocks for Lignocellulosic Biofuels. *Science* **2010,** *329* (5993), 790-792; (c) Rude, M. A.; Schirmer, A., New microbial fuels: a biotech perspective. *Curr. Opin. Microbiol.* **2009,** *12* (3), 274-281.

8. Buist, P. H., Exotic biomodification of fatty acids. *Nat. Prod. Rep.* **2007,** *24*, 1110-1127.

9. Qui, Y.; Tittiger, C.; Wicker-Thomas, C.; Le Goff, G.; Young, S.; Wajnberg, E.; Fricaux, T.; Taquet, N.; Blomquist, G. J.; Feyereisen, R., An insect-specific P450 oxidative decarbonylase for cuticular hydrocarbon biosynthesis. *Proc. Natl. Acad. Sci. (USA)* **2012,** *109*, 14858 - 14863.

10. Dennis, M.; Kolattukudy, P. E., A Cobalt-Porphyrin Enzyme Converts a Fatty Aldehyde to a Hydrocarbon and Co. *Proc. Natl. Acad. Sci. U. S. A.* **1992,** *89* (12), 5306-5310.

11. Unpublished, *structure solved by Joint Center of Structural Genomics (protein database entry PDB|2OC5|A)*.

12. Feig, A. L.; Lippard, S. J., Reactions of non-heme iron(II) centers with dioxygen in biology and chemistry. *Chem. Rev.* **1994,** *94* (3), 759-805.

13. Das, D.; Eser, B. E.; Han, J.; Sciore, A.; Marsh, E. N. G., Oxygen-Independent Decarbonylation of Aldehydes by Cyanobacterial Aldehyde Decarbonylase: A New Reaction of Diiron Enzymes. *Angew. Chem. Intl. Ed.* **2011,** *50* (31), 7148-7152.

14. Warui, D. M.; Li, N.; N√∏rgaard, H.; Krebs, C.; Bollinger, J. M.; Booker, S. J., Detection of Formate, Rather than Carbon Monoxide, As the Stoichiometric Coproduct in Conversion of Fatty Aldehydes to Alkanes by a Cyanobacterial Aldehyde Decarbonylase. *J. Am. Chem. Soc.* **2011,** *133* (10), 3316-3319.

15. (a) Li, N.; Norgaard, H.; Warui, D. M.; Booker, S. J.; Krebs, C.; Bollinger, J. M., Conversion of fatty aldehydes to alka(e)nes and foramte by a cyanobacterial aldehyde decarbonylase: crypric redox by an unusual dimetal oxygenase. *J. Am. Chem. Soc.* **2011,** *133*, 7148-7152; (b) Li, N.; Chang, W.-C.; Warui, D. M.; Booker, S. J.; Krebs, C.; Bollinger, J. M., Evidence for Only Oxygenative Cleavage of Aldehydes to Alk(a/e)nes and Formate by Cyanobacterial "Aldehyde Decarbonylase". *Biochemistry* **2012,** *ASAP*.

16. Newcomb, M.; Toy, P. H., Hypersensitive radical probes and the mechanisms of cytochrome P450-catalyzed hydroxylation reactions. *Acc. Chem. Res.* **2000,** *33* (7), 449-455.

17. Bowry, V. W.; Ingold, K. U., A Radical Clock Investigation of Microsomal Cytochrome-P-450 Hydroxylation of Hydrocarbons - Rate of Oxygen Rebound. *J. Am. Chem. Soc.* **1991,** *113* (15), 5699-5707.

18. Valentine, A. M.; LeTadic-Biadatti, M. H.; Toy, P. H.; Newcomb, M.; Lippard, S. J., Oxidation of ultrafast radical clock substrate probes by the soluble methane monooxygenase from Methylococcus capsulatus (Bath). *J. Biol. Chem.* **1999,** *274* (16), 10771-10776.

19. Baldwin, J. E.; Adlington, R. M.; Domaynehayman, B. P.; Knight, G.; Ting, H. H., USE OF THE CYCLOPROPYLCARBINYL TEST TO DETECT A RADICAL-LIKE

INTERMEDIATE IN PENICILLIN BIOSYNTHESIS. *Journal of the Chemical Society-Chemical Communications* **1987,** (21), 1661-1663.

20. Huang, H.; Chang, W.-C.; Pai, P. J.; Romo, A.; Mansoorabadi, S. O.; Russell, D. H.; Liu, H.-w., Evidence for Radical-Mediated Catalysis by HppE: A Study Using Cyclopropyl and Methylenecyclopropyl Substrate Analogues. *J. Am. Che. Soc.* **2012,** *ASAP*.

21. Schlosser, M.; Christmann, K. F., Trans-Selective Olefin Syntheses. *Angew. Chem. Intl. Ed* **1966,** *5* (1), 126-126.

22. (a) Furukawa, J.; Kawabata, N.; Nishimura, J., Synthesis of cyclopropanes by the reaction of olefins with dialkylzinc and methylene iodide. *Tetrahedron* **1968,** *24* (1), 53-58; (b) Lebel, H. l. n.; Marcoux, J.-F. o.; Molinaro, C.; Charette, A. B., Stereoselective Cyclopropanation Reactions. *Chem. Rev.* **2003,** *103* (4), 977-1050.

23. De Mico, A.; Margarita, R.; Parlanti, L.; Vescovi, A.; Piancatelli, G., A Versatile and Highly Selective Hypervalent Iodine (III)/2,2,6,6-Tetramethyl-1-piperidinyloxyl-Mediated Oxidation of Alcohols to Carbonyl Compounds. *J. Org. Chem* **1997,** *62* (20), 6974-6977.

24. Eser, B. E.; Das, D.; Han, J.; Jones, P. R.; Marsh, E. N., Oxygen-independent alkane formation by non-heme iron-dependent cyanobacterial aldehyde decarbonylase: investigation of kinetics and requirement for an external electron donor. *Biochemistry* **2011,** *50* (49), 10743-50.

25. Bowry, V. W.; Lusztyk, J.; Ingold, K. U., Calibration of a New Horologery of Fast Radical Clocks - Ring-Opening Rates for Ring-Alkyl-Substituted and Alpha-Alkyl-Substituted Cyclopropylcarbinyl Radicals and for the Bicyclo[2.1.0]Pent-2-Yl Radical. *J. Am. Chem. Soc.* **1991,** *113* (15), 5687-5698.

26. Souda, P.; Ryan, C. M.; Cramer, W. A.; Whitelegge, J., Profiling of integral membrane proteins and their post translational modifications using high-resolution mass spectrometry. *Methods* **2011,** *55* (4), 330-336.

27. Cao, F.; Chen, Y.; Cierpicki, T.; Liu, Y.; Basrur, V.; Lei, M.; Dou, Y., An Ash2L/RbBP5 Heterodimer Stimulates the MLL1 Methyltransferase Activity through Coordinated Substrate Interactions with the MLL1 SET Domain. *PLoS One* **2010,** *5* (11), e14102.

Chapter 3

Mechanistic Insights from Reaction of α-Oxiranyl-Aldehydes with Cyanobacterial Aldehyde Deformylating Oxygenase

The work described in this chapter was performed in collaboration with Dr. Debasis Das, who performed kinetic analyses of substrate reactivities, and Dr. Bishwajit Paul, who synthesized the substrate analogues and corresponding product standards. It has been published in the *American Chemical Society Chemical Biology,* **2013**, *9*, 570-577.

3.1 Introduction

Following my work with the cyclopropyl species, a study by the Bollinger Laboratory utilized stopped-flow U.V.-visible spectroscopy and rapid quench Mossbauer spectroscopy to provide evidence in support of the formation of a Fe^{III}/Fe^{III} peroxide or peroxy-semialdehyde species in cADO.[1] This species was relatively stable, t½ ~ 400 s at 5 ºC, but once additional electrons in the form of reduced O-methoxy-phenazine methosulfate were added it rapidly decayed. The proposed catalytic mechanism for cADO was altered to fit these findings, and proceeds according to the mechanism shown in Figure 3.1B.[2,3] Evidence for a radical mechanism for C – C bond scission was provided through my studies of cADO with the β-substituted cyclopropyl aldehyde radical clock as described in chapter 2. Ring-opening of the cyclopropyl ring was

observed, consistent with homolytic cleavage of the formyl group.[4] Though a lower limit for the formed radical was derived, a more accurate measurement of the lifetime of the radical formed as a result of homolytic cleavage was needed to flesh out the catalytic mechanism of cADO. Also of note are recent experimental observations of oxidative products arising from the reaction of cADO with medium-chain aldehydes, which led to a conflicting mechanistic proposal involving heterolytic C-C bond scission (Figure 3.1C). In order to address these disparities and more accurately measure the aforementioned radical lifetime, an alternative functionality was explored.

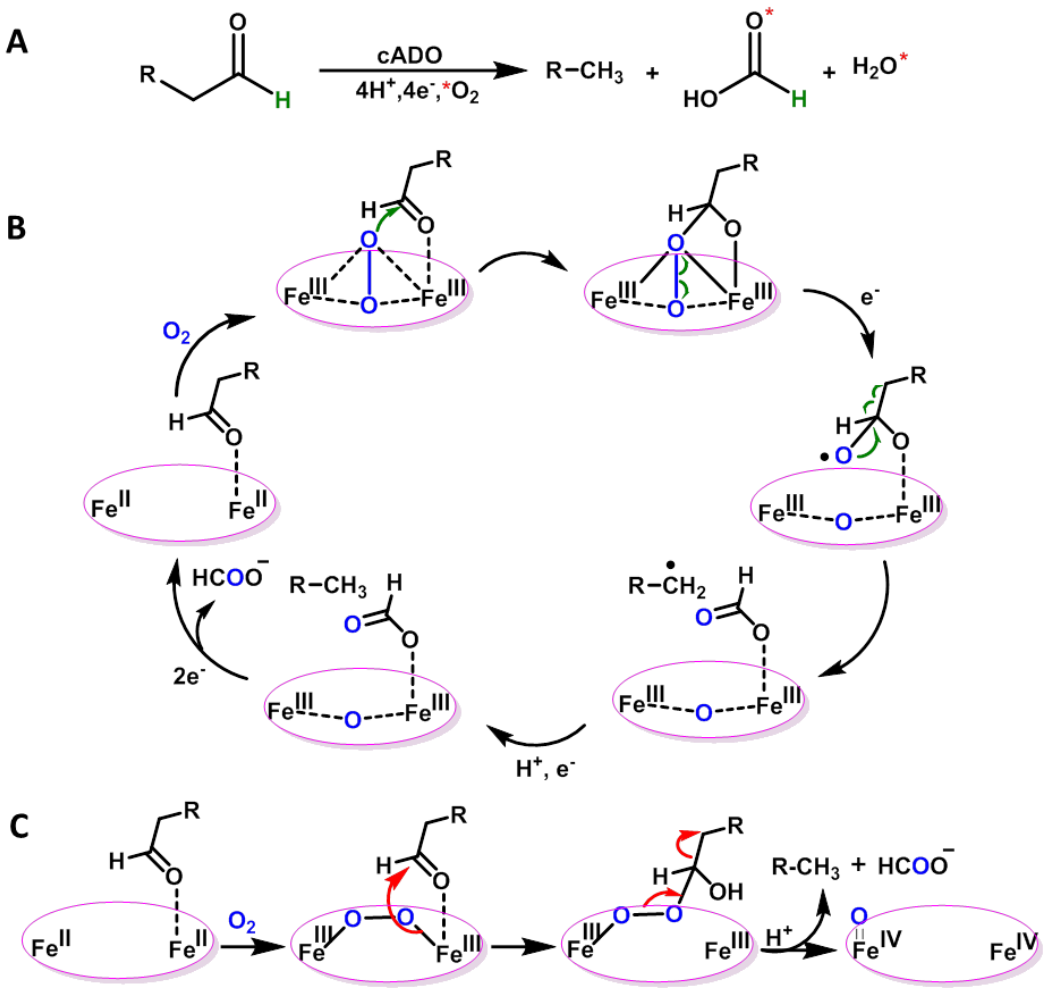

Figure 3.1. A. Deformylation reaction catalyzed by cADO. B. Proposed mechanism of cADO involving homolytic cleavage of the C1-C2 bond of aldehyde by di-iron peroxo species. C. A recently proposed mechanism for deformylation involving heterolytic cleavage of the C1-C2 bond.

The substrate-binding site of cADO comprises a narrow hydrophobic channel that terminates at the metal center.[5] The scope for substrate modification is, therefore, limited by steric constraints. However, examination of the structure, as well as the work with β-cyclopropyl additions accomplished in Chapter 2, suggested that aldehydes containing 3-membered rings adjacent to the aldehyde carbon could be accommodated with minimal

perturbation of the structure. We therefore synthesized analogs of dodecanal and octadecanal *trans*-3-nonyloxirane-2-carbaldehyde, **1**, and *trans*-3-pentadecanyloxirane-2-carbaldehyde, **2** bearing an oxirane ring adjacent to the aldehyde carbon (Figure 3.2). We reasoned that introducing the oxiranyl functionality at the site of C-C bond scission should provide insights into the mechanism of deformylation by altering the stability of intermediates. The oxiranyl radical has a significantly slower rate of radical ring opening than the cyclopropylcarbinyl species, and the introduction of the 3-membered oxirane ring adjacent to the aldehyde carbon would allow the stereochemistry of proton transfer to be investigated.

Figure 3.2. Structures of *trans*-3-nonyloxirane-2-carbaldehyde, **1**, and *trans*-3-pentadecanyloxirane-2-carbaldehyde, **2** used in these studies.

3.2 Materials and Methods

3.2.1 Materials

Anhydrous solvents such as dichloromethane, n-hexane, ethyl acetate and diethyl ether were used without further distillation. Bases such as DIBAL-H, DBU were used directly from reagent grade bottle. Reactions were monitored by thin-layer chromatography (TLC) with visualization by potassium permanganate ($KMnO_4$) stains and 2,4-dinitrophenyl hydrazine (DNP) stains. All glass-wares were oven-dried before use. Column

chromatography was performed with silica-gel mesh size 100-200 μm (Fisher Scientific, USA). The removal of solvent and other volatile impurities were done under reduced pressure using rotatory evaporator in a water bath of < 37 °C. NMR spectra were measured in $CDCl_3$ at ambient temperature unless otherwise noted. Hexadecane, undecanal, decane were obtained from Sigma-Aldrich. Trans-2-dodecenol, hexadecanal, heptadecanal was obtained from TCI America. Phenazine methosulfate (PMS), ferrous ammonium sulfate from Sigma Aldrich. NADH, 2-Nitrophenylhydrazine, EDC were obtained from Acros Organics. Potassium chloride, HEPES were from Fisher chemicals. D_2O (99.9%) and DMSO-d_6 (99.9%) were from Cambridge Isotope Laboratories, Inc. All other reagents were of the purest grade commercially available and used without further purification.

3.2.2 Synthesis of α-Oxiranyl Aldehydes

The synthesis of *trans*-3-nonyloxirane-2-carbaldehyde, ((*E*)-2,3-epoxydodecanal), **1**, was accomplished by standard methods starting from commercially available (E)-dodec-2-en-1-ol. *Trans*-3-pentadecanyloxirane-2-carbaldehyde, ((*E*)-2,3-epoxyoctadecanal) **2** (Figure 3.2), was accomplished by standard methods utilizing the Horner-Wittig reaction of hexadecanal with ethyl-2-(diethoxylphosphoryl) acetate to obtain the corresponding α-unsaturated carboxylic acid ethyl ester that was subsequently elaborated to **1** and **2**.[4,6] Authentic standards of nonyloxirane and pentadecanyloxirane were synthesized by epoxidation of 1-undecene and 1-pentadecene using metachloroperbenzoic acid.[6] Full details of the synthetic procedures may be found in Appendix B.

3.2.3 Enzyme Assays

The purification of recombinant *N. punctiformes* cADO from *E. coli* was performed as described previously.[4] Assays were performed in 100 mM HEPES buffer, pH 7.2, containing 100 mM KCl and 10% glycerol under microaerobic conditions and employing phenazine methosulfate (PMS) and NADH as the auxiliary reducing system as described previously.[4] Aldehydes substrates were made up as a 10 mM stock solution in DMSO. A typical assay contained 10 µM cADO, 20 µM ferrous ammonium sulfate, 300 µM aldehyde substrate, 100 µM phenazine methosulfate (PMS) and 2 mM NADH in a total volume of 500 µL. Assays were shaken at 37 °C at 200 rpm. Reactions were quenched by addition of 500 µL ethyl acetate and vigorous vortexing, followed by centrifugation at 14000 rpm for 30 min to separate the organic phase. The ethyl acetate layer was collected and 8 µL of sample subjected to GC-MS analysis as described previously.

3.2.4 Formate Determination

Formate was determined to be the co-product of reaction of **1** and **2** with cADO by reaction with 2-Nitrophenylhydrazine, as described previously.[7,4]

3.2.5 Deuterium Incorporation Assays

To investigate deuterium incorporation into alkane products, assays were performed in 100 mM HEPES buffer containing 100 mM KCl in 99.9% D_2O, pD 7.2. Substrates were made up as 10 mM stock solutions in 99.9% DMSO-d6. cADO was added as a concentrated stock solution in non-deuterated buffer such that the final H_2O concentration did not exceed 2%. The enzyme was incubated in the buffer for 1 h prior

to initiating the reaction by addition of substrate. Assays were shaken at 37 °C for 2 h at 200 rpm. Products were extracted and analyzed as described in previous enzyme assays.

3.2.6 Preparation of NMR Samples for Stereospecificity Analysis

Assays were performed as described above except that phosphate buffer was substituted for HEPES buffer which otherwise interfered with the NMR spectra. Assays were carried out either in 10 mM potassium phosphate, pH 7.2, containing 50 mM KCl in H_2O or 10 mM potassium phosphate, pD 7.2, containing 50 mM KCl in D_2O (99.9%). Aldehyde solutions were made up as a stock solution in DMSO or DMSO-d6 for the respective experiments. A typical assay contained 40 μM *Np* cADO, 80 μM ferrous ammonium sulfate, 100 μM PMS, 2 mM NADH and 400 μM substrate in a total volume of 500 μL. For assays performed in deuterated buffer, the final H_2O concentration was ~5% after adding all the assay components. Ten identical 500 μL reactions were set up in each buffer and shaken at 37 °C at 200 rpm for 2 h. The reaction mixtures were sequentially extracted with a total volume of 1 mL $CDCl_3$ (99.9%). The $CDCl_3$ layers were washed with D_2O, dried over sodium sulfate and filtered before analysis by ^1H NMR.

3.3 Results and Discussion

3.3.1 Reaction of 1 and 2 with cADO

Initially Dr. Debasis Das and I examined the activity of **1** under both air-saturated and micro-aerobic conditions and compared its activity with that of dodecanal. Typical assays contained 10 μM cADO, 300 μM substrate, and an auxiliary reducing system

comprising NADH, 2 mM, as the reductant and PMS, 100 μM, the electron mediator, as described previously. Under fully aerobic conditions very little activity was observed with either **1** or dodecanal, most likely because the non-enzymatic reaction of O_2 with reduced PMS depleted the reducing system before significant turn-over could occur. All subsequent experiments were therefore performed micro-aerobically, as described previously. Under micro-aerobic conditions cADO catalyzed the conversion **1** to 2-nonyloxirane and dodecanal to undecane at approximately similar rates (apparent k_{cat} = 0.016 ± 0.001 min^{-1} and 0.01 ± 0.001 min^{-1} respectively). In both cases the reaction was linear for several hours during which time about 3 turnovers occurred (Figure 3.3). Formate was formed as the co-product, as expected (Figure 3.4).

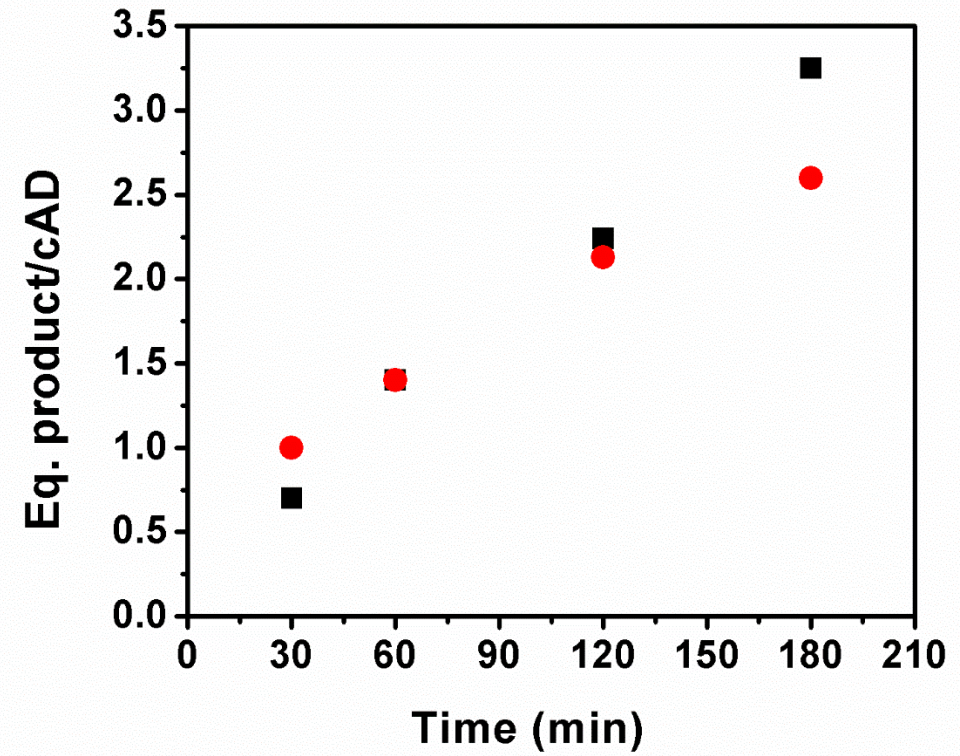

Figure 3.3. Comparison of the rates of deformylation of **1** (■) and dodecanal (●) by cADO.

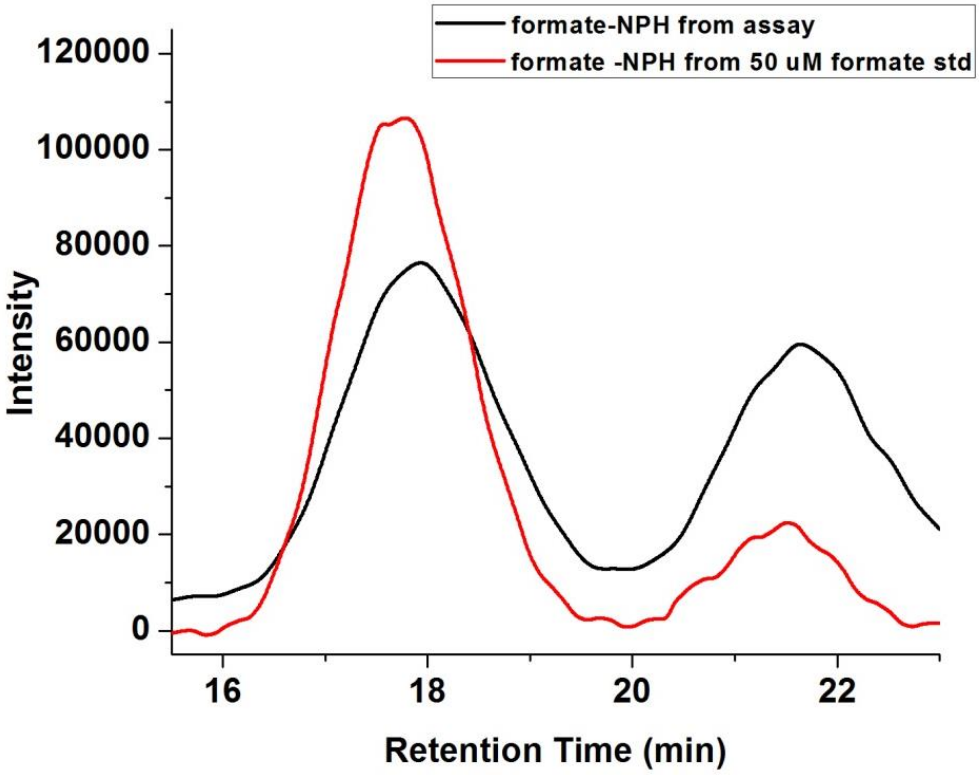

Figure 3.4. Overlaid HPLC traces of formate NPH-derivative from 50 µM standard formate (in red) and the formate-NPH obtained from the formate produced from **2** by *Np* cADO (in black).

The sluggish nature of the cADO reaction has been noted previously in investigations by various laboratories.[8,7,9] A recent study examined the relative rates of reaction of aliphatic aldehydes with chain lengths ranging from 18 to 4 carbons.[10] Interestingly, it was found that the enzyme is more active with either long-chain (C18 – C14) or short-chain (C9 – C5) aldehydes whereas medium chain aldehydes, including dodecanal, were turned over considerably more slowly. Therefore, we were curious whether faster rates of turn-over could be obtained by increasing the chain length of the alkyl-oxiranyl-carbaldehyde. We examined the activity of **2** with cADO and compared it with the "fast" substrate octadecanal. We found that **2** was converted to 2-

pentadecanyloxirane and formate about twice as fast, apparent k_{cat} = 0.029 ± 0.001 min^{-1} as **1** was converted to 2-nonyloxirane, although octadecanal was found to turn over ~ 7-fold faster than dodecanal, in agreement with previous measurements.[11,10]

We were curious whether the slow turnover of **1** and **2** might be due to these compounds inactivating the enzyme, as we previously observed mechanism-based inactivation, resulting in covalent modification of the enzyme, in the reaction of cADO with a β-substituted cyclopropyl aldehyde designed to function as a radical clock.[4] However, LC-ESI-MS analysis of the enzyme after reaction with the oxiranyl aldehydes established that neither **1** nor **2** covalently modified the enzyme (Figure 3.5). Moreover, the time course of the reaction does not show evidence for time-dependent inhibition of the enzyme. The slow reactions of **1** and **2** with cADO therefore appear to be intrinsic to their chemical functionality.

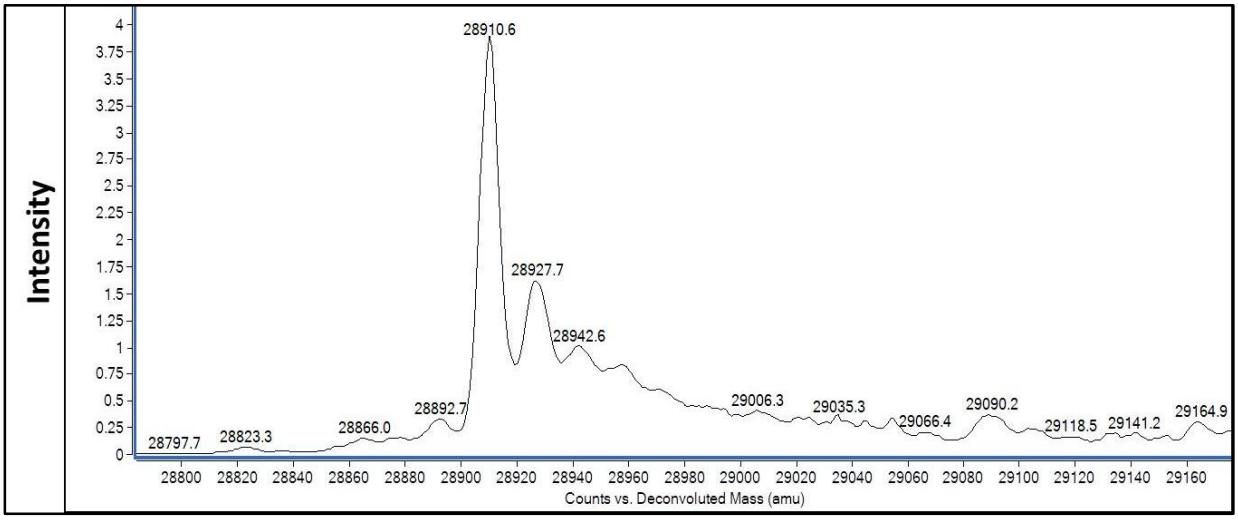

Figure 3.5. Deconvoluted mass spectrum of compound **2** treated *Np* cADO. The calculated Mr = 28910.6 is identical to that of the recombinant enzyme as isolated from *E. coli*.

3.3.2 Stereochemistry of proton transfer

Previous studies have established that the proton in the product alkane derives from the solvent in the cADO-catalyzed reaction;[8,7] this is in contrast to the decarbonylation reactions catalyzed by the insect and plant enzymes in which the aldehyde hydrogen is transferred to the alkane.[12,13] However, the stereochemistry of this step has not been determined for any of these enzymes. I took advantage of the oxirane ring generated by the reaction of **1** with cADO to examine the stereochemistry of proton transfer. Reactions were stepped up containing 40 μM cADO, 400 μM **1**, 2 mM NADH and 100 μM PMS in 10 mM potassium phosphate buffer, pH/pD 7.2 in either H_2O or D_2O. After 2 h incubation at 37 °C the products of the reaction, together with unreacted substrate, were extracted with $CDCl_3$, dried and their ^1H NMR spectra recorded.

The oxirane protons (Figure 3.6A) are clearly separated from other resonances and comprise a broad multiple due to H_a, δ = 2.89 ppm, (J_1 = 3.22, J_2 = 5.83 Hz) and overlapping doublet-of-doublets due to H_b, δ = 2.73 ppm, (J_1 = 3.90, J_2 = 5.08 Hz) and a doublet-of-doublets due to H_c, δ = 2.45 ppm, (J_1 = 2.75 Hz; J_2 = 5.07 Hz). For the reaction performed in H_2O, integration of H_a, H_b and H_c reveals, as expected, equal intensities for all 3 protons (Figure 3.6B). For the reaction performed in D_2O, however both H_b and H_c are equally reduced in intensity to 0.63 relative to H_a (Figure 3.6C), indicating that the deuteron can be transferred with equal probability to either face of the oxirane ring. It is evident that the intensities of H_b and H_c are not reduced to the theoretical value of 0.50. We attribute this to residual protons in the D_2O buffer, which are estimated to comprise ~ 5 % of the solvent. Proton incorporation is most likely enhanced by a solvent kinetic isotope effect.

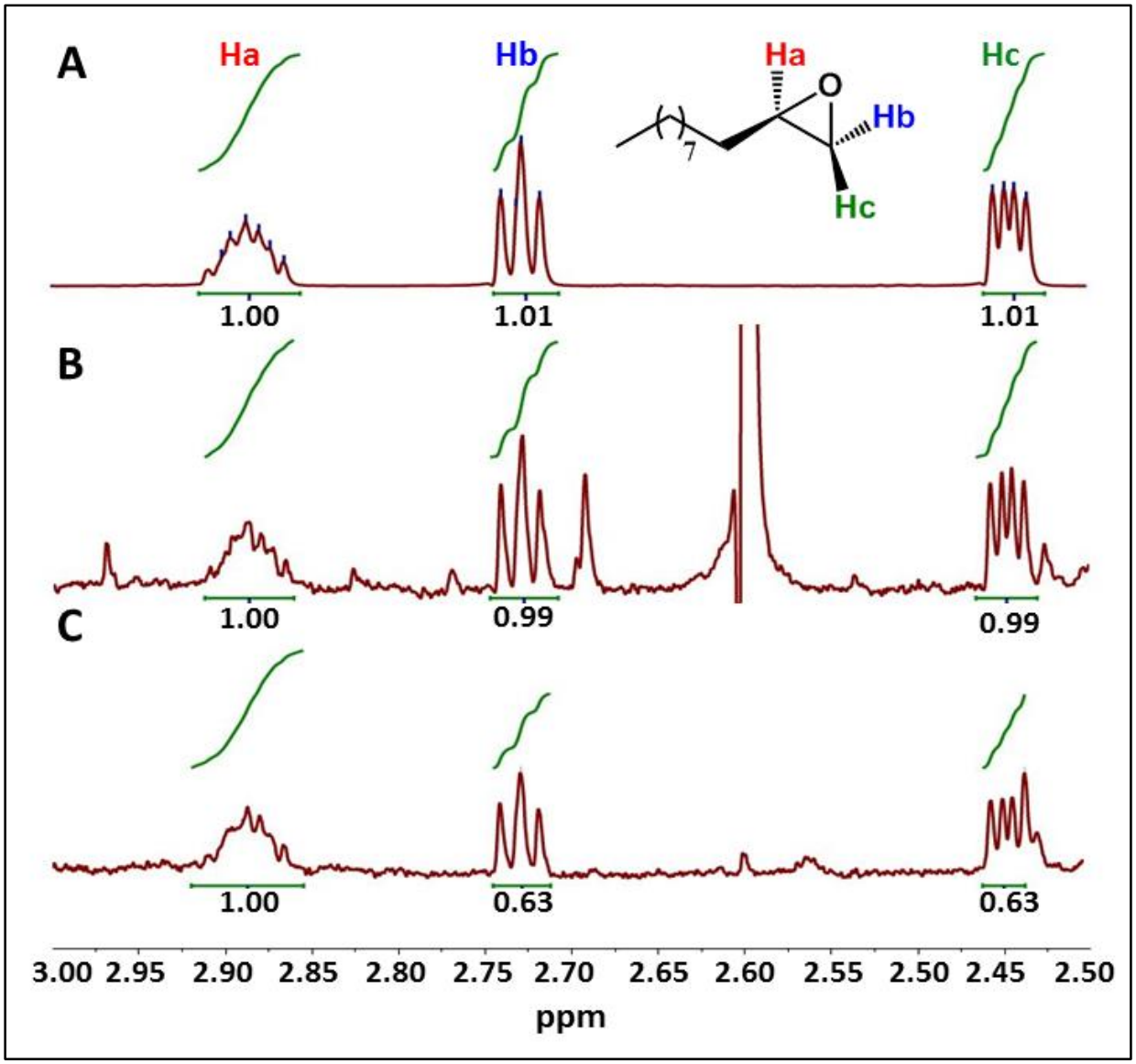

Figure 3.6. Stereochemistry of proton addition to 2-nonyloxirane. ^{1}H-NMR spectra of the oxirane ring protons H_a, H_b and H_c are shown. **A**: an authentic standard of racemic 2-nonyloxirane (for clarity the structure of the (R)-enantiomer is drawn); B: products of the reaction of **1** with cADO in H_2O; C: products of the reaction of **1** with cADO in D_2O. In each case integrations are relative to H_a.

This observation provides evidence for the existence of an intermediate species, most likely the 3-nonyloxiran-2-yl radical that is able to undergo rapid rotation about the

C – C bond to the alkyl group before delivery of the solvent-derived proton. Oxiranyl radicals are known to be pyramidal at the carbon center,[14] indicating little or no delocalization of the radical onto the oxygen, and undergo rapid inter-conversion between *cis*- and *trans*- forms. For un-substituted oxiranyl radicals the rate of inter-conversion is especially fast, ~10^7 s^{-1} at –110 ºC.[15] Thus, the observed stereochemical scrambling of deuterium indicates that inter-conversion between *cis*- and *trans*- radicals occurs much faster than proton delivery to form the product.

3.3.3 Evidence for Rearrangement of Oxiranyl Radical Intermediates

During the course of our investigations we consistently noticed small amounts of decane (Figure 3.7A) and hexadecane (Figure 3.7B) in the products of the reaction of **1** and **2** respectively with cADO. Further investigations established that the appearance of these products was linearly dependent on enzyme concentration, and that they were formed in direct proportion to the major 2-alkyloxirane products (Figure 3.7B *inset*). Furthermore, the appearance of these n-2 alkanes was dependent on the presence of all the components in the assay, including the substrates (Figure 3.8 and 3.9). These observations suggested that they were derived from reaction of the oxiranyl-aldehydes with the enzyme. The reaction products were confirmed by GCMS using authentic standards, as shown in Figure 3.13 and 3.14.

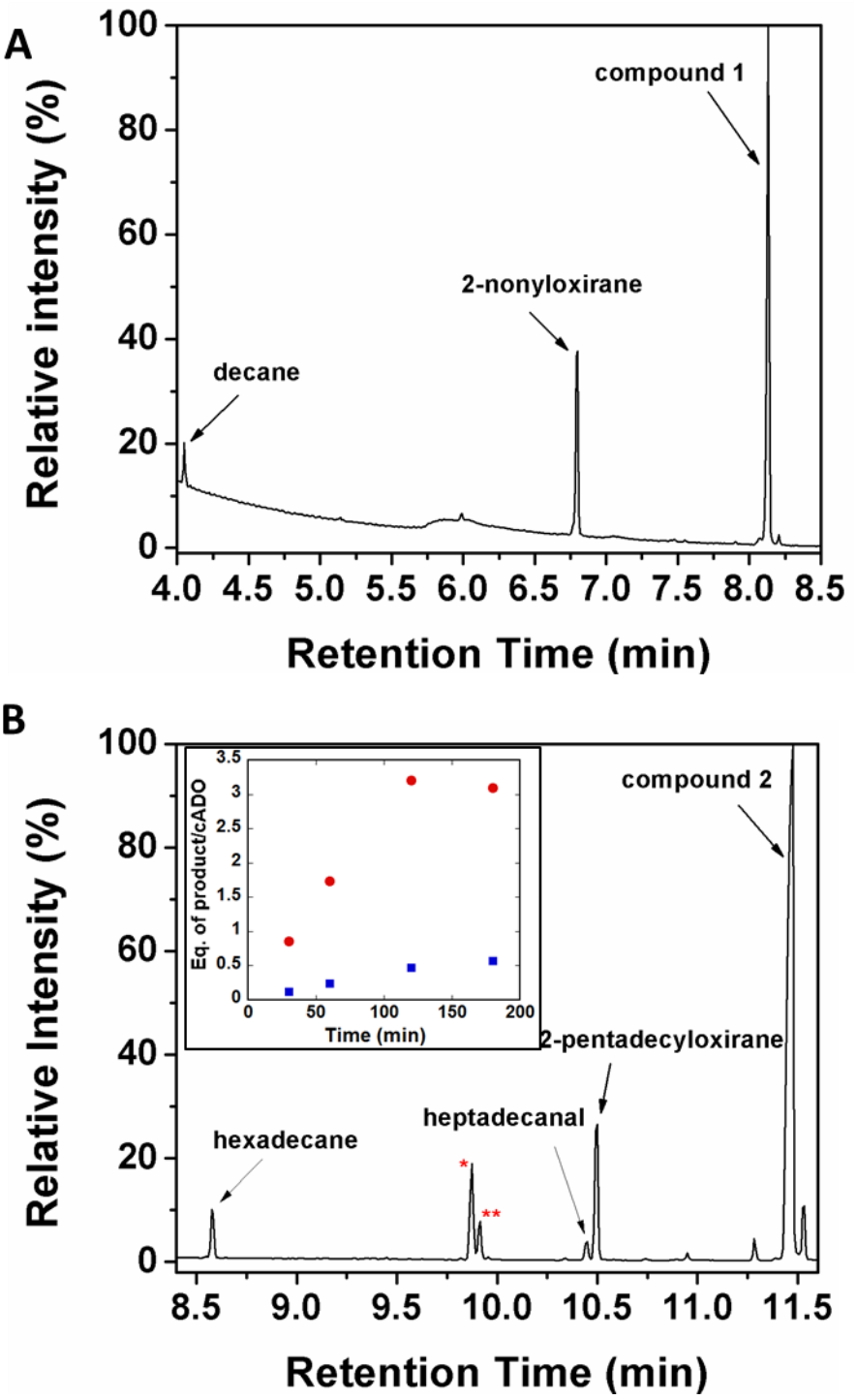

Figure 3.7. Formation of n-2 alkanes from **1** and **2** by cADO. **A**: GC-MS chromatograph of the products of reaction of **1** with cADO. **B**: GC-MS traces of the products of reaction of **2** with cADO; in this case small amounts of enzymatically-derived heptadecanal are resolved in the chromatograph. *Inset:* comparison of the rates of formation of 2-pentadecyloxirane (●) and hexadecane (■) from **2**. Peaks identified by * and ** are contaminants.

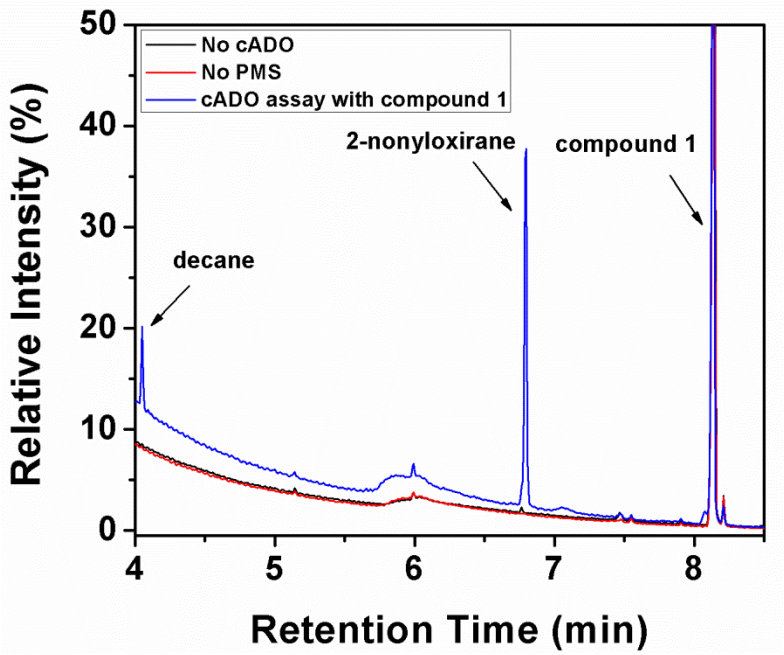

Figure 3.8. Overlaid chromatographs of conversion of **1** to 2-nonyloxirane by *Np* cADO and the control experiments where *Np* cADO or PMS were omitted.

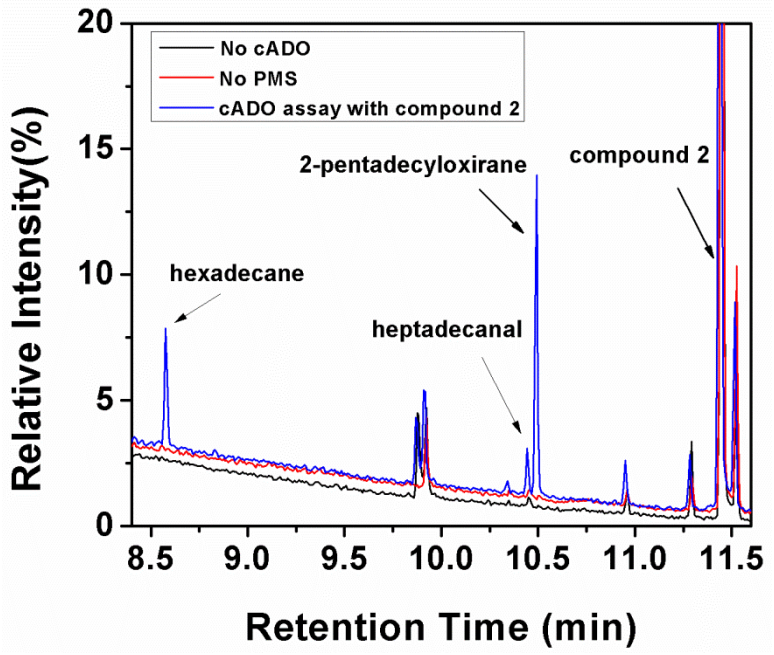

Figure 3.9. Overlaid chromatographs of conversion of **2** to 2-pentadecyloxirane by *Np* cADO and the control experiments where *Np* cADO or PMS were omitted.

Oxirane rings can be rearranged to carbonyl compounds by Lewis acid catalysts.[16] We therefore considered the possibility that the diferric form of cADO might catalyze the rearrangement of 2-nonyloxirane and 2-pentadecanyloxirane to undecanal and heptadecanal, respectively, which would then undergo deformylation to decane and hexadecane. However, no alkanes were formed when either 2-nonyloxirane or 2-pentadecanyloxirane (Figure 3.10) were incubated with the diferric enzyme alone. Neither was rearrangement of these compounds observed when they were incubated with the enzyme with the other components of the assay for prolonged periods.

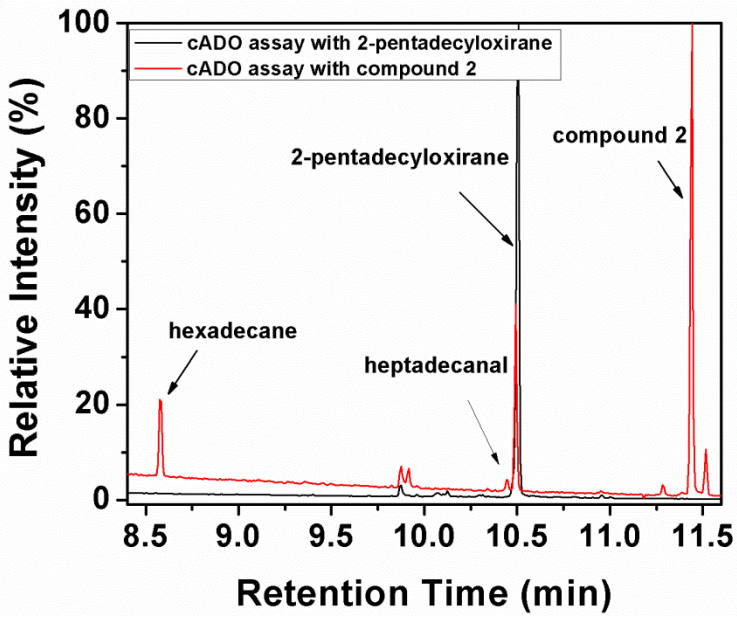

Figure 3.10. Overlaid chromatographs of *Np* cADO assay with 2-pentadecyloxirane and *Np* cADO assay with compound **2**.

These observations suggest that the n-2 alkanes most likely arise through partitioning of an intermediate formed in the deformylation of **1** and **2** by cADO between two reaction pathways. To explain the formation of the n-2 alkanes we considered a

variant of the deformylation mechanism in which after homolytic cleavage of the C_α-CO bond to form the 3-alkyloxiran-2-yl radical and formate, ring-opening of this radical occurs to generate the C_α radical of the n-1 aldehyde. Quenching of this radical would thus generate the n-1 aldehyde that could subsequently undergo deformylation (Figure 3.11). Ring-opening reactions of alkyloxiranyl radicals are well documented in the literature.[15,17]

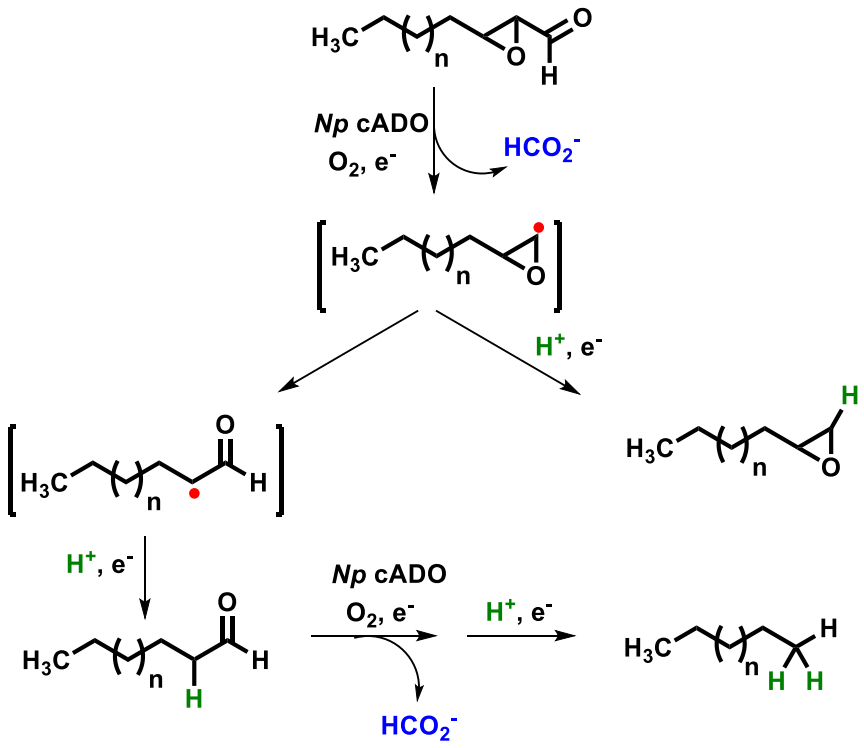

Figure 3.11. Mechanism for the conversion of oxiranyl aldehydes to C_{n-1} oxiranes and C_{n-2} alkanes involving a branched pathway that arises through the slow rearrangement of an oxiranyl radical intermediate.

This mechanism predicts that n-1 aldehydes should be formed as intermediates. Close examination of the gas chromatograph for the reaction of **2** with cADO revealed the presence of a minor peak at 10.46 min that eluted just before 2-pentadecanyloxirane (Figure 3.7B). The intensity of the peak increased with time during the course of the

reaction (Figure 3.12) and was dependent upon all the components of the assay being present. The mass spectrum of the compound matched that of heptadecanal and the peak co-eluted with an authentic standard of heptadecanal (Figure 3.13). It was similarly possible to detect the formation of undecanal in the reaction products formed through the reaction with cADO with **1**, although in this case it was necessary to modify the chromatography conditions to separate undecanal from 2-nonyloxirane (Figure 3.14).

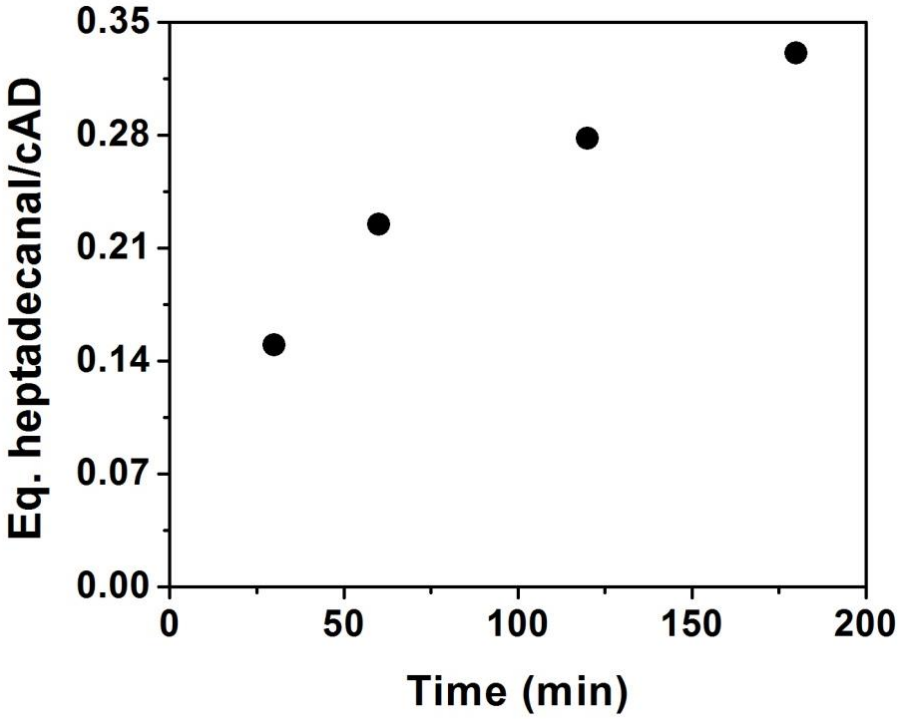

Figure 3.12. A time course of accumulation of heptadecanal in the reaction of *Np* cADO with **2.**

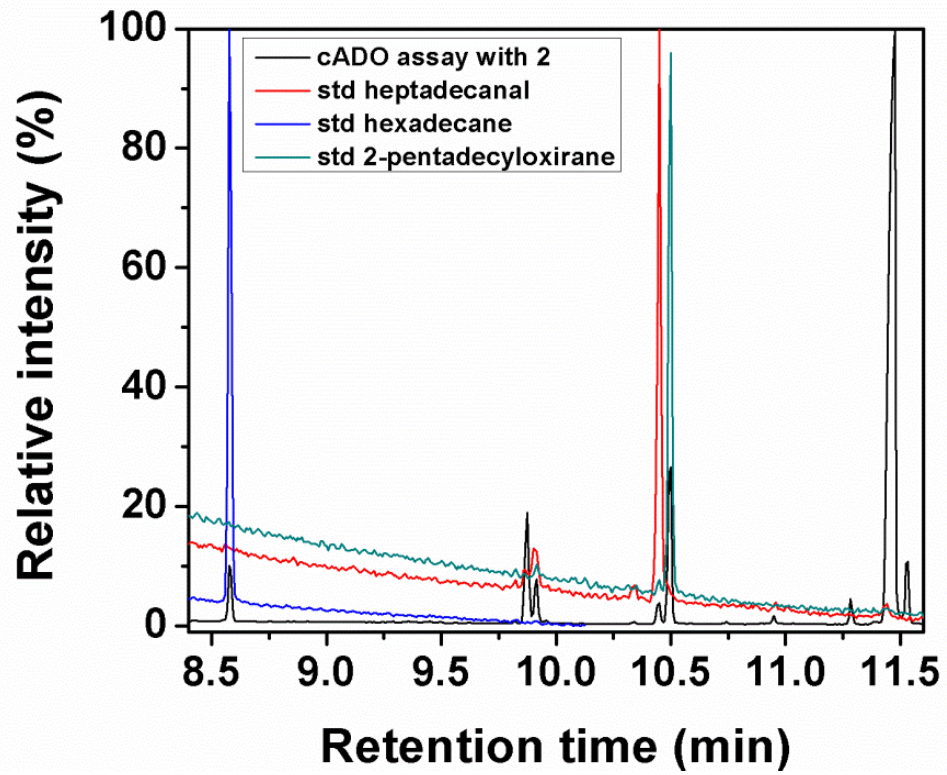

Figure 3.13. Overlaid chromatographs of reaction of **2** with *Np* cADO with standard samples of heptadecanal, hexadecane and compound 2-pentadecyloxirane.

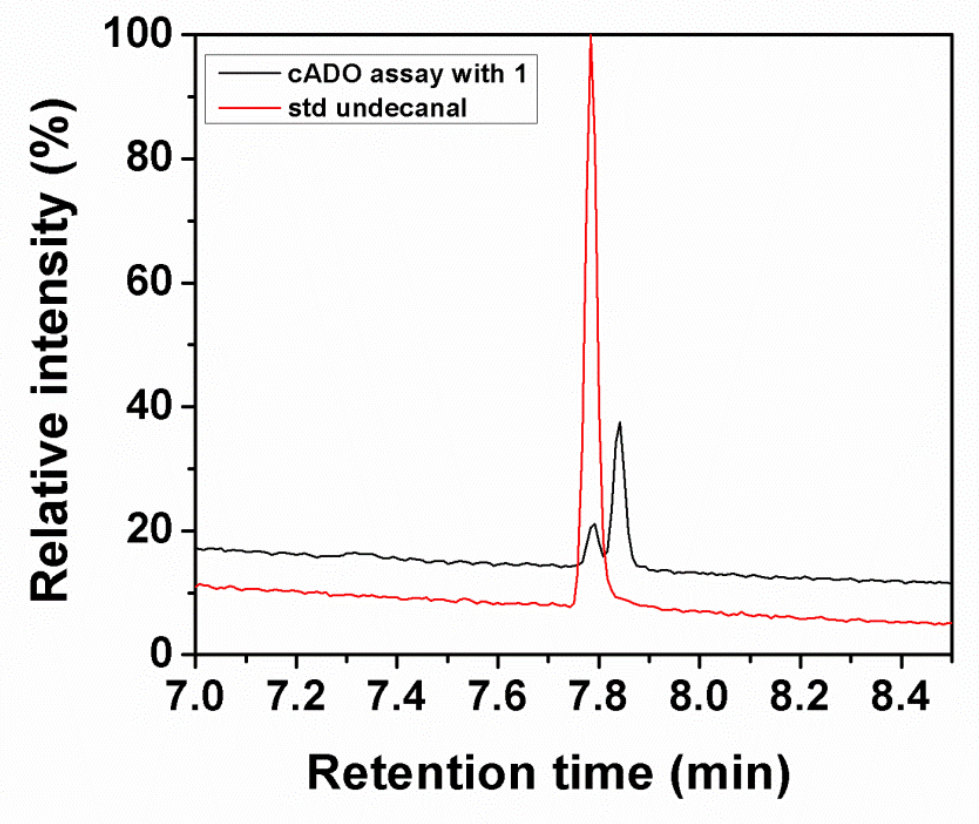

Figure 3.14. Overlaid chromatographs of *Np* cADO assays with compound **1** and standard undecanal. To separate undecanal from 2-nonyloxirane, the oven temperature was held initially at 70 °C for 2 min and then gradually increased to 120 °C at 20 °C/min and finally increased to 160 °C at 5 °C/min. This allowed the peak that originally eluted at 6.79 min be resolved into two separate peaks and eluting at 7.80 min and 7.87 min. The peak at 7.80 min overlaid well with an authentic standard undecanal.

A further prediction of the mechanism is that the alkanes derived from **1** or **2** should incorporate two protons from the solvent during the course of the reaction. To evaluate this prediction, the reaction of **2** in D_2O was investigated. cADO was reacted with **2** for 2 h under the usual conditions in assay buffer in which the D_2O content was ~ 97 %. The products of the reaction were extracted and analyzed by GC-MS. The molecular ion for hexadecane was clearly visible and shifted by 2 mass units to m/z = 228.2 from the

expected value of m/z = 226.2 for unlabeled material (Figure 3.15). A smaller peak at m/z = 227.2 corresponding to mono-deuterated heptadecane was also present, which may be explained by incomplete deuteration of the solvent combined with a solvent isotope effect.

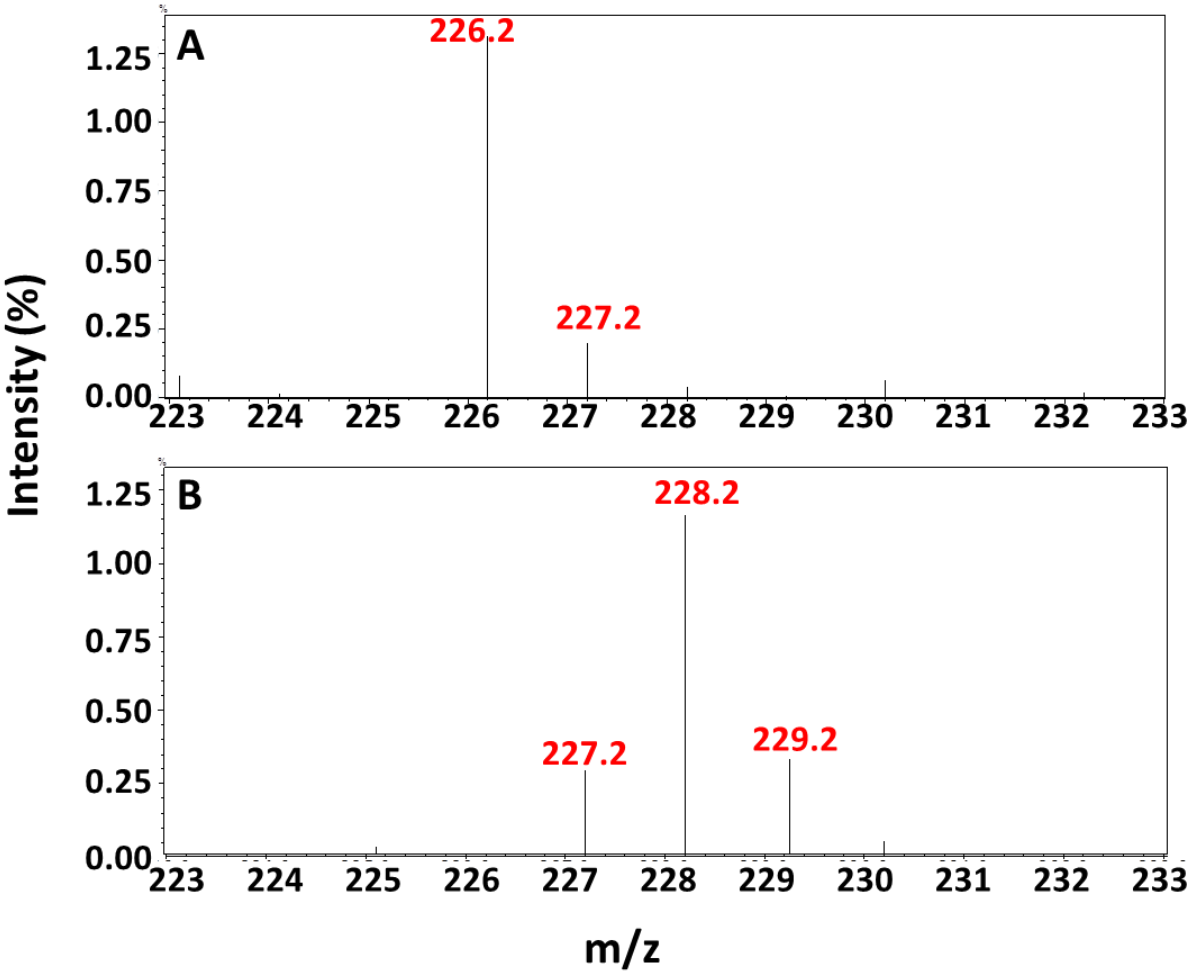

Figure 3.15. GC-MS analysis of hexadecane (m/z = 226.2) produced from reaction of **2** with cADO. **A:** in H_2O buffer; **B:** in D_2O buffer. The molecular ion for hexadecane produced in D_2O buffer is shifted by 2 mass units to m/z = 228.2.

3.4 Conclusions

To investigate the electron-requiring steps following initial formation of the metal peroxide species we synthesized and examined the reaction of cADO with an aldehyde bearing a strategically placed cyclopropyl group that could act as a radical clock, as described in Chapter 2.[4] This substrate partitioned between two pathways when reacted with cADO. In the productive pathway, ring-opening of the cyclopropyl group occurred to give 1-octadecene, providing support for a radical mechanism for C-C bond cleavage. Whereas in a non-productive reaction, alkylation of the protein occurred after deformylation, resulting in inactivation of the enzyme.

The previously studied radical clock generated a cyclopropylcarbinyl radical, useful for measuring the lifetimes of radical intermediates when they are of similar duration to the well-characterized ring-opening reactions so that product partitioning ratios can be measured. Because only the ring-opened product was observed, all that could be inferred was that the lifetime of the intermediate radical species was significantly in excess of 10 ns.[4] However, oxiranyl radicals, although not as extensively studied, also undergo ring-opening rearrangements, but at much slower rates that allow them to be used as slow radical clocks. The rate constant for rearrangement of the 3-methyloxiran-3-yl radical to the corresponding acetonyl radical has been measured as 3.1×10^4 s^{-1} at 25 ºC.[18] The rate constant for the rearrangement of the 3-methyloxiran-2-yl radical to the corresponding propanal-derived radical, which serves as a better reference for the reaction of oxiranyl aldehydes with cADO, has not been measured directly but is estimated to occur about an order of magnitude more slowly.[15] From the observed partitioning ratios between alkyloxirane and n-2 alkane, the products derived from the

reaction of **1** and **2** with cADO, we estimate that the rate constant for proton-coupled electron transfer in the final step of the reaction is ~ 10^4 s^{-1} at 25 ºC and is unlikely to be faster than 10^5 s^{-1}, using the rate constant for rearrangement of the 3-methyloxiran-3-yl radical as an upper limit,.

Recently, an interesting observation has been made that cADO catalyzes the oxidation of alkanes derived from deformylation of C9 and C10 aldehydes to the corresponding n-1 alcohols and aldehydes, albeit extremely slowly.[3] However, the enzyme was unable to oxidize alkanes or alcohols in the absence of aldehydes. To accommodate these findings, a mechanism was proposed in which the deformylation step occurred by heterolytic mechanism to generate a reactive Fe-superoxide species, akin to that generated in P450 reactions, that was responsible for the subsequent oxidative chemistry. Oxiranes can be rearranged to aldehydes by strong, hindered bases[19,20] and so, in principle, a mechanism involving heterolytic C – C bond cleavage and the formation of an oxiranyl carbanion could be operating. However, this is less likely for the following reasons.

The heterolytic mechanism predicts that it should be possible to form up to 1 equivalent of product under the assay conditions resulting from the initial reaction of the apo-enzyme, Fe(II) and O_2. However, no evidence was found for any turnover unless PMS and NADH were included.[7,4] The reaction of cADO with a cyclopropyl aldehyde radical clock substrate, discussed above and in chapter 2, provides strong support for a radical mechanism. It was suggested that ring opening could be a secondary reaction arising from reaction of the cyclopropylalkane product with the Fe-superoxide species to generate a cyclopropylcarbinyl radical in a P450-like manner.[3] But the products from

such a reaction should bear a hydroxyl group; in practice the product was found to be (unoxidized) octadecene. Lastly, spectroscopic evidence has recently been published supporting the formation of a diferric peroxide or preoxyhemiacetal intermediate in the reaction of cADO, as mentioned above.[1] This species was stable until the addition of the reductant necessary to initiate homolytic bond cleavage; in contrast a heterolytic mechanism would imply that it could undergo spontaneous conversion to the putative Fe-superoxide species.

3.5 References

1. Pandelia, M. E.; Li, N.; Norgaard, H.; Warui, D. M.; Rajakovich, L. J.; Chang, W. C.; Booker, S. J.; Krebs, C.; Bollinger, J. M., Substrate-Triggered Addition of Dioxygen to the Diferrous Cofactor of Aldehyde-Deformylating Oxygenase to form a Diferric-Peroxide Intermediate. *Journal of the American Chemical Society* **2013**, Epub Aug 29, 2013. DOI: 10.1021/ja405047b.

2. Li, N.; Norgaard, H.; Warui, D. M.; Booker, S. J.; Krebs, C.; Bollinger, J. M., Conversion of fatty aldehydes to alka(e)nes and foramte by a cyanobacterial aldehyde decarbonylase: crypric redox by an unusual dimetal oxygenase. *Journal of the American Chemical Society* **2011,** *133*, 7148-7152.

3. Aukema, K. G.; Makris, T. M.; Stoian, S. A.; Richman, J. E.; Münck, E.; Lipscomb, J. D.; Wackett, L. P., Cyanobacterial aldehyde deformylase oxygenation of aldehydes yields n-1 aldehydes and alcohols in addition to alkanes. *ACS Catalysis* **2013,** *3*, 2228-2238.

4. Paul, B.; Das, D.; Ellington, B.; Marsh, E. N., Probing the mechanism of cyanobacterial aldehyde decarbonylase using a cyclopropyl aldehyde. *J Am Chem Soc* **2013,** *135* (14), 5234-5237.

5. Unpublished, *structure solved by Joint Center of Structural Genomics (protein database entry PDB|2OC5|A)*.

6. Barret, A. G. M.; Head, J.; Smith, M. L.; Stock, N. S.; White, A. J. P.; Williams, D. J., Fleming-Tamao Oxidation and Masked Hydroxyl Functionality: Total Synthesis of (+)-Pramanicin and Structural Elucidation of the Antifungal Natural Product (-)-Pramanicin. *The Journal of Organic Chemistry* **1999,** *64*, 6005-6018.

7. Das, D.; Eser, B. E.; Han, J.; Sciore, A.; Marsh, E. N. G., Oxygen-independent decarbonylation of aldehydes by cyano-bacterial aldehyde decarbonylase: a new reaction of di-iron enzymes. *Angewandte Chemie International Edition* **2011,** *50*, 7148-7152.

8. Warui, D. M.; Li, N.; Norgaard, H.; Krebs, C.; Bollinger, J. M.; Booker, S. J., Detection of Formate, Rather than Carbon Monoxide, As the Stoichiometric Coproduct in Conversion of Fatty Aldehydes to Alkanes by a Cyanobacterial Aldehyde Decarbonylase. *J. Am. Chem. Soc.* **2011,** *133*, 3316-3319.

9. Andre, C.; Kim, S. W.; Yu, X. H.; Shanklin, J., Fusing catalase to an alkane-producing enzyme maintains enzymatic activity by converting the inhibitory byproduct H2O2 to the cosubstrate O2. *Proceedings of the National Academy of Sciences of the United States of America* **2013,** *110* (8), 3191-3196.

10. Khara, B.; Menon, N.; Levy, C.; Mansell, D.; Das, D.; Marsh, E. N.; Leys, D.; Scrutton, N. S., Production of propane and other short-chain alkanes by structure-based

engineering of ligand specificity in aldehyde-deformylating oxygenase. *Chembiochem : a European journal of chemical biology* **2013,** *14* (10), 1204-8.

11. Eser, B. E.; Das, D.; Han, J.; Jones, P. R.; Marsh, E. N. G., Oxygen-Independent Alkane Formation by Non-Heme Iron-Dependent Cyanobacterial Aldehyde Decarbonylase: Investigation of Kinetics and Requirement for an External Electron Donor. *Biochemistry* **2011,** *50* (49), 10743-10750.

12. Cheesbrough, T. M.; Kolattukudy, P. E., Alkane Biosynthesis by Decarbonylation of Aldehydes Catalyzed by a Particulate Preparation from Pisum-Sativum. *Proceedings of the National Academy of Sciences of the United States of America-Biological Sciences* **1984,** *81* (21), 6613-6617.

13. Reed, J. R.; Quilici, D. R.; Blomquist, G. J.; Reitz, R. C., Proposed mechanism for the cytochrome P450-catalyzed conversion of aldehydes to hydrocarbons in the house fly, Musca domestica. *Biochemistry* **1995,** *34* (49), 16221-16227.

14. Behrrns, G.; Schulte-Frohliiid, D., Proof of the Pyramidal Configuration of the Oxi-ranyl Radical: Two Isomers of the 3-Methyl-2-oxi-ranyl Radical. *Angewandte Chemie international Edition* **1973,** *12*, 932-933.

15. Itzel, H.; Fischer, H., Electron Spin Resonance of Oxiranyl Radicals in Solution : Configurational Stabilities and Rearrangement Reactions. *Helvetica Chimia Acta* **1976,** *59*, 880-901.

16. Suda, K.; Kikkawa, T.; Nakajima, S.; Takanami, T., Highly regio- and stereoselective rearrangement of epoxides to aldehydes catalyzed by high-valent metalloporphyrin complex, Cr(TPP)OTf. *Journal of the American Chemical Society* **2004,** *126* (31), 9554-9555.

17. Padwa, A.; Das, N. C., Oxirane Radicals. The Thermal Decomposition of t-Butyl Cis- and trans-a,b- 6-Diphenylperglycidates. *The Journal of Organic Chemistry* **1969,** *34* (4), 816-821.

18. Weber, M.; Fischer, H., Absolute Rate Constants for the â-Scission and Hydrogen Abstraction Reactions of the tert-Butoxyl Radical and for Several Radical Rearrangements: Evaluating Delayed Radical Formations by Time-Resolved Electron Spin Resonance. *Journal of the American Chemical Society* **1999,** *121*, 7381-7388.

19. Yanagisawa, A.; Yasue, K.; Yamamoto, H., Selective lsomerization of 1,2-Epoxyalkanes to Aldehydes with Lithium Dialkylamides. *Journal of the Chemical Society Chemical Communication* **1994**, 2013-2014.

20. Satoh, T., Oxiranyl Anions and Aziridinyl Anions. *Chemical Reviews* **1996,** *96*, 3303-3325.

Chapter 4

An unusual iron-dependent oxidative aldehyde deformylation reaction mimicking the reaction catalyzed by insect aldehyde decarbonylase

The work described in this chapter was accomplished in collaboration with Dr. Bishwajit Paul, Dr. Debasis Das, Mr. Andrew Vitek and Professor Paul Zimmerman. Experiments pertaining to protonation stereospecificity were performed by Dr. Bishwajit Paul, and computational modeling was performed by Mr. Andrew Vitek and Professor Paul Zimmerman. This chapter is based on a manuscript currently under consideration for publication in *Chemical Science*.

4.1 Introduction

The mechanisms of both P450[1] and non-heme iron oxygenases[2] have been extensively studied. A hallmark of these enzymes is the wide variety of oxidative transformations that they catalyze, including hydroxylations,[3] decarbonylations,[4] demethylations,[5] and epoxidations,[6] amongst others. How enzymes discriminate between the different reaction pathways available to the reactive high-valent iron-oxo species that are initially generated at the active site continues to challenge our understanding of their mechanisms. For the aldehyde decarbonylase enzymes, this discrimination involves directing the reactive iron-oxygen species towards C-C bond

cleavage to effect removal of the aldehyde carbon rather than simply effecting C-H bond cleavage that would result in oxidation of the aldehyde to a carboxylic acid.[7] Despite its identity as a cytochrome P450 enzyme, the insect aldehyde decarbonylase (CYP4G1) remains poorly understood.

Studies of metal complexes that mimic the active sites of enzymes have played an important role in elucidating the mechanisms of both non-heme[7k, 8] and P450[9] iron oxygenases; for example, in probing the ability of different iron-oxo intermediates[7k, 8b, c, 10] and different spin-states[8a, 8d] to catalyze nucleophilic deformylations and electrophilic oxidations of aldehydes (and other substrates). Here we describe an unanticipated reaction involving the oxidative deformylation of an α-cyclopropyl aldehyde to produce CO_2 and a cyclopropyl alkane that is catalyzed by aqueous Fe^{2+} ions in the presence of oxygen or by Fe^{3+} in the presence of H_2O_2. The reaction mimics the oxidative deformylation catalyzed by the insect p450 aldehyde decarbonylase.[11] The presence of the cyclopropyl group is essential for the deformylation as simple n-aldehydes only undergo oxidation to carboxylic acids under these conditions. An atomistic reaction mechanism determined by computational reaction discovery tools shows that C-C bond-breaking is favored in α-cyclopropyl compared to alkyl aldehydes, providing a plausible explanation for the observed reactivity.

The studies detailed in chapters 2 and 3 utilized α-oxiranyl- and β-cyclopropyl-substituted long-chain aldehydes to probe the mechanism of cADO.[7e, 7i] These sterically undemanding substrate modifications provided valuable insight into the mechanism of deformylation, pointing to a radical mechanism for C–C bond cleavage.[7i] Therefore, I was motivated to synthesize the α-cyclopropyl-substituted dodecanal derivative (**1**) to further

probe the enzyme mechanism. I reasoned that introducing a cyclopropyl- group at the site of C–C bond scission would significantly destabilize any radical intermediate potentially generated on C2, so that **1** might function either as an inhibitor or a very slow substrate.

4.2 Materials and Methods

4.2.1 Materials

Ferrous ammonium sulfate was purchased from Sigma-Aldrich. NADH and ferric chloride were from Acros Organics. D_2O (99.9%) and DMSO-d_6 (99.9%) were obtained from Cambridge Isotope Laboratories, Inc. Hydrogen peroxide (30% in water) and ferrous chloride were from Fischer Scientific.

4.2.2 Synthesis of cyclopropyl aldehydes

The synthesis of *trans*-2-nonylcyclopropane-1-carbaldehyde (α-cyclopropyl dodecanal, **1**) was accomplished by standard methods starting from commercially available (*E*)-dodec-2-en-1-ol, in which the cyclopropyl group is positioned α- to the carbonyl group (See Appendix C). Briefly, the alcohol group on **(***E***)**-dodec-2-en-1-ol was protected as TBDMS silyl ether followed by the conversion of the double bond to a cyclopropyl group using diethylzinc and diiodomethane to yield the *trans*-stereoisomer. Finally, the deprotection of TBDMS group by methanolic hydrochloric acid, followed by the TEMPO oxidation of the alcohol yielded the desired *trans*-2-nonylcyclopropane-1-carbaldehyde (**1**)**.**

4.2.3 Assays

Enzymatic assays were performed as described previously.[7i] For nonenzymatic assays, concentrated stocks of aldehydes (**1**, dodecanal, α-oxiranyl dodecanal) in DMSO (10 mM) and iron (II) ammonium sulfate in H_2O (10 mM) were prepared in a glove box. Standard assays consisted of 100 µM ferrous ammonium sulfate and 300 - 500 µM **1** in 10 mM sodium acetate buffer (pH 5.0) at a total volume of 500 µL. Vials were removed from the glove box and exposed to air briefly before capping and incubating at 37 °C and 200 rpm for 10 min (at which point reaction completion was apparent). Assays were quenched with the addition of 50 mM EDTA and organics extracted in ethyl acetate. To study the pH dependence of the reaction, assays were conducted in aqueous buffer over the pH range 4 – 10 (10 mM Na acetate pH 4 - 6, 10 mM HEPES pH 6 - 8, 1 mM CHES pH 8 - 10) that contained 100 µM Fe^{2+} and 500 µM **1** at 37 C with shaking at 200 rpm for 15 min. The products of the reaction were then extracted, derivatized and analyzed by GCMS.

Carboxylic acid quantification was accomplished using the standard diazomethane derivatization protocol.[12] The organic extract from the standard assay mentioned above was treated with a few drops of diazomethane solution and the esterified product analyzed by GCMS.

4.2.4 Solvent Proton Incorporation

Assays were prepared as described above in either H_2O or D_2O (99%). Aldehyde solutions were made up as a stock solution in d_6-DMSO to facilitate subsequent ^{1}H-NMR analyses. A typical assay contained 1 mM ferrous ammonium sulfate and 500 µM **d_3-1**

(Compound **1A**) in a total volume of 4 mL. For assays performed in D_2O, the final H_2O concentration was <~1% after adding all the assay components. Five identical 4 mL reactions were set up in each assay condition and shaken at 37 °C at 200 rpm for 15 min. The reaction mixtures were sequentially extracted with a total volume of 1.2 mL $CDCl_3$ (99.9%). The $CDCl_3$ layers were dried over sodium sulfate and filtered before analysis by ^1H NMR. Spectra were acquired at 700 MHz (Varian) at 22 °C.

4.2.5 HRMS analysis of C_1 products

Compound **1** (^{13}C-labelled at the carbonyl-carbon (**1B**) or unlabeled) and $Fe(NH_3)_6SO_4$ were dissolved in air-saturated H_2O to 500 µM and 1 mM, respectively in a final volume of 2 mL. Samples were incubated in sealed 5 mL round bottom flasks equipped with HRMS adapters and incubated at 37 °C and 200 rpm for 30 min (completion). The headspace was analyzed by a VG 70-250-S magnetic sector mass spectrometer and total ion counts collected.

4.2.6 Computational methods

All quantum chemical calculations were performed by Mr. Andrew Vitek and Professor Paul Zimmerman through density functional theory (DFT) using the Q-Chem 4.3 *ab initio* quantum chemistry package. Gas-phase geometry optimizations were carried out with the unrestricted Perdew-Burke-Ernzerhof (PBE) density functional[13] and double-zeta, polarized 6-31G* basis set.[14] Frequency calculations were performed on all structures to confirm that optimizations led to stable minima or transition states. PBE with the triple-zeta, polarized cc-pVTZ basis set was used to calculate single point energies with the SMD solvation model[15] using H_2O as the implicit solvent. Thermodynamic

corrections were applied to the solvated energies using the PBE/6-31G* level of theory and a temperature of 300 K. Research discovery tools developed by the Zimmerman group were used to determine the deformylation mechanism that results in CO_2 and n-1 alkane formation. This strategy proceeds as follows: 1) a graph-based structure generator hypothesizes potential intermediates that are plausibly one elementary step away from starting reactants,[16] 2) the growing string method determines the exact transition state and minimum energy reaction path for each proposed elementary step,[17] and 3) steps 1-2 are repeated for thermodynamically and kinetically feasibly intermediates until complete, low-barrier pathways for product formation are found. These methods allow for efficient exploration of the relevant chemical space and discovery of plausible reaction paths with little or no knowledge of the elementary steps involved.[18]

4.3 Results and Discussion

4.3.1 Reaction of α-cyclopropyl-aldehyde with iron and oxygen

Compound **1** was synthesized by standard methods, as described in Experimental Procedures. Initial studies on the reaction of **1** with cADO suggested that the compound might undergo deformylation, as indicated by the appearance of a peak at 5.9 min that co-eluted with an authentic standard of 1,2-cyclopropyl-undecane (**2**) (Figure 4.1). However, subsequent control experiments established that the deformylation reaction did not depend on cADO, and, in fact, required only aqueous Fe^{2+} and O_2 to occur. The auxiliary reducing system, which is necessary for cADO activity, was found to inhibit the non-enzymatic reaction.

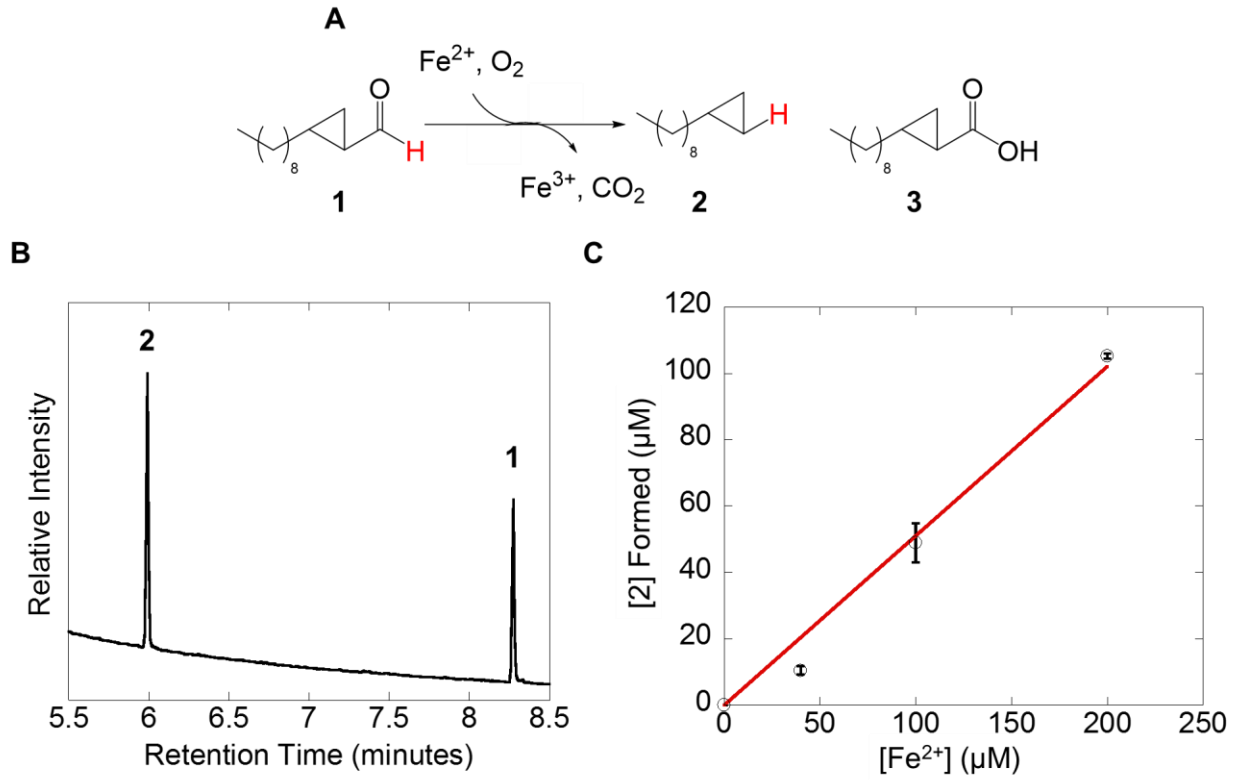

Figure 4.1. Reaction of **1** with Fe^{2+} and O_2 results in deformylation and oxidation. **A**, Scheme depicting reaction of **1** with Fe^{2+} and O_2. **B**, GCMS trace demonstrating conversion of 500 μM **1** to 1,2-cyclopropyl undecane (**2**) by 500 μM Fe^{2+}. **C**, Dependence of the formation of **2** on [Fe^{2+}] from 500 μM **1**.

The deformylation of **1** occurred in competition with the more conventional oxidation of the aldehyde group to the corresponding 2,3-cyclopropy-dodecanoic acid (**3**). In H_2O, the ratio of alkane, **2**, to carboxylic acid, **3**, formed was ~1:5 (Figure 4.2). The pH dependence of the reaction was investigated over the pH range 4 – 10. The formation of **2** and **3** was favored by slightly acid acidic conditions, although the pH-dependencies of the reactions were not identical. The formation of **2** exhibited a simple pH-dependence with an apparent pK_a of 7.2, whereas the formation of **3** exhibited more complex pH-dependent behavior with an apparent titration point at pH 8.4 (Figure 4.3).

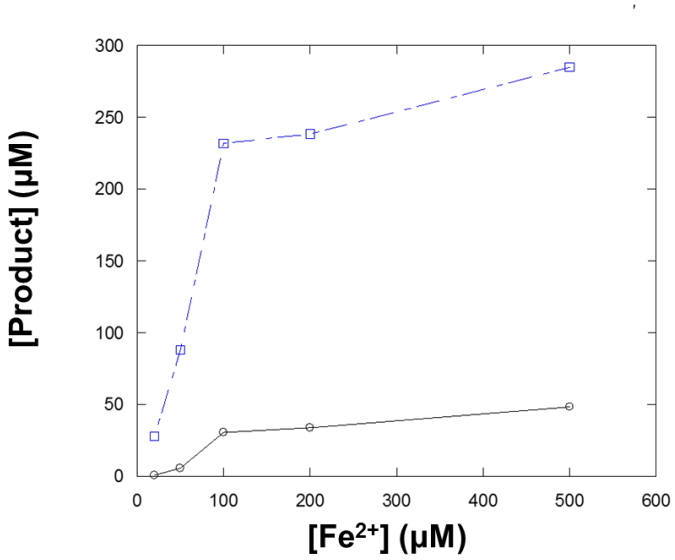

Figure 4.2. Fe^{2+} Dependence of **1** turnover to both alkane (black) and carboxylic acid (blue) products. Assays contained 500 μM **1** and were run to apparent completion.

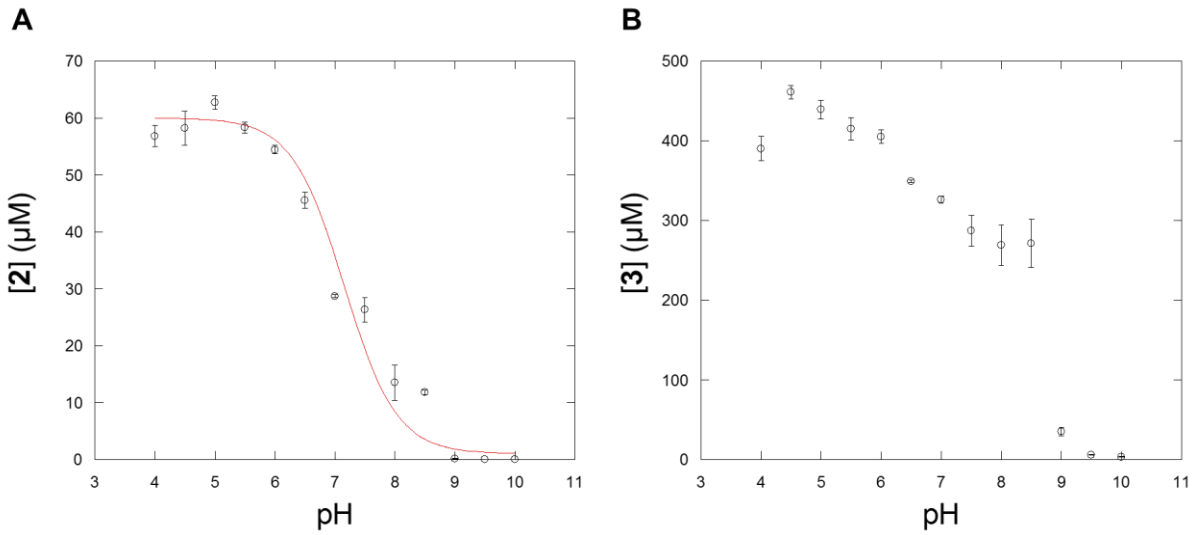

Figure 4.3. pH Dependence of reaction of 500 μM **1** with 100 μM Fe^{2+} and O_2. **A**, Formation of **2** as a function of pH. **B**, Formation of **3** as a function of pH. Assays run to completion.

Control experiments using dodecanal, dodecenal and α-oxiranyl dodecanal failed to detect any n-1 alkane products under the same conditions. Instead these aldehydes,

as expected, were exclusively oxidized to dodecanoic acid, dodecenoic acid and 2,3-oxiranyl dodecanoic acid, respectively (Figure 4.4). These results pointed to the unusual role of the cyclopropyl group in directing the oxidative chemistry of **1** towards deformylation.

Further investigation of the stoichiometry with which **2** and **3** were formed with respect to the amount of Fe^{2+} in the reaction revealed that the formation of **2** was linearly dependent on the concentration of Fe^{2+} supplied, with an approximate slope of 2 (Figure 4.1). In contrast, several equivalents of carboxylic acid, **3**, were formed per Fe^{2+} ion, an observation that is in accord with the well-documented ability of transition metal ions to catalyze the oxidation of aldehydes to carboxylic acids.[19] This observation suggested that Fe^{2+} might be acting to reduce O_2 to hydrogen peroxide and that the deformylation of **1** may occur through a metal peroxide intermediate. To test this, assays were conducted under anaerobic conditions in which 300 μM of **1** was reacted with 100 μM of Fe^{3+} and 1 – 10 mM hydrogen peroxide. Under these conditions **1** was converted to **2** and **3** in approximately the same ratios as observed with Fe^{2+} and O_2. This observation indicates that an iron-bound peroxide species is likely the oxidant in the reaction. Although Fe^{3+} and hydrogen peroxide were shown to function in the reaction, experimentally it proved easier to conduct further studies using Fe^{2+} and O_2 as the oxidant.

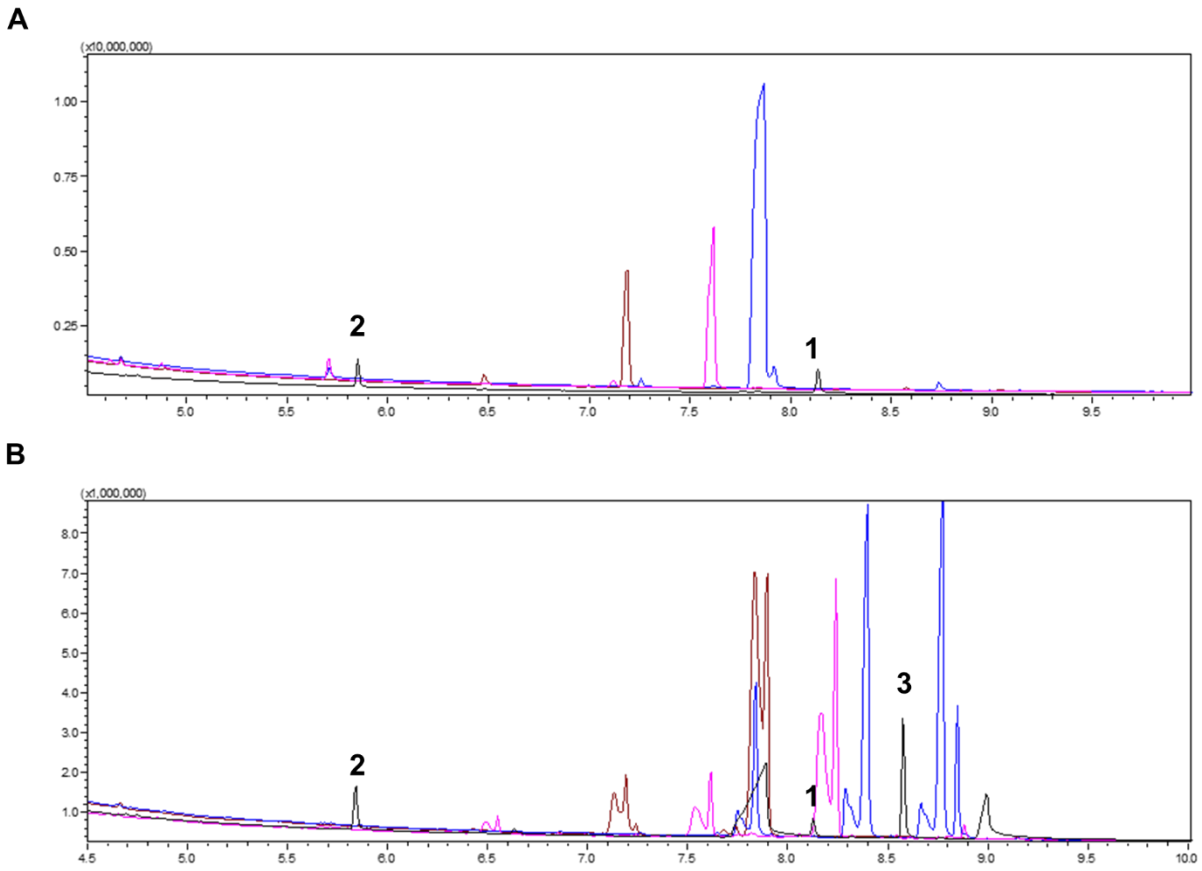

Figure 4.4. Deformylation Dependence on Substrate Identity. **A**, Substrate peaks of dodecanal (Brown), dodecenal (Pink) and 2,3-oxiranyl dodecanal (Blue) were visible at 7.2 minutes, 7.6 minutes and 7.8 minutes, respectively. Alkane formation was exclusive to α-cyclopropyl (Black), with substrate (**1**) at 8.1 minutes and product (**2**) at 5.9 minutes. **B**, Diazomethane derivatized samples. Substrate peaks remained visible, but significant formation of dodecanoic acid (Brown, 7.9 minutes), dodecenoic acid (Pink, 8.2 minutes), and 2,3-oxiranyl dodecanoic acid (Blue, 8.4 and 8.7 minutes) is present. The α-cyclopropyl species is again in black, with the associated carboxylic acid (**3**) at 8.6 minutes. Assays contained 100 μM Fe^{2+} and 500 μM substrate, and were run to completion.

4.3.2 Fate of the aldehyde carbon

To determine the fate of the carbonyl carbon, **1** was synthesized with the carbonyl carbon ^{13}C-labeled and reacted with Fe^{2+} and O_2 in water containing 10% D_2O. The

products of reaction were then analyzed *in situ* by ^{13}C NMR. The only ^{13}C-labeled material evident from the spectrum was the carboxylic acid arising by oxidation of the aldehyde. Therefore it seemed likely that the aldehyde carbon was converted to CO_2 in the reaction. To examine this possibility, the reaction was conducted in sealed flasks and the headspace analyzed by HRMS. The reaction of unlabeled **1** resulted in a 2.5-fold increase in CO_2 above background, whereas reaction of **1B** resulted in the appearance of the expected $^{13}CO_2$ peak at m/z = 45 (Figure 4.5). Interestingly the production of CO_2 as a byproduct mimics the poorly-understood insect p450 enzyme (CYP4G1) that catalyzes the oxidative decarbonylation of fatty aldehydes.[11a, 20]

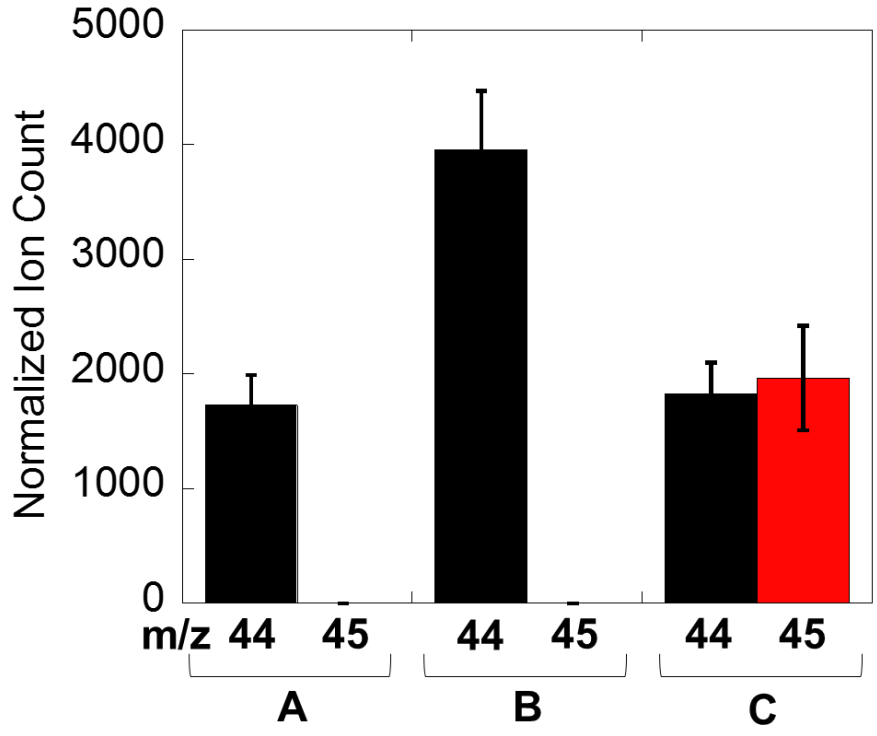

Figure 4.5. Normalized total ion counts of m/z = 44 and m/z = 45 Da peaks in gas phase above reactions. ***A****:* 0 μM **1**, 1000 μ M Fe^{2+}; ***B****:* 500 μM unlabeled **1** and 1000 μM Fe^{2+}AS; ***C***: 500 μM Compound **1B** and 1000 μM Fe^{2+}. Peaks were normalized to atmospheric N_2 ion counts.

4.3.3 Fate of the aldehyde proton

Experiments on the insect p450 enzyme indicated that the aldehyde hydrogen was retained in the n-1 alkane.[11a, 20] To determine the fate of the aldehyde hydrogen in the reaction of **1** Dr. Bishwajit Paul initially synthesized **1** with the aldehyde proton deuterium-labeled. However, reaction of deuterium-labeled **1** with Fe^{2+} and O_2 resulted in the compound being converted almost entirely to the carboxylic acid, **3,** with negligible formation of **2**. This indicated that a significant kinetic isotope effect was operating against the formation of **2**, thereby favoring the alternate reaction pathway leading to the formation of **3**. The unfavorable isotopic branching made it unfeasible to examine the deuterium content of **2** by NMR or MS. Dr. Paul therefore adapted his approach by synthesizing Compound **1A** (**1** labeled with 3 deuterium atoms, one at the α-carbon and two on the cyclopropyl methylene carbon). This allowed him to test, instead, whether *protium* was transferred from the aldehyde carbon.

Compound **1A** was reacted with Fe^{2+} and O_2 in either H_2O or D_2O and the product, **2**, recovered and analyzed by ^{1}H-NMR. The spectra, shown in Figure 4.6, were identical whether the reaction was carried out in H_2O or D_2O, indicating that the proton in the product was transferred from the aldehyde rather than the solvent. Moreover, protonation appeared to be equally favored on either the *trans* or *cis* face of the cyclopropyl ring. This suggests a mechanism in which C – C bond scission precedes hydrogen transfer.

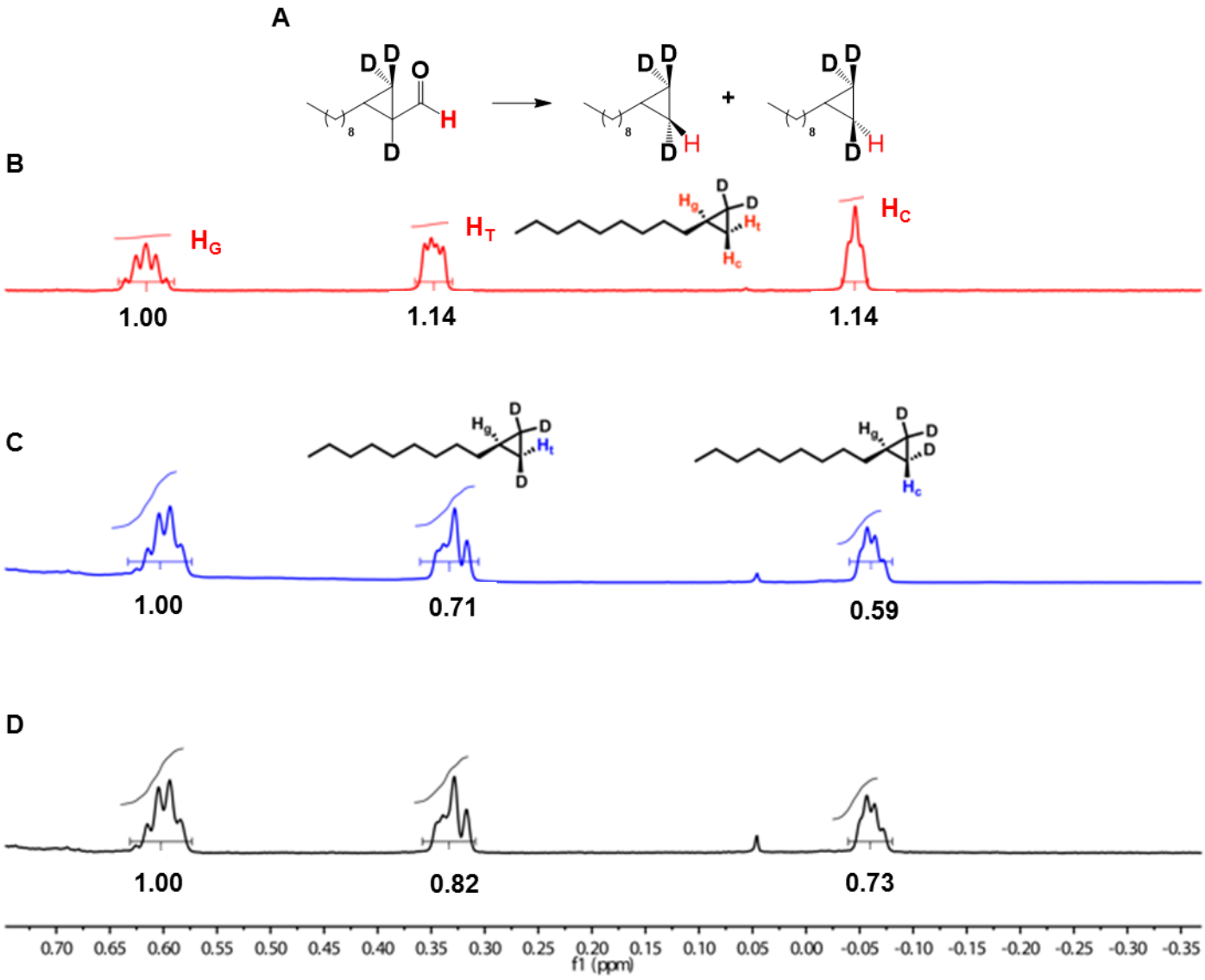

Figure 4.6. Aldehyde proton is retained in the alkane product stereo-randomly. ***A:*** General reaction scheme; ***B****:* Di-deuterated 1-nonylcyclopropane standard (Compound **2A**); ***C***: Compound **1A** reacted in H_2O; ***D***: Compound **1A** reacted in D_2O. The protium content at H_t and H_c does not depend on the isotopic composition of the solvent.

4.3.4 Computational search of potential reaction pathways

To gain further insight into the atomistic details of this very unusual reaction, and in particular the role of the cyclopropyl substituent in directing **1** towards deformylation, we turned to computational simulations. Reaction discovery methods[25,26, 17] developed

by the Zimmerman group were used to search for potential pathways leading to the observed reaction products for **1**. These methods allow for exploration and evaluation of chemically reasonable elementary steps and produce active reaction paths by identifying the most kinetically and thermodynamically feasible elementary steps. Based on the experimental observations above, the fully hydrated Fe^{3+}-OOH species was used as the starting point for computational studies. To simplify the calculations methylcyclopropyl-carbaldehyde was used to approximate **1**. The metal-peroxide was modeled in the protonated form as the deformylation reaction proceeds only at acidic pH values.

Figure 4.7 depicts the decarbonylation mechanism for the model α-cyclopropyl aldehyde with high (Fe^{III} hextet) and low spin (Fe^{III} quartet) iron complexes. The starting structures for high and low spin complexes are stabilized by two hydrogen-bonds between the water ligands of the iron-aquo species and the carbonyl of the aldehyde substrate. The starting structure for the low spin complex lies 6.1 kcal/mol above the high spin complex. The decarbonylation is initiated by insertion of the aldehyde into the peroxy group of the starting iron complex with barriers of 14.3 and 20.9 kcal/mol above the starting structures (high and low spin, respectively). Insertion is followed by rotation about the C-O bond of the inserted aldehyde, which primes the acidic proton of the inserted substrate for abstraction by an iron hydroxide species. These rotations have moderate barriers of 9.1 and 5.8 kcal/mol for high and low spin complexes, respectively. Rotation about the C-O bond is followed by homolytic cleavage of the O-O bond with barriers of 5.4 and 2.6 kcal/mol for the high and low spin states, respectively. This intermediate is stabilized by two hydrogen-bonding interactions – one between the hydroxyl proton of the aldehyde fragments and the iron-oxo radical group and another between the radical

oxygen of the aldehyde fragment and a neighboring water ligand. The last step of the decarbonylation is the C-C bond scission between the alkyl and carbonyl groups of the aldehyde substrate. In this step, the cyclopropyl and carbonyl C-C bond is broken. The cyclopropyl group abstracts the carbonyl hydrogen atom to form a stable alkane. The iron-oxo group abstracts the hydroxyl proton of the carbonyl group to form CO_2 and the resulting iron-hydroxide complex. This last step has a barrier of 10.6 and 3.4 kcal/mol for high and low spin complexes, respectively.

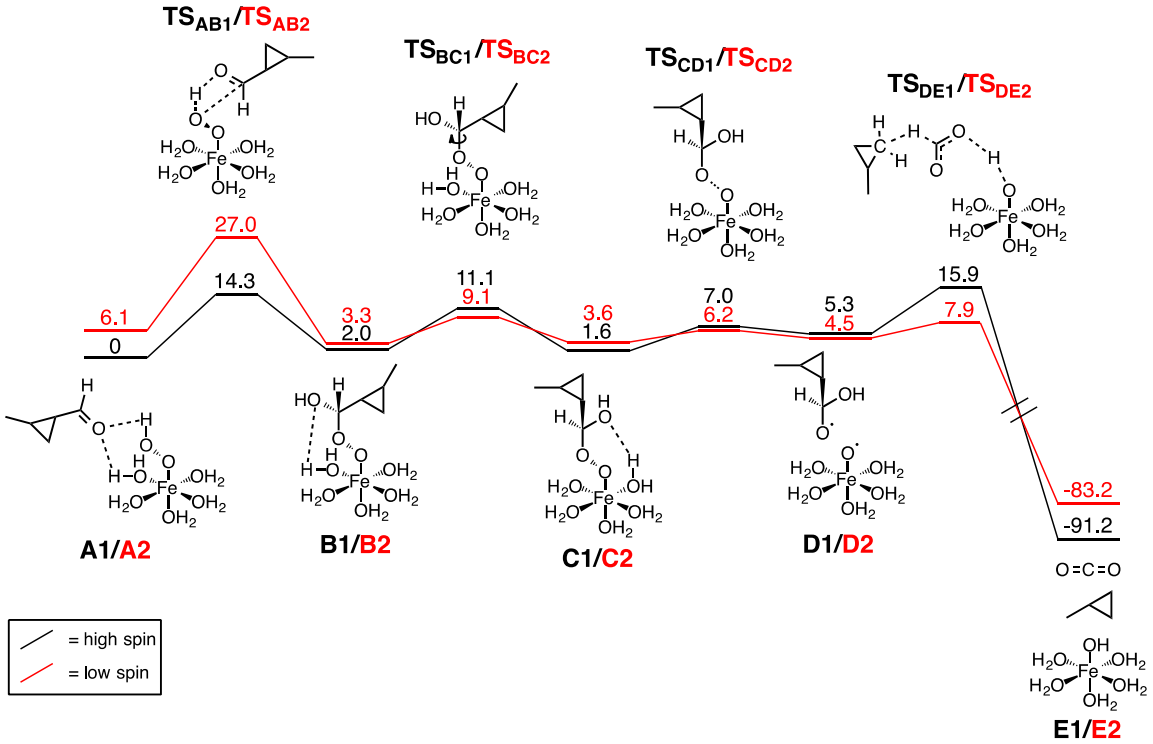

Figure 4.7. Decarbonylation mechanism for α-cyclopropyl. Energy barriers based on a high (black) and low (red) spin iron complex are depicted.

Despite little intuition about how the mechanism might proceed, the computational reaction search identified a plausible mechanism for deformylation, shown in Figure 4.8. This mechanistic pathway represents the most kinetically and thermodynamically feasible

pathway that was located for deformylation starting from Fe^{3+}-OOH and **1**, identified from among over 3,000 elementary reaction steps that were screened. Pathways leading to carboxylic acid products that are initiated by direct H-abstraction by Fe^{3+}-OO^{-} are also possible, and have been described in the literature.[19] While we herein focus on the novel deformylation pathway, competing pathways leading to carboxylic acid formation should be understood as feasible and operating simultaneously.

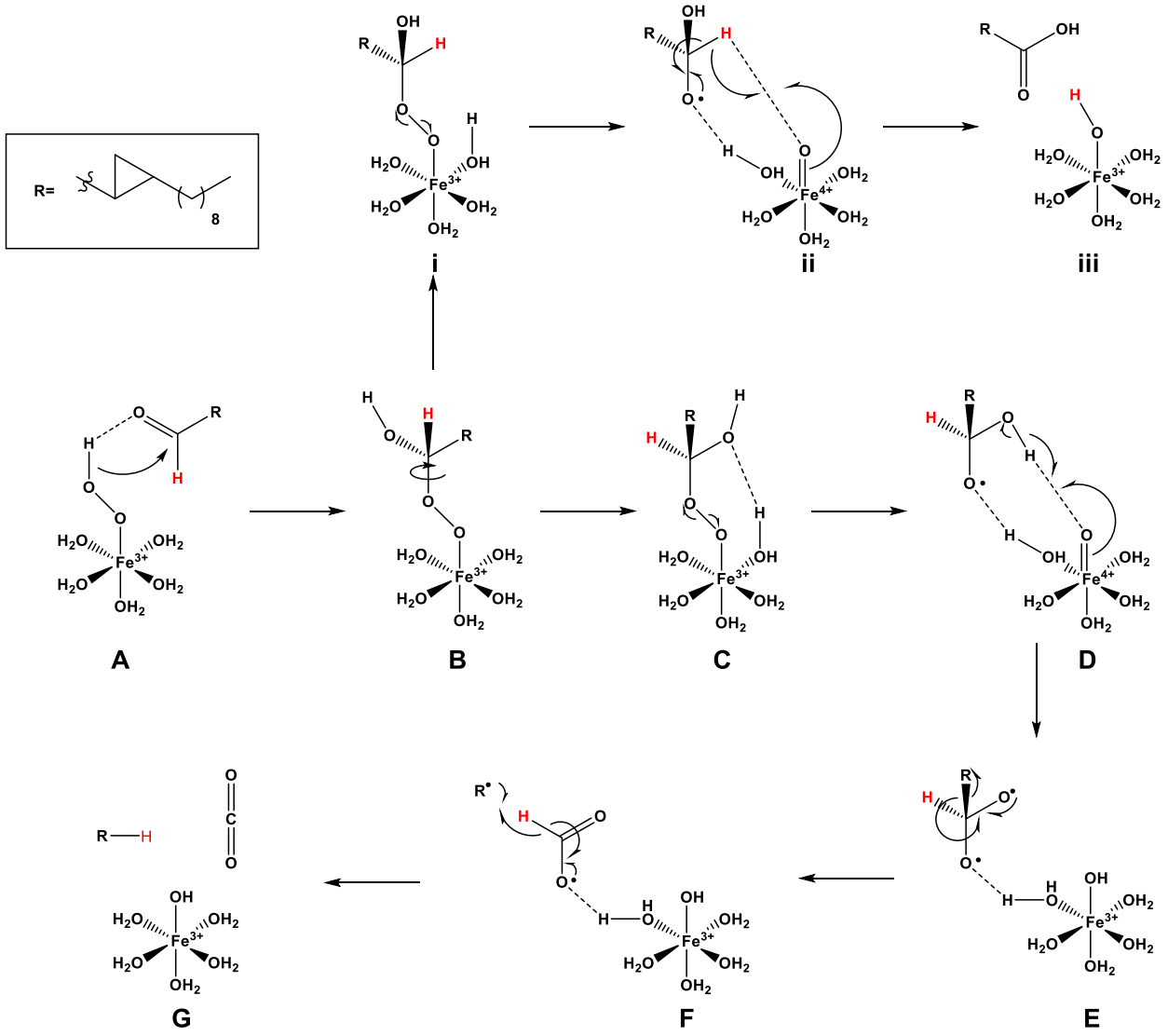

Figure 4.8. Decarbonylation and oxidation mechanisms for **1** predicted by computational reaction pathway discovery.

The computationally predicted mechanism involves the aldehyde first binding to the Fe^{3+}-OOH complex through hydrogen bonds between the peroxy- and H_2O ligands (**A,** in Figure 4.8). The reaction is initiated by nucleophilic attack of the aldehyde substrate by the metal-bound peroxide to form the metal-peroxyhemiacetal, **B** in Figure 4.8. Formation of the metal-peroxyhemiacetal is followed by a rotation about the C-O bond (**B**, in Figure 4.8) to position either the proton on the acetal oxygen (**C**, in Figure 4.8) or the carbonyl hydrogen (**i**, in Figure 4.8) close to the Fe–O peroxide bond. Next, homolytic fission of the weak O-O bond generates the high valent iron-oxo species and the acetal radical, **C-D**. This step is predicted to be accompanied by a change in the spin state of iron from a high spin hextet to a low spin quartet. Deformylation is initiated by abstraction of the acetal O-H hydrogen by the high valent iron-oxo species (**D** in Figure 4.8), with the resulting acetal di-radical fragmenting to generate a formyl radical and a reactive cyclopropyl radical (**E-F** in Figure 4.8) that immediately abstracts the formyl-hydrogen to generate CO_2 and **2** (**F-G** in Figure 4.8). Importantly, this step retains the aldehyde H in the cyclopropyl ring. Interestingly, rotation about the C-O bond in **B** can also bring the aldehyde carbon in close proximity to the Fe–O peroxide bond (**i** in Figure 4.8). In this configuration homolysis of the peroxide O-O bond leads to C-H abstraction and consequent oxidation of the aldehyde to the carboxylic acid, **3** (**ii** and **iii** in Figure 4.8). Along the paths shown in Figure 4.8, the rate-limiting step for deformylation of **1** is computed to be the initial formation of the iron-peroxyhemiacetal with a barrier of 8.1 kcal/mol. Whereas this does not agree with the experimental finding that C-H scission is rate-limiting, as indicated by a large deuterium isotope effect, the difference in the

calculated energy barriers for C-H bond-cleavage and iron-peroxyhemiacetal formation (6.7 and 8.1 kcal/mol) are within the expected error of the DFT method.

While steps **A** – **C** are well precedented,[7e, 21] steps **D** to **G** are quite unusual. These steps, however, are supported by the deuterium-labelling results described above and, significantly, were identified independently of the experimental results; i.e. the reaction search was not constrained by the requirement that aldehyde hydrogen be retained in the product alkane.

The reaction pathway searches found an exactly analogous deformylation pathway that appeared to be feasible for n-propanal. While the level of theory employed (PBE/SMD) is expected provide only semi-quantitative barriers along the reaction path, the n-propanal pathway was found to have barriers that were 2.2 kcal/mol (A→B) and 1.6 kcal/mol (C→E) higher in energy than the cyclopropyl-forming pathway. The higher barriers indicate that deformylation is slower for the non-cyclopropyl substrate, where carboxylic acid formation will be more competitive. Further studies were also undertaken to calculate the potential energy surface for the individual steps in the hypothesized mechanism using various density functionals (Figure 4.9). These studies supported the feasibility of the pathways identified in the reaction search, but did not lead to qualitatively different results.

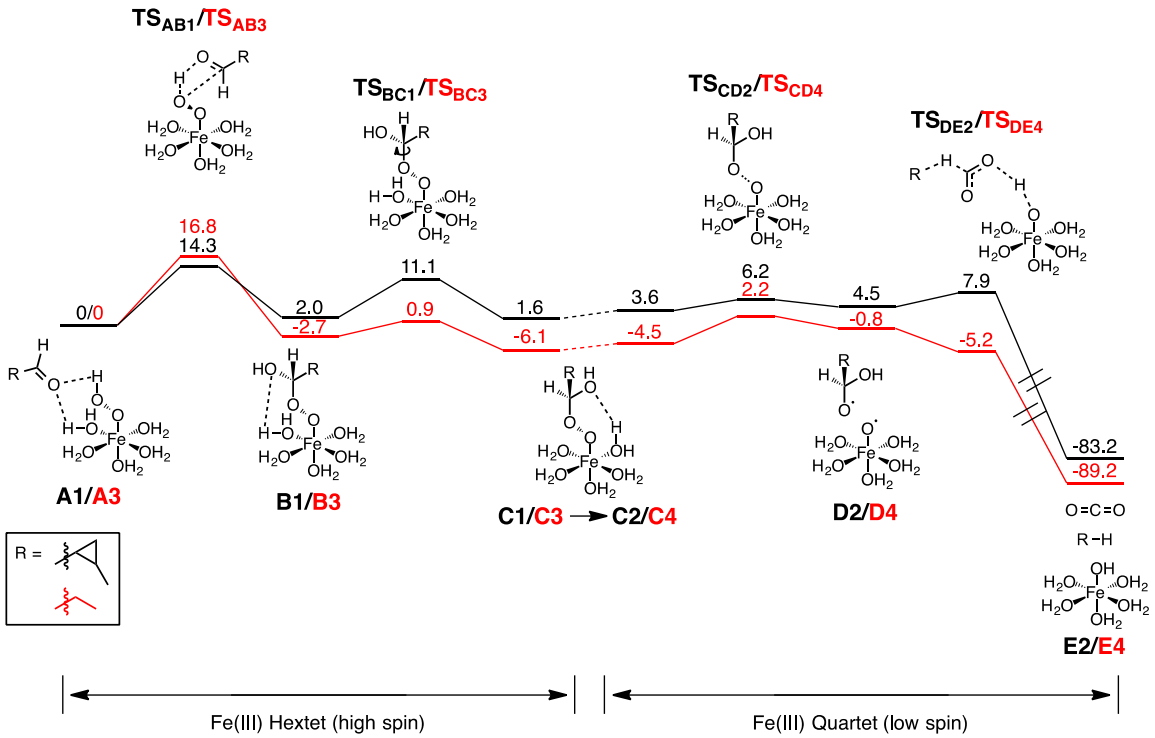

Figure 4.9. Comparison of α-cyclopropyl aldehyde and n-aldehyde reaction pathways.

The deformylation reaction we identified for **1** represents a highly unusual mode of oxidation for an aldehyde because in this case the aldehyde carbon is completely oxidized to CO_2 while the α-carbon is reduced by transfer of the aldehyde hydrogen. The reaction mimics that catalyzed by insect P450 aldehyde decarbonylase, CYP4G1, and it is somewhat surprising that a very simple oxidizing system – either aqueous Fe^{2+} and O_2, or Fe^{3+} and hydrogen peroxide – is able to recapitulate the reaction of a rather complex enzyme.[11a, 20] This is the first non-enzymatic example of this type of oxidative deformylation of an aldehyde to generate CO_2 and an alkane.

An obvious question is how does appending a simple cyclopropyl ring adjacent to the aldehyde carbon alter the oxidation pathway? The oxidation of aldehydes to carboxylic acids in the presence of oxygen and transition metal complexes[19] (and metallo-enzymes[7a]) is by far the more common pathway and, indeed predominates in the reaction

of **1**. These reactions have been extensively studied and shown to proceed by various mechanisms involving reactive oxygen species.[19b, 22] The key step in the reaction is abstraction of the aldehyde hydrogen atom by a reactive oxygen species, e.g. metal-peroxo or metal-oxo, or a transition metal, to generate an acyl radical, followed by formation of the corresponding peroxyacid and subsequent auto-oxidation (Figure 4.10).[19, 22] For the observed deformylation of **1** to occur, this reaction pathway must somehow be suppressed.

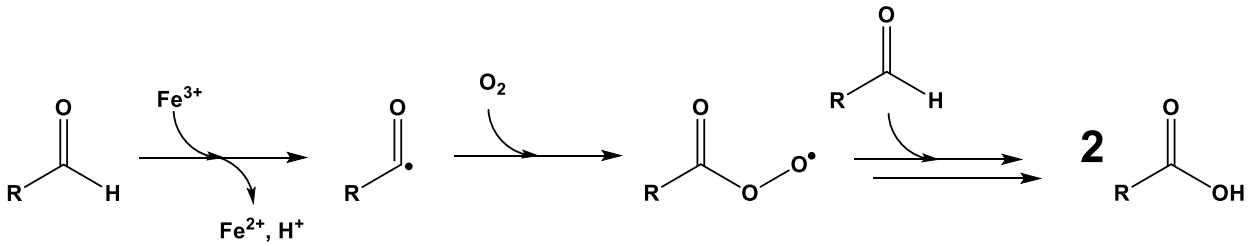

Figure 4.10. Auto-oxidation of aldehydes by molecular oxygen. Radical abstraction of aldehyde hydrogen results in carbonyl radical species, which can then interact with molecular oxygen to form a peroxyacid. This can then react with further aldehydes to give multiple equivalents of carboxylic acid.[19a]

A less commonly encountered mode of aldehyde reaction is oxidative decarbonylation to release of the aldehyde carbon as formate. A well-studied example is the deformylation of cyclohexane carbaldehyde by metal peroxides that has been shown to proceed by an eliminative mechanism that results in the formation of cyclohexene and formate.[23] Enzymatic reactions that liberate formate include the P450-dependent deformylation of cyclohexane carbaldehyde catalyzed by CYP2B4 and the aromatization reaction of androst-4-ene-3,17-dione to estrone catalyzed by aromatase.[24] Under reductive conditions this deformylation pathway can lead to the formation of alkanes, rather than alkenes. This was recently demonstrated for an iron(III)peroxo complex that under reducing conditions effectively deformylated phenylpropionaldehyde to yield

formate and ethylbenzene.[7k] This reaction mimics that of cyanobacterial aldehyde deformylating oxygenase (cADO), in which the intermediate alkyl radical, formed after release of the aldehyde carbon as formate, is reduced to form the alkane product.[4, 7a, 7e, 7i]

4.4. Conclusions

These studies on an α-cyclopropyl-aldehyde originally designed as a mechanistic probe of the reaction catalyzed by cADO have uncovered a novel mode of a non-enzymatic deformylation that occurs in the presence of Fe^{2+} and O_2. Computational reaction pathway searches identified a plausible mechanistic pathway that is in accord with isotope-labeling studies. The discussion above suggests how the cyclopropyl group may fine-tune the energetics of the reaction to favor deformylation over oxidation. It may be possible to incorporate more sophisticated stereo-electronic control into the design of either the substrate aldehyde or iron complex to bias the reaction further in favor of deformylation. I propose that the cyclopropyl group may influence the reaction pathway in two ways. First, the well-established electron-withdrawing nature of the cyclopropyl group[25] would make the aldehyde more electrophilic, thereby facilitating the formation of the initial metal-peroxyhemiacetal complex, **B** in Figure 4.8. DFT calculations support this notion and indicate that the transition state for metal-peroxyacetal formation is about 2 kcal*mol^{-1} lower for **1** than for dodecanal (Figure 4.9). Metal-peroxyhemiacetal formation is not required for carboxylic acid formation, as this can proceed through direct abstraction of the aldehyde hydrogen by the metal-peroxide complex.[19b, 26]

Second, the positioning of the cyclopropyl group does not allow a radical α-elimination mechanism to operate that would result in the formation of formate and an

alkene, as is seen for the oxidative deformylation of cyclohexane carbaldehyde.[7e] Moreover, formation of the postulated cyclopropyl radical is energetically very unfavorable; therefore the formyl radical formed in step **C** is likely insufficiently reactive undergo C–C bond cleavage to release formate as occurs in the reaction of cyclohexane carbaldehyde.[23] Instead, hydrogen abstraction from the acetal oxygen by the high-valent iron-oxo species is presumed to provide the energetic driving force for the reaction. The acetal di-radical species thus formed would be expected to break down rapidly to give formyl and cyclopropyl radicals, at which point the cyclopropyl radical would be perfectly positioned to abstract the formyl hydrogen. This would result in the energetically favorable formation of CO_2 and transfer of the aldehyde hydrogen to the cyclopropyl group.

The arguments advanced suggest how the cyclopropyl group may fine-tune the energetics of the reaction to favor deformylation over oxidation. In the context of understanding enzymatic deformylation reactions, which was the initial impetus for these studies, it is noted that an enzyme could affect more precise stereo-electronic control of the reaction pathway. First, the electrophilicity of the aldehyde could be increased by various mechanisms such as general or Lewis acid catalysis. Second, by controlling the orientation of the substrate with respect to the iron center, hydrogen atom abstraction by the reactive iron-oxo species could be directed towards the acetal O-H bond and away from the aldehyde C-H bond and C-H bonds on the α-carbon. These studies provide further insight into how enzymes may control reactive iron-oxo species to catalyze the diverse range of iron-dependent oxidative transformations observed in biology.

4.5 References

1. Hrycay, E.; Bandiera, S., Monooxygenase, Peroxidase and Peroxygenase Properties and Reaction Mechanisms of Cytochrome P450 Enzymes. In *Monooxygenase, Peroxidase and Peroxygenase Properties and Mechanisms of Cytochrome P450*, Hrycay, E. G.; Bandiera, S. M., Eds. Springer International Publishing: 2015; Vol. 851, pp 1-61.

2. Kovaleva, E. G.; Lipscomb, J. D., Versatility of biological non-heme Fe(II) centers in oxygen activation reactions. *Nat. Chem. Biol.* **2008,** *4* (3), 186-93.

3. Merkx, M.; Kopp, D. A.; Sazinsky, M. H.; Blazyk, J. L.; Muller, J.; Lippard, S. J., Dioxygen Activation and Methane Hydroxylation by Soluble Methane Monooxygenase: A Tale of Two Irons and Three Proteins. *Angew. Chem., Int. Ed. Engl.* **2001,** *40*, 2782-2807.

4. Schirmer, A.; Rude, M. A.; Li, X.; Popova, E.; Cardayre, S. B., Microbial Biosynthesis of Alkanes. *Science* **2010,** *329*, 559-562.

5. Cascella, B.; Mirica, L. M., Kinetic analysis of iron-dependent histone demethylases: alpha-ketoglutarate substrate inhibition and potential relevance to the regulation of histone demethylation in cancer cells. *Biochemistry* **2012,** *51* (44), 8699-701.

6. (a) Liu, P.; Murakami, K.; Seki, T.; He, X.; Yeung, S.-M.; Kuzuyama, T.; Seto, H.; Liu, H., Protein Purification and Function Assignment of the Epoxidase Catalyzing the Formation of Fosfomycin. *J. Am. Chem. Soc.* **2001,** *123*, 4619-4620; (b) Liu, P.; Liu, A.; Yan, F.; Wolfe, M. D.; Lipscomb, J. D.; Liu, H., Biochemical and Spectroscopic Studies on (S)-2-Hydroxypropylphosphonic Acid Epoxidase: A Novel Mononuclear Non-heme Iron Enzyme. *Biochemisty* **2003,** *42*, 11577-11586.

7. (a) Marsh, E. N.; Waugh, M. W., Aldehyde Decarbonylases: Enigmatic Enzymes of Hydrocarbon Biosynthesis. *ACS Catal.* **2013,** *3* (11); (b) Andre, C.; Kim, S. W.; Yu, X.-H.; Shanklin, J., Fusing catalase to an alkane-producing enzyme maintains enzymatic activity by converting the inhibitory byproduct H2O2 to the cosubstrate O2. *Proc. Natl. Acad. Sci.* **2013,** *110* (8), 3191-3196; (c) Aukema, K. G.; Makris, T. M.; Stoian, S. A.; Richman, J. E.; Münck, E.; Lipscomb, J. D.; Wackett, L. P., Cyanobacterial aldehyde deformylase oxygenation of aldehydes yields n-1 aldehydes and alcohols in addition to alkanes. *ACS Catal.* **2013,** *3* (10), 2228-2238; (d) Buer, B. C.; Paul, B.; Das, D.; Stuckey, J. A.; Marsh, E. N. G., Insights into Substrate and Metal Binding from the Crystal Structure of Cyanobacterial Aldehyde Deformylating Oxygenase with Substrate Bound. *ACS Chem. Biol.* **2014,** *9* (11), 2584-2593; (e) Das, D.; Ellington, B.; Paul, B.; Marsh, E. N., Mechanistic insights from reaction of alpha-oxiranyl-aldehydes with cyanobacterial aldehyde deformylating oxygenase. *ACS Chem. Biol.* **2014,** *9* (2), 570-7; (f) Das, D.; Eser, B. E.; Han, J.; Sciore, A.; Marsh, E. N. G., Oxygen-Independent Decarbonylation of Aldehydes by Cyanobacterial Aldehyde Decarbonylase: A New Reaction of Diiron Enzymes. *Angew. Chem., Int. Ed. Engl.* **2011,** *50* (31), 7148-7152; (g) Li, N.; Nørgaard,

H.; Warui, D. M.; Booker, S. J.; Krebs, C.; Bollinger, J. M., Conversion of Fatty Aldehydes to Alka(e)nes and Formate by a Cyanobacterial Aldehyde Decarbonylase: Cryptic Redox by an Unusual Dimetal Oxygenase. *J. Am. Chem. Soc.* **2011,** *133* (16), 6158-6161; (h) Pandelia, M. E.; Li, N.; Nørgaard, H.; Warui, D. M.; Rajakovich, L. J.; Chang, W.-c.; Booker, S. J.; Krebs, C.; Bollinger, J. M., Substrate-Triggered Addition of Dioxygen to the Diferrous Cofactor of Aldehyde-Deformylating Oxygenase to Form a Diferric-Peroxide Intermediate. *J. Am. Chem. Soc.* **2013,** *135* (42), 15801-15812; (i) Paul, B.; Das, D.; Ellington, B.; Marsh, E. N., Probing the mechanism of cyanobacterial aldehyde decarbonylase using a cyclopropyl aldehyde. *J. Am. Chem. Soc.* **2013,** *135* (14), 5234-7; (j) Rajakovich, L. J.; Nørgaard, H.; Warui, D.; Chang, W.-c.; Li, N.; Booker, S. J.; Krebs, C.; Bollinger, J. M.; Pandelia, M.-E., Rapid Reduction of the Diferric-Peroxyhemiacetal Intermediate in Aldehyde-Deformylating Oxygenase by a Cyanobacterial Ferredoxin: Evidence for a Free-Radical Mechanism. *J. Am. Chem. Soc.* **2015**; (k) Shokri, A.; Que, L., Jr., Conversion of Aldehyde to Alkane by a Peroxoiron(III) Complex: A Functional Model for the Cyanobacterial Aldehyde-Deformylating Oxygenase. *J. Am. Chem. Soc.* **2015,** *137* (24), 7686-91; (l) Waugh, M. W.; Marsh, E. N. G., Solvent Isotope Effects on Alkane Formation by Cyanobacterial Aldehyde Deformylating Oxygenase and Their Mechanistic Implications. *Biochemistry* **2014,** *53* (34), 5537-5543.

8. (a) Jensen, K. B.; McKenzie, C. J.; Nielsen, L. P.; Pedersen, J. Z.; Svendsen, H. M., Deprotonation of low-spin mononuclear iron(III)-hydroperoxide complexes give transient blue species assigned to high-spin iron(III)-peroxide complexes. *Chem. Commun.* **1999,** (14), 1313-1314; (b) Annaraj, J.; Suh, Y.; Seo, M. S.; Kim, S. O.; Nam, W., Mononuclear nonheme ferric-peroxo complex in aldehyde deformylation. *Chem. Commun.* **2005,** (36), 4529-31; (c) Cho, J.; Jeon, S.; Wilson, S. A.; Liu, L. V.; Kang, E. A.; Braymer, J. J.; Lim, M. H.; Hedman, B.; Hodgson, K. O.; Valentine, J. S.; Solomon, E. I.; Nam, W., Structure and reactivity of a mononuclear non-haem iron(III)-peroxo complex. *Nature* **2011,** *478* (7370), 502-5; (d) Shan, X.; Rohde, J.; Koehntop, K. D.; Zhou, Y.; Bukowski, M. R.; Costas, M.; Fujisawa, K.; Que, L., Jr., X-ray Absorption Spectroscopic Studies of High-Spin Nonheme (Alkylperoxo)iron(III) Intermediates. *Inorg. Chem.* **2007,** *46*, 8410-8417.

9. Goh, Y. M.; Nam, W., Significant Electronic Effect of Porphyrin Ligand on the Reactivities of High-Valent Iron(IV) Oxo Porphyrin Cation Radical Complexes. *Inorg. Chem.* **1999,** *38* (5), 914-920.

10. Pirovano, P.; Magherusan, A. M.; McGlynn, C.; Ure, A.; Lynes, A.; McDonald, A. R., Nucleophilic reactivity of a copper(II)-superoxide complex. *Angew. Chem., Int. Ed. Engl.* **2014,** *53* (23), 5946-50.

11. (a) Reed, J. R.; Vanderwel, D.; Choi, S.; Pomonis, J. G.; Reitz, R. C.; Blomquist, G. J., Unusual mechanism of hydrocarbon formation in the housefly: Cytochrome P450 converts aldehyde to the sex pheromone component (Z)-9-tricosene and CO2. *Proc. Natl. Acad. Sci.* **1994,** *91*, 10000-10004; (b) Qiu, Y.; Tittiger, C.; Wicker-Thomas, C.; Le Goff, G.; Young, S.; Wajnberg, E.; Fricaux, T.; Taquet, N.; Blomquist, G. J.; Feyereisen, R., An

insect-specific p450 oxidative decarbonylase for cuticular hydrocarbon biosynthesis. *Proc. Natl. Acad. Sci.* **2012,** *109* (37), 14858-14863.

12. Hudlicky, M., An improved apparatus for the laboratory preparation of diazomethane. *J. Org. Chem.* **1980,** *45* (26), 5377-5378.

13. Perdew, J. P.; Burke, K.; Ernzerhof, M., Generalized Gradient Approximation Made Simple. *Phys. Rev. Lett.* **1996,** *77* (18), 3865-3868.

14. Rassolov, V. A.; Pople, J. A.; Ratner, M. A.; Windus, T. L., 6-31G* basis set for atoms K through Zn. *J. Chem. Phys.* **1998,** *109* (4), 1223-1229.

15. Marenich, A. V.; Cramer, C. J.; Truhlar, D. G., Universal Solvation Model Based on Solute Electron Density and on a Continuum Model of the Solvent Defined by the Bulk Dielectric Constant and Atomic Surface Tensions. *J. Phys. Chem. B* **2009,** *113* (18), 6378-6396.

16. (a) Zimmerman, P. M., Automated discovery of chemically reasonable elementary reaction steps. *J. Comput. Chem.* **2013,** *34* (16), 1385-1392; (b) Zimmerman, P. M., Navigating molecular space for reaction mechanisms: an efficient, automated procedure. *Mol. Simul.* **2014,** *41* (1-3), 43-54.

17. (a) Zimmerman, P. M., Growing string method with interpolation and optimization in internal coordinates: Method and examples. *J. Chem. Phys.* **2013,** *138* (18), 184102; (b) Zimmerman, P. M., Reliable Transition State Searches Integrated with the Growing String Method. *J. Chem. Theory Comput.* **2013,** *9* (7), 3043-3050; (c) Zimmerman, P. M., Single-ended transition state finding with the growing string method. *J. Comput. Chem.* **2015,** *36* (9), 601-611.

18. Nett, A. J.; Zhao, W.; Zimmerman, P. M.; Montgomery, J., Highly Active Nickel Catalysts for C–H Functionalization Identified through Analysis of Off-Cycle Intermediates. *J. Am. Chem. Soc.* **2015,** *137* (24), 7636-7639.

19. (a) McNesby, J. R.; Heller, C. A., Oxidation of Liquid Aldehydes by Molecular Oxygen. *Chem. Rev.* **1954,** *54* (2), 325-346; (b) Chudasama, V.; Fitzmaurice, R. J.; Caddick, S., Hydroacylation of a,b-unsaturated esters via aerobic C–H activation. *Nat. Chem.* **2010,** *2*, 592-596.

20. Reed, J. R.; Quilici, D. R.; Blomquist, G. J.; Reitz, R. C., Proposed Mechanism for the Cytochrome P450-Catalyzed Conversion of Aldehydes to Hydrocarbons in the House Fly, Musca domestica. *Biochemisty* **1995,** *34*, 16221-16227.

21. Rat, S.; Menage, S.; Thomas, F.; Niviere, V., Non-heme iron hydroperoxo species in superoxide reductase as a catalyst for oxidation reactions. *Chem. Commun.* **2014,** *50*, 14213-14216.

22. Walling, C., Autoxidation. In *Active Oxygen in Chemistry*, Foote, C.; Valentine, J.; Greenberg, A.; Liebman, J., Eds. Springer Netherlands: 1995; Vol. 2, pp 24-65.

23. Vaz, A. D.; Pernecky, S. J.; Raner, G. M.; Coon, M. J., Peroxo-iron and oxenoid-iron species as alternative oxygenating agents in cytochrome P450-catalyzed reactions: switching by threonine-302 to alanine mutagenesis of cytochrome P450 2B4. *Proc. Natl. Acad. Sci.* **1996,** *93* (10), 4644-4648.

24. (a) Meunier, B.; de Visser, S. P.; Shaik, S., Mechanism of oxidation reactions catalyzed by cytochrome p450 enzymes. *Chem. Rev.* **2004,** *104* (9), 3947-80; (b) Newcomb, M.; Hollenberg, P. F.; Coon, M. J., Multiple mechanisms and multiple oxidants in P450-catalyzed hydroxylations. *Arch. Biochem. Biophys.* **2003,** *409* (1), 72-79.

25. Parker, W., *Alicyclic Chemistry*. Royal Society of Chemistry: 1975.

26. van der Donk, W. A.; Krebs, C.; Bollinger, J. M., Substrate activation by iron superoxo intermediates. *Curr. Opin. Struct. Biol.* **2010,** *20* (6), 673-683.

Chapter 5

Conclusions and Future Directions

5.1 Conclusions

The discovery of the soluble, stable cyanobacterial aldehyde decarbonylase (cADO) that was amenable to heterologous expression and purification was met with keen interest by the scientific community. At last, *in vitro* characterization of an enzyme responsible for hydrocarbon biosynthesis could be accomplished, greatly advancing understanding of biofuel production and aiding the push for renewable energy. Early studies demonstrated cADO to be a small (29kDa) 4-helix bundle protein in the di-iron oxygenase family of enzymes, including methane monooxygenase, ferritin and class 1 ribonucleotide reductase.[1] cADO utilizes molecular oxygen, aldehydes of varying chain length and 4 electrons from an external reducing system to catalyze a redox-neutral deformylation, producing formate and n-1 alkanes.[1c, 2] Further mechanistic characterizations have spectroscopically identified a stable peroxy-hemiacetal as a key intermediate in the mechanism of catalysis.[3] In our laboratory, Dr. Matthew Waugh identified an iron-bound water as the source of the proton electron transfer that quenches the alkyl species and determined the solvent isotope effect associated with this step.[4] Multiple crystal structures of cADO have been solved, identifying multiple modes of substrate binding, possible candidates for mutagenic studies, and modes of active site access for water.[5] Despite such advances, much remained to be understood about just

how the decarbonylation of aldehydes was accomplished in Nature. In particular, the nature and stereospecificity of the C-C bond scission step remained undetermined, and little mechanistic characterization of the other aldehyde decarbonylase enzymes had yet been accomplished.

5.1.1 cADO Effects the Homolytic Scission of the C_α-CO Bond

Though the products of the cADO-catalyzed deformylation of aldehydes were known, whether the key C-C bond scission proceeded via homolysis or heterolysis had yet to be determined. Early EPR work indicated the presence of a radical intermediate in the reaction via trapping,[6] but a conflicting study suggested heterolysis to account for the side reaction of cADO therein studied. Through the use of a β-cyclopropyl aldehyde radical clock, we demonstrated that deformylation proceeded through C-C bond homolysis, as evidenced by the sole production of soluble octadecene through radical ring opening. Because no enzyme-based non-rearranged product was detected, the lifetime of the formed cyclopropylcarbinyl radical was calculated to be ≥10 ns.[7]

In order to address this, further studies utilizing an α-oxiranyl aldehyde radical clock were performed. Because the oxiranyl group better stabilizes radicals than cyclopropyl functionalities, this substrate allowed us to more accurately probe the lifetime of the species resulting from C-C bond hemolysis. By measuring the partitioning between non-rearranged and rearranged products of cADO-catalyzed deformylation, we were able to determine that lifetime of the formed alkyl radical is between 10-100μs.[8]

5.1.2 Stabilization of the Alkyl Radical in the Active Site is Necessary for Enzyme Stability

Despite yielding useful information as to the nature of C-C bond scission by cADO, the β-cyclopropyl aldehyde species acted as a mechanism-based inhibitor of the enzyme. No more than 1 turnover was ever observed with the substrate, with the enzyme incapable of further catalysis thereafter. In order to understand this unusual behavior, we subjected cADO to MS analysis before and after inactivation by the β-cyclopropyl substrate. Between 60-80% of inactive enzyme was found to contain a 251 Da covalent modification corresponding to the deformylated substrate. Further analysis identified a phenylalanine residue in the hydrophobic binding pocket as the site of covalent modification, relatively far removed from the diiron active site.[7] The remainder of the enzyme sample, despite showing no evidence of covalent modification, was similarly inactive.

We reasoned that the radical opening of the cyclopropyl ring, which moved the alkyl radical from C1 to C4 of the molecule, interacted with cADO in one of 3 ways. The radical could either be A) quenched by a solvent-exchangeable amino acid side chain, resulting in soluble 1-octadecene and active enzyme; B) covalently modify cADO and thereby inactivate it; or C) radically abstract a hydrogen from a non-exchangeable group in cADO, resulting in soluble product and an enzyme radical which could cross-link and inhibit catalysis. Thus it was determined that confinement of formed radical species to the diiron active site of cADO is necessary to maintain active enzyme. Exposure of the substrate binding pocket, even only a few Ångstroms removed from the diiron center, compromises the stability of cADO.

5.1.3 Radical Quenching by Electron Proton Transfer is Stereorandom

In addition to elucidating the rate constant for electron proton transfer, the α-oxiranyl aldehyde species allowed us to probe the stereospecificity of the very same step. Through isotopic labeling and NMR analysis, it was determined that the proton could be added to either face of the oxirane ring with equal probability. This indicated that the oxiranyl radical formed after homolysis was free to rotate within the active site during reaction.[8] From this, we could conclude that enzymatic hydrocarbon production from aldehydes is not strongly dependent on tight, static substrate orientation within the active site in cyanobacteria. Proton electron transfer was equally favoured on both sides of the oxiranyl species after C-C bond homolysis.

5.1.4 Aldehyde Decarbonylation by CYP4G1 Depends on Stereo-Electronic Control of the Substrate

Building on the mechanistic details gleaned from our previous substrates, we synthesized an α-cyclopropyl aldehyde radical clock to investigate the stereochemistry of electron proton addition after bond homolysis without the multiple rearrangements seen in the oxiranyl substrate. To our surprise, decarbonylation of the substrate was nonenzymatic and required only Fe^{2+} and O_2. Through isotopic labelling, we determined that this decarbonylation produced CO_2 and exhibited retention of the aldehyde hydrogen in the n-1 alkane. Unlike cADO, this nonenzymatic system mimicked what little was known of the insect cytochrome P450 decarbonylase, CYP4G1.[9] Testing of the related α-oxiranyl and alkyl species showed that the decarbonylation was unique to the α-cyclopropyl moiety.

In order to glean some understanding of how the group in the cyclopropyl position rendered aldehydes amenable to such a novel decarbonylation, we utilized a computational approach through collaboration with Prof. Paul Zimmerman and Mr. Andrew Vitek. Mechanistic simulations provided an energetically feasible mechanism for the reaction (and so a reasonable understanding of CYP4G1 catalysis), and partitioning between oxidation and decarbonylation correlated to the electronic properties of the carbonyl carbon. While the electron-donating nature of the oxiranyl species and the neutral nature of the alkyl species allowed only for oxidation, the electron-withdrawing nature of the cyclopropyl group resulted in a more electrophilic aldehyde group, resulting in partial decarbonylation. Thus we were able to conclude that CYP4G1 likely exerts stereo-electronic control over the substrate aldehydes to increase the electrophilicity of the carbonyl carbon, thus diverting from standard P450 chemistry and catalyzing the observed oxidative decarbonylation.

5.2 Future Directions

As recent studies continue to expand our understanding of the manner in which enzymes might catalyze decarbonylation, and thus produce biofuels, we must turn our eyes towards industrial applications. Due to its inherently sluggish, and heretofore insufficiently understood nature, cADO is unlikely to be of great importance in the development of large-scale microbial alkane production. As such, I would not continue the study of cADO for its industrial applications, but instead purely to further understanding of enzyme-catalyzed decarbonylation of aldehydes. The many insights into biochemical aldehyde decarbonylation gleaned from its study, however, will be of

great use in protein and pathway engineering in years to come. For industrial application, I would instead continue to characterize enzymes implicated in hydrocarbon production, and look for much higher basal activity rates, such as that found with the P450 decarboxylase, $OleT_{JE}$.

5.2.1 Further Characterization of cADO

Although significant work by our laboratory and others focusing on cADO has established a strong, well-supported mechanism to explain aldehyde decarbonylation by cADO, much remains in question about this most unusual enzyme. Two questions in particular need be answered before further work can implement aldehyde decarbonylation in a system for maximized hydrocarbon production; first, why is overall turnover by cADO so sluggish, when the individually studied steps are so rapid, and second, how does cADO direct transition metal chemistry towards decarbonylation rather than the more common hydroxylation reactions based in iron chemistry?

To address the first question, we need to look more closely at cADO conformational dynamics and how substrate interacts with the enzyme. Long chain fatty aldehydes have poor solubilities, and necessitate the use of DMSO in our systems. Genetic studies and pull-down assays could be utilized to search for biological substrate delivery systems, which could help to increase the measured rate of cADO *in vivo*. Early NMR studies of cADO were inconclusive, but did indicate that cADO is a highly dynamic protein based on significant line broadening in all conditions tested. Substrate analogues designed for increased solubility could increase the frequency with which cADO interacts

with, and binds, substrate molecules and further investigate the source of the sluggish nature of aldehyde decarbonylation by this enzyme.

While initial interest in cADO stemmed primarily from its potential as a biofuel production system, the unusual nature of the chemistry catalyzed thereby has maintained interest in the enzyme despite its poor activity. The majority of enzyme catalysis using transition metal ligands centers around oxidation reactions, and the structurally similar methane monooxygnease (MMO) directly oxidizes methane to produce methanol in a very well-characterized reaction. Unlike this and other iron-based enzymes, cADO catalyzes the redox-neutral deformylation of aldehyde substrates. In order to understand this, Dr. Matthew Waugh began work on electrochemical characterization of the diiron site in cADO, but initial studies were inconclusive. By studying the reduction potential of the iron site in cADO in comparison to that in similar proteins with different catalyses, we might better understand how to direct oxidative chemistry towards hydrocarbon production. Further characterization by Electron Paramagnetic Resonance and Mössbauer spectroscopy could additionally aide in our understanding of decarbonylation.

5.2.2 Protein Engineering

With the ever-accelerating advancement of computing technology, great strides have been made in the field of bioinformatics and, in particular, in protein structure and function prediction. It is now feasible to accurately predicting protein structure and function based purely on primary amino acid sequence, as well as utilizing such knowledge in *de novo* enzyme design and synthesis. The CASP protein structure and function prediction competition has done much to accelerate the development of software

aimed towards structural and functional predictions based entirely on peptide sequence, and our understanding of this field grows with each passing year. Utilizing the knowledge of biochemical decarbonylation gained from X-ray structures of cADO and related enzymes lacking the same function, spectroscopic studies of decarbonylases and the work described in this thesis, the goal of designing a stable enzyme for decarbonylation lacking the inherent issues associated with known aldehyde decarbonylases might at last be realized. Work by the Bollinger laboratory, as well as recent electrochemical data obtained by Dr. Matthew Waugh, has amply demonstrated that the chemical steps accomplished by cADO are quite fast, while the overall activity exhibited by the enzyme is surprisingly slow. I believe that the primary inhibitor of cADO activity is the unwieldy, hydrophobic nature of the currently-studied substrate and its likely tendency to prefer the substrate binding channel of cADO to the aqeous environment to which it is ideally released. By working to design a protein optimized for substrate binding/product release, electron flow, and radical decarbonylation, we might at last produce an enzyme of great use in industrial-scale hydrocarbon biosynthesis.

5.2.3 Substrate Analogue Studies of $OleT_{JE}$

First discovered in 2011 by the Schirmer Laboratory, $OleT_{JE}$ catalyzes the direct decarboxylation of fatty acids to yield 1-alkene products.[10] Though technically a peroxygenase in the P450 family, a recent work demonstrated that, through fusion with a reductase domain, decarboxylation could be driven by NADPH alone.[11] This makes $OleT_{JE}$ a highly attractive target for biological hydrocarbon production. Such a system would remove the necessity of engineering a cell line for reduction of fatty acids to their

corresponding fatty aldehydes, greatly reducing the metabolic burden placed upon the cell. In addition, the apparent activity of the enzyme is much higher than that of previously studied decarbonylases. While the basic characterization of the enzyme has already been largely accomplished, the mechanism by which its heme-based decarboxylation is carried out has yet to be explored.

5.3 References

1. (a) Khara, B.; Menon, N.; Levy, C.; Mansell, D.; Das, D.; Marsh, E. N. G.; Leys, D.; Scrutton, N. S., Production of Propane and Other Short-Chain Alkanes by Structure-Based Engineering of Ligand Specificity in Aldehyde-Deformylating Oxygenase. *Chembiochem* **2013,** *14* (10), 1204-1208; (b) Krebs, C.; Bollinger, J. M.; Booker, S. J., Cyanobacterial alkane biosynthesis further expands the catalytic repertoire of the ferritin-like "di-iron-carboxylate" proteins. *Current opinion in chemical biology* **2011,** *15* (2), 291-303; (c) Wallar, B. J.; Lipscomb, J. D., Dioxygen Activation by Enzymes Containing Binuclear Non-Heme Iron Clusters. *Chemical Reviews* **1996,** *96* (7), 2625-2658.

2. (a) Blazyk, J. L.; Gassner, G. T.; Lippard, S. J., Intermolecular Electron-Transfer Reactions in Soluble Methane Monooxygenase: A Role for Hysteresis in Protein Function. *Journal of the American Chemical Society* **2005,** *127* (49), 17364-17376; (b) Li, N.; Nørgaard, H.; Warui, D. M.; Booker, S. J.; Krebs, C.; Bollinger, J. M., Conversion of Fatty Aldehydes to Alka(e)nes and Formate by a Cyanobacterial Aldehyde Decarbonylase: Cryptic Redox by an Unusual Di-metal Oxygenase. *Journal of the American Chemical Society* **2011,** *133* (16), 6158-6161.

3. Pandelia, M. E.; Li, N.; Nørgaard, H.; Warui, D. M.; Rajakovich, L. J.; Chang, W.-c.; Booker, S. J.; Krebs, C.; Bollinger, J. M., Substrate-Triggered Addition of Dioxygen to the Diferrous Cofactor of Aldehyde-Deformylating Oxygenase to Form a Diferric-Peroxide Intermediate. *J. Am. Chem. Soc.* **2013,** *135* (42), 15801-15812.

4. Waugh, M. W.; Marsh, E. N. G., Solvent Isotope Effects on Alkane Formation by Cyanobacterial Aldehyde Deformylating Oxygenase and Their Mechanistic Implications. *Biochemistry* **2014,** *53* (34), 5537-5543.

5. Buer, B. C.; Paul, B.; Das, D.; Stuckey, J. A.; Marsh, E. N. G., Insights into Substrate and Metal Binding from the Crystal Structure of Cyanobacterial Aldehyde Deformylating Oxygenase with Substrate Bound. *ACS Chem. Biol.* **2014,** *9* (11), 2584-2593.

6. Das, D.; Eser, B. E.; Han, J.; Sciore, A.; Marsh, E. N. G., Oxygen-Independent Decarbonylation of Aldehydes by Cyanobacterial Aldehyde Decarbonylase: A New Reaction of Diiron Enzymes. *Angew. Chem., Int. Ed. Engl.* **2011,** *50* (31), 7148-7152.

7. Paul, B.; Das, D.; Ellington, B.; Marsh, E. N., Probing the mechanism of cyanobacterial aldehyde decarbonylase using a cyclopropyl aldehyde. *J. Am. Chem. Soc.* **2013,** *135* (14), 5234-7.

8. Das, D.; Ellington, B.; Paul, B.; Marsh, E. N., Mechanistic insights from reaction of alpha-oxiranyl-aldehydes with cyanobacterial aldehyde deformylating oxygenase. *ACS Chem. Biol.* **2014,** *9* (2), 570-7.

9. (a) Reed, J. R.; Quilici, D. R.; Blomquist, G. J.; Reitz, R. C., Proposed Mechanism for the Cytochrome P450-Catalyzed Conversion of Aldehydes to Hydrocarbons in the House Fly, Musca domestica. *Biochemisty* **1995,** *34*, 16221-16227; (b) Reed, J. R.; Vanderwel, D.; Choi, S.; Pomonis, J. G.; Reitz, R. C.; Blomquist, G. J., Unusual mechanism of hydrocarbon formation in the housefly: Cytochrome P450 converts aldehyde to the sex pheromone component (Z)-9-tricosene and CO2. *Proc. Natl. Acad. Sci.* **1994,** *91*, 10000-10004.

10. Rude, M. A.; Baron, T. S.; Brubaker, S.; Alibhai, M.; Del Cardayre, S. B.; Schirmer, A., Terminal Olefin (1-Alkene) Biosynthesis by a Novel P450 Fatty Acid Decarboxylase from Jeotgalicoccus Species. *Applied and Environmental Microbiology* **2011,** *77* (5), 1718-1727.

11. Liu, Y.; Wang, C.; Yan, J.; Zhang, W.; Guan, W.; Lu, X.; Li, S., Hydrogen peroxide-independent production of α-alkenes by OleT(JE) P450 fatty acid decarboxylase. *Biotechnology for Biofuels* **2014,** *7*, 28-28.

Appendices

Appendix A

Syntheses for Chapter 2

Synthesis of 2-(2-tetradecylcyclopropyl)acetaldehyde (6)

Synthesis of the β-cyclopropyl octadecanal substrate was carried out by Dr. Bishwajit Paul as Described in Figure A.1. Synthesis of individual species is described below.

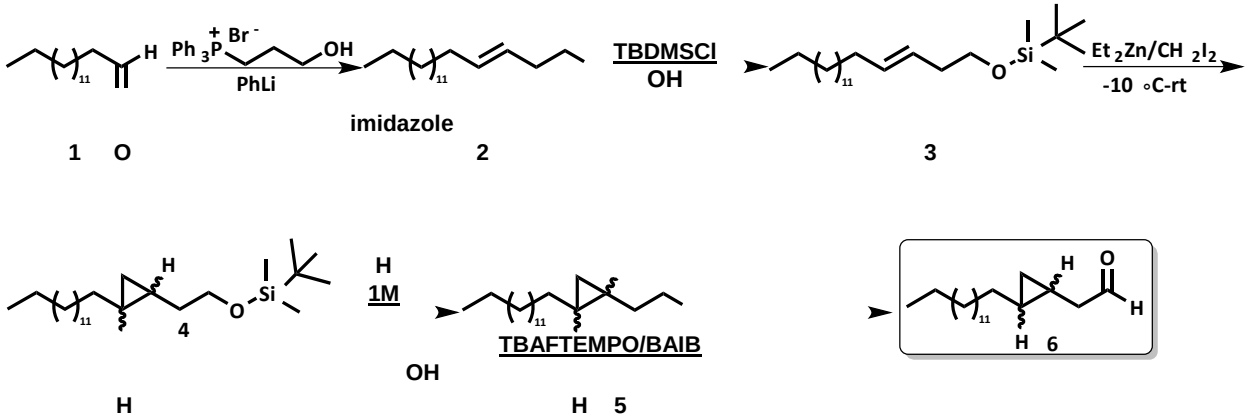

Figure A.1. Synthesis of 2-(2-tetradecylcyclopropyl)acetaldehyde (**6**)

Synthesis of Pentadecanal (1)

Oxidation of 1-pentadecanol to pentadecanal **(1)** was performed using TEMPO/BAIB strategy according to a literature procedure.[1] To a solution of 1-pentadecanol (1 g, 4.4 mmol) were added (2,2,6,6-Tetramethylpiperidin-1yl)oxyl (TEMPO, 68.6 mg, 0.44 mmol) and bis(acetoxy)iodobenzene (BAIB, 1.7 g, 5.3 mmol) in dichloromethane at room temperature. The reaction was stirred at room

temperature for 3 hours. The solvent was removed under reduced pressureusing a rotatory evaporator and the crude mixture was applied to a silica-gel column equilibrated in n-hexane. The column was developed by slowly increasing the polarity of the solvent using a gradient of 0 to 1 % ethylacetate in hexane to obtain **1** (850 mg, 85%). The compound was pure as judged by NMR (Figure A.2). ^{1}H NMR (400 MHz, $CDCl_3$) δ 9.84 (t, *J* = 6.8 Hz, 1H), 2.47 (t, *J* = 6.8 Hz, 2H), 1.40 (t, *J* = 7.2 Hz, 22H), 1.38-1.32 (m, 22H), 0.94 (t, *J* = 6.8 Hz, 3H). ^{13}C NMR (100 MHz, $CDCl_3$), δ 202.92, 43.89, 31.89,
29.65, 29.63, 29.62, 29.61, 29.55, 29.40, 29.35, 29.33, 29.14, 22.66, 22.06, 14.09.

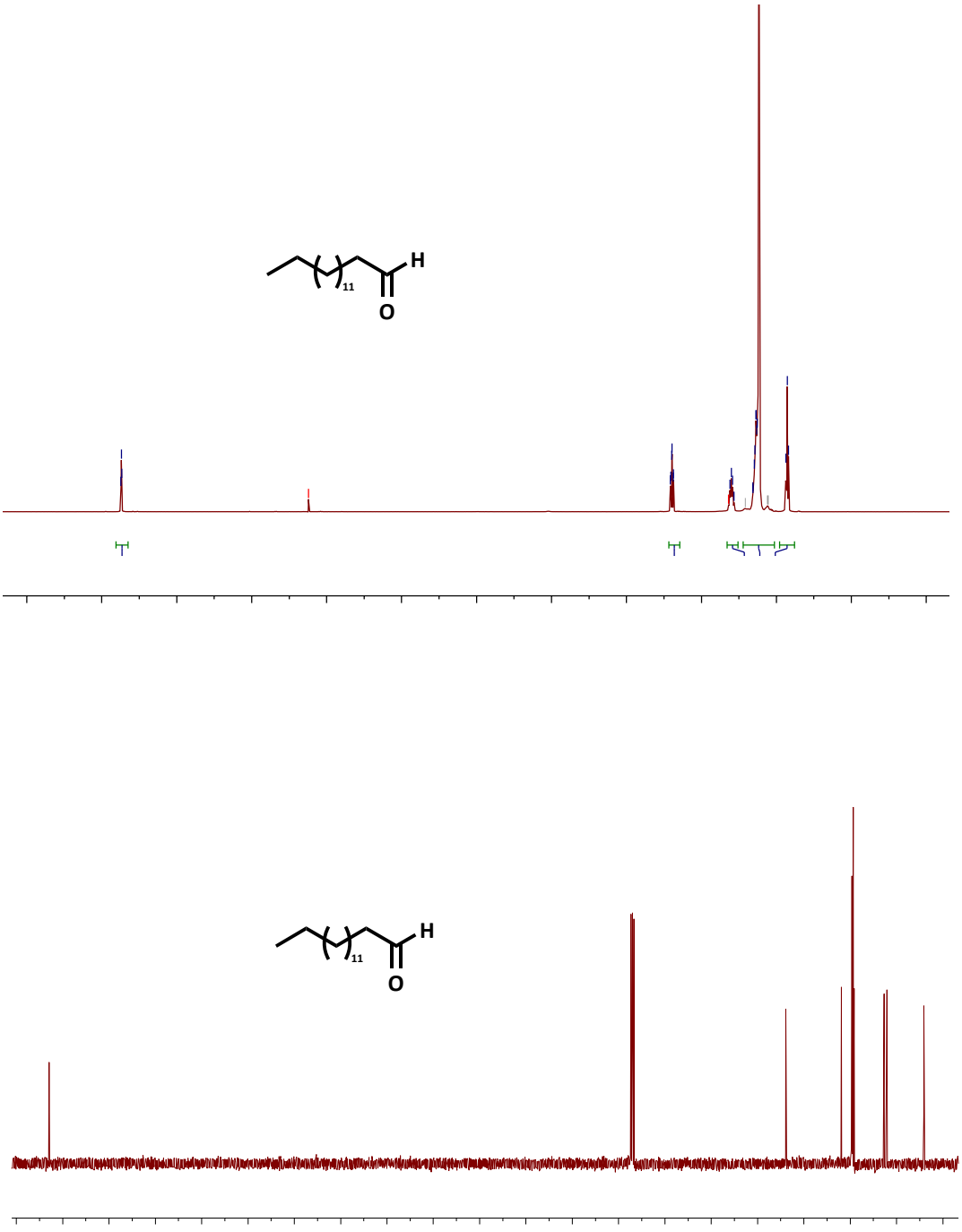

Figure A.2. ^{1}H and ^{13}C NMR spectrum of compound **1** in CDCl3.

Synthesis of *trans*-octadec-3-en-1-ol (2)

The Wittig reaction of **1** with 3hydroxypropyl-triphenylphosphosonium bromide was performed according to a literature procedure.[2] To a suspension of 3-hydroxypropyl-triphenylphosphosonium bromide (2 g, 4.98 mmol) in tetrahydrofuran (THF), 1.5 equivalents (3.7 ml) of phenyllithium (1.2 M dissolved THF) was added dropwise under nitrogen at room temperature. The reaction was stirred at room temperature for 30 min. The reaction mixture was cooled to -78 °C in a dry ice/acetone mixture bath for 15 min, followed by dropwise addition of pentadecanal (563 mg, 2.5 mmol) (**1**) (dissolved in minimum volume of THF). After the addition was complete, the reaction mixture was warmed to -30 °C, followed by addition of 0.5 equivalent of phenyl lithium (1.2 ml) to obtain predominantly the *trans*-product**.** The reaction was allowed to warm to room temperature with stirring over 30 min. Finally, the reaction was cooled to -78 °C and quenched by addition of 1.8 ml 6M hydrochloric acid and 5 ml of water. After warming to room temperature the aqueous phase was extracted with diethyl ether (3 x 20 ml), washed with brine, dried over sodium sulphate and concentrated under reduced pressure by rotatory evaporator. The crude mixture was subjected to silica gel column chromatography in n-hexane/EtoAc mixture in which the gradient of the solvent was gradually increased from neat n-hexane to 4 % EtoAc/nhexane to obtain **2** (460 mg, 68 %) as a predominant *trans* isomer. The compound was pure as judged by NMR (Figure A.3) and TLC. Its identity was confirmed by high resolution electron-impact MS (*m/z*): calculated 268.2766; observed 268.2761. ^{1}H NMR

(400 MHz, $CDCl_3$) δ 5.54-5.48 (m, 1H), 5.42-5.37 (m, 1H), 3.60 (t, *J* = 6.3 Hz, 2H), 2.24

(q, *J* = 6.5 Hz, 2H), 1.99 (q, *J* = 7.0 Hz, 2H), 1.32-1.26 (m, 23H), 0.86 (t, *J* = 6.8 Hz, 3H);

^{13}C NMR (100 MHz, CDCl) 134.42, 125.49, 61.99, 35.96, 32.66, 31.90, 29.68, 29.67, 3

δ 29.63, 29.61, 29.55, 29.60, 29.49, 29.44, 29.34, 29.18, 22.67, 14.10.

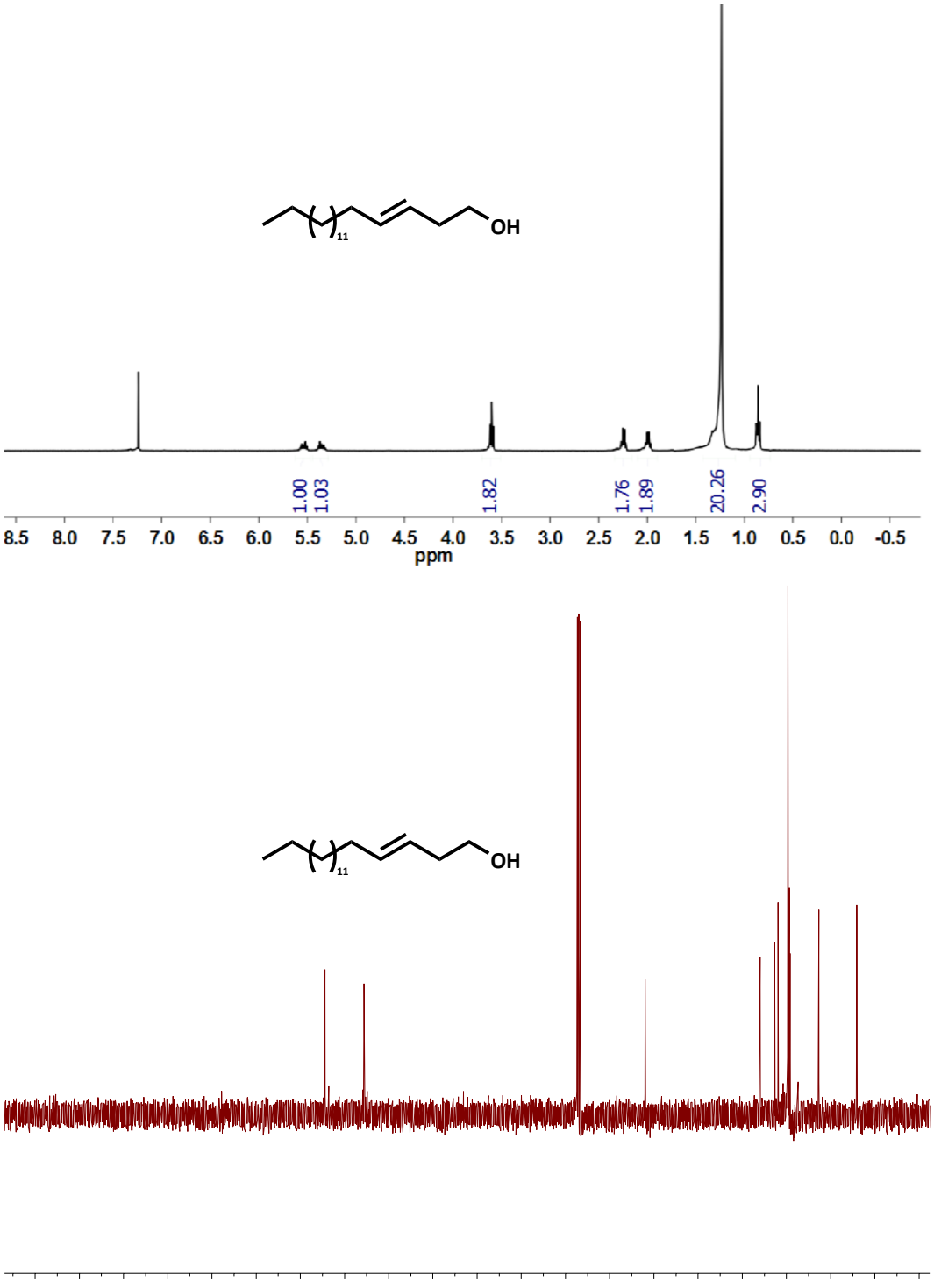

Figure A.3. ^{1}H and ^{13}C-NMR spectrum of compound **2** in $CDCl_3$

Synthesis of *trans*-*tert*-butyldimethyl(octadec-3-en-1-yloxy)silane (3)

The alcohol functional group in **2** was protected by *tert*-Butyl-dimethylsilyl group (TBDMS) using a literature procedure.[3] To a solution of **2** (100 mg, 0.37 mmol) in anhydrous dicholoromethane (DCM) at 0 °C were added imidazole (40 mg, 0.59 mmol), and catalytic amount of DMAP. TBDMS chloride (66 mg, 0.44 mmol) was added to the reaction mixture resulting in the formation of white suspension. The reaction mixture was gradually warmed to room temperature and stirred overnight. The reaction mixture was diluted with DCM (50 ml) and washed with water (2 X 5 ml). The organic layer was separated, dried over anhydrous sodium sulphate and concentrated on a rotatory evaporator. The crude mixture was purified by silica-gel chromatography using 1 % ethylacetate/n-hexane as the eluting solvent to yield **3** (120 mg, 85%). The compound was pure as judged by NMR (Figure A.4) and TLC. ^{1}H NMR (400 MHz, $CDCl_3$) δ 5.525.46 (m, 1H), 5.42-5.35 (m, 1H), 3.62 (t, *J* = 7.0 Hz, 2H), 2.22 (q, *J* = 6.8 Hz, 2H), 2.11 (q, *J* = 6.8 Hz, 2H), 1.32-1.26 (m, 22H), 0.95-0.85 (m, 12H), 0.07 (s, 6H); ^{13}C NMR (100 MHz, $CDCl_3$) δ 132.65, 131.91, 126.27, 125.43, 63.39, 63.06, 33.86, 32.72, 31.96, 31.15, 29.74, 29.73, 29.72, 29.70, 29.39, 25.97, 25.95, 22.72, 18.99, 18.37, 14.13, -5.25, -5.26.

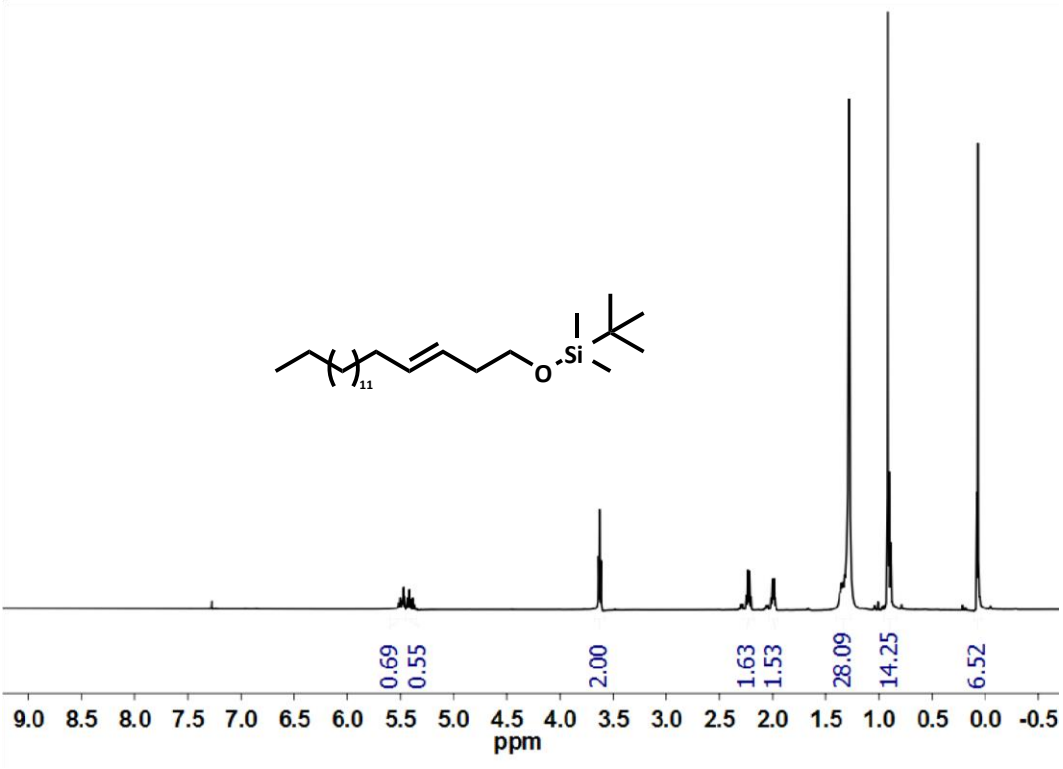

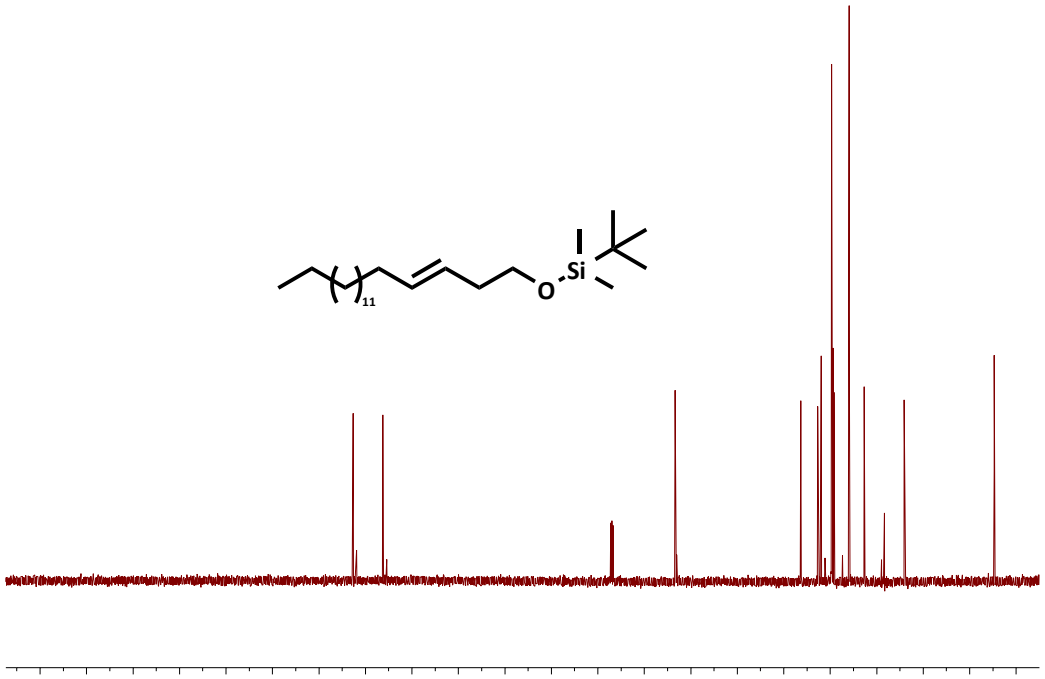

Figure A.4. ^{1}H and ^{13}C-NMR spectrum of compound **3** in CDCl3.

Synthesis of *tert*-butyldimethyl(2-(2-tetradecylcyclopropyl)ethoxy)silane (4)

3 was converted to **4** based on literature procedures.[4,5] To a solution of **3** (120 mg, 0.31 mmol) in anhydrous dichloromethane at -10 °C were added diethyl zinc (70 µl, 0.7 mmol) and diiodomethane (100 µl, 1.2 mmol). The reaction mixture was warmed to room temperature and stirred for 48 hours. Upon completion of the reaction as judged by TLC, the crude mixture was concentrated on a rotatory evaporator. **4** was purified by silica-gel column chromatography using 1% ethylacetate/n-hexane as the eluting solvent and was obtained as predominant the *trans*-stereoisomer (40 mg, 30 %). The compound was > 90% pure as judged by NMR (Figure A.) and TLC. ^{1}H NMR (400 MHz, $CDCl_3$) δ 3.673.58 (m, 2H), 2.15-2.11 (m, 2H), 1.36-1.25 (m, 22H), 0.90-0.85 (m, 12H), 0.43-0.37 (m, 1H), 0.19-0.13 (m, 2H), 0.06-0.03 (m, 6H); ^{13}C NMR (100 MHz, $CDCl_3$) δ 63.35, 37.69, 34.25, 31.95, 30.32, 29.73, 29.69, 29.65, 29.60, 29.55, 29.50 29.40, 29.22, 26.03, 25.99, 25.97, 22.72, 18.51, 18.38, 15.29, 14.15, 11.45, -5.26.

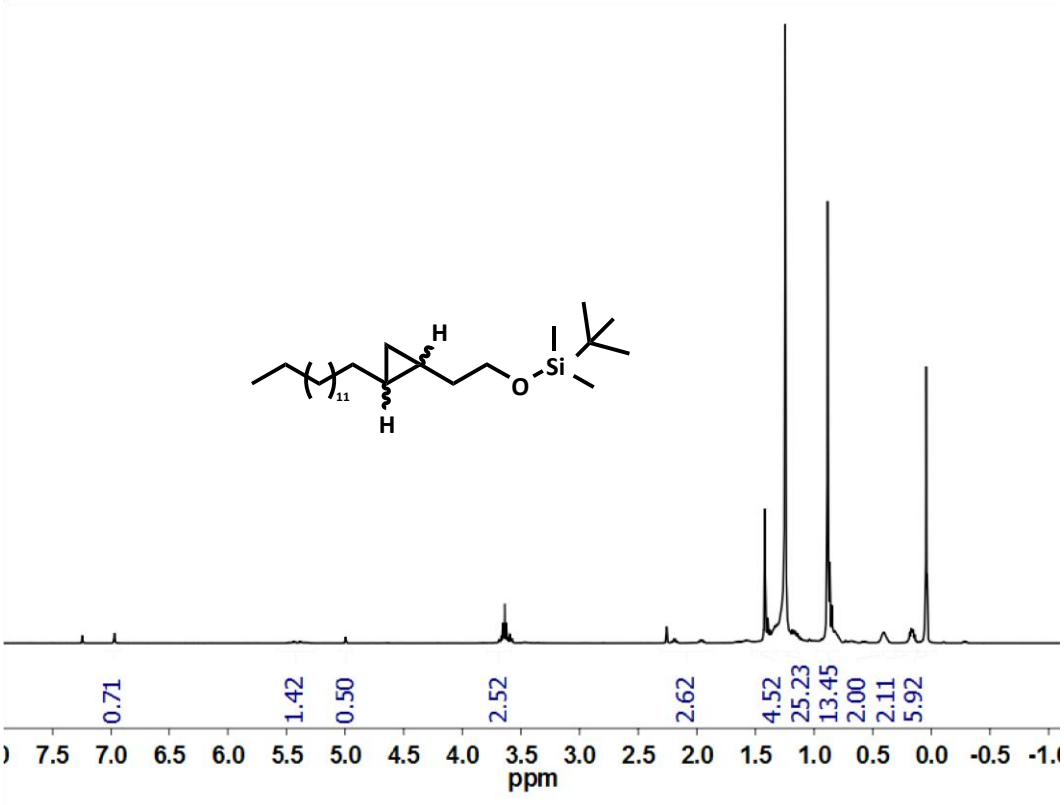

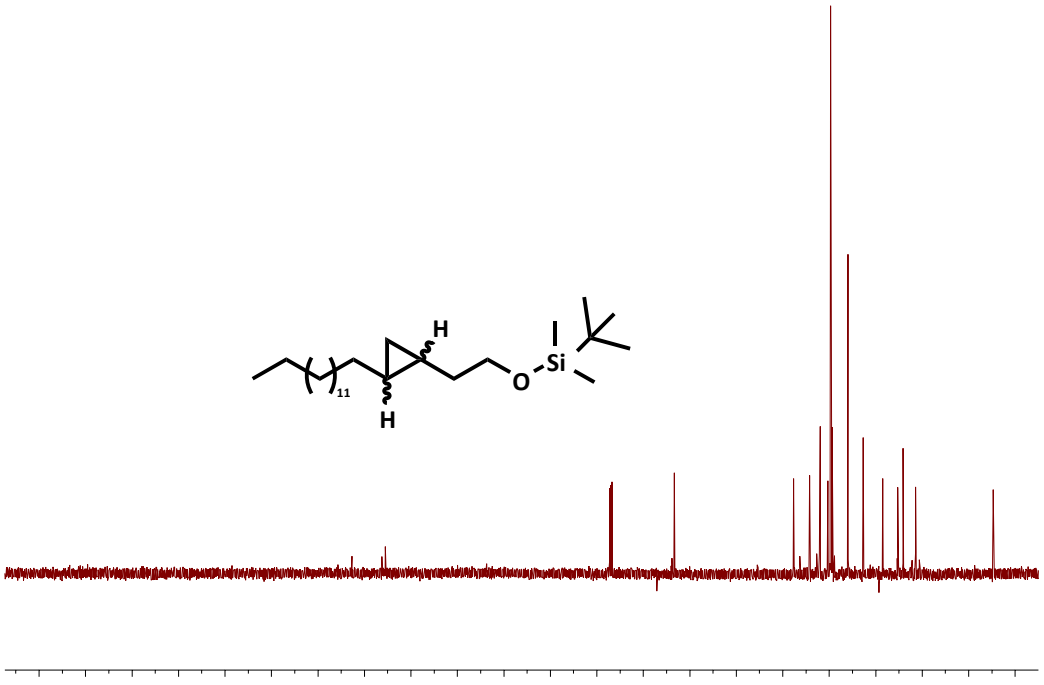

Figure A.5. ^{1}H and ^{13}C NMR spectrum of compound **4** in CDCl3.

Synthesis of (2-tetradecylcyclopropyl)ethanol (5)

1 ml of 1.0 M TBAF in THF was added to a solution of **4** (120 mg, 0.304 mmol) in anhydrous THF at room temperature. The reaction mixture was stirred for 3 h under nitrogen. The reaction mixture was diluted with 50 ml dichloromethane and washed with water (2 x 5 ml) and brine (2 x 2 ml). The organic layer was dried over sodium sulphate and concentrated by rotatory evaporation to afford the crude product as yellow oil that was further subjected to silica-gel chromatography using 1% ethylacetate/n-hexane as the eluting solvent and yielded **5** as a white solid (70 mg, 85%). The compound was > 85% pure as judged by NMR (Figure A.6) and TLC. ^{1}H NMR (400 MHz, $CDCl_3$) δ 3.73-3.68 (m, 2H), 2.15-2.11 (m, 2H), 1.491.47 (m, 2H), 1.45-1.36 (m, 22H), 0.90 (t, *J* = 6.8 Hz, 3H), 0.47-0.42 (m, 2H), 0.24-0.21 (m, 2H); ^{13}C NMR (100 MHz, $CDCl_3$) δ 63.52, 63.18, 62.00, 37.22, 35.98, 34.18, 32.69, 31.93, 31.74, 30.09, 29.71, 29.67, 29.64, 29.54, 29.52, 29.47, 29.41, 29.38, 29.22, 28.86, 26.11, 25.65, 22.70, 18.38, 18.38, 15.16, 15.11, 14.13, 12.12, 11.33, 10.57.

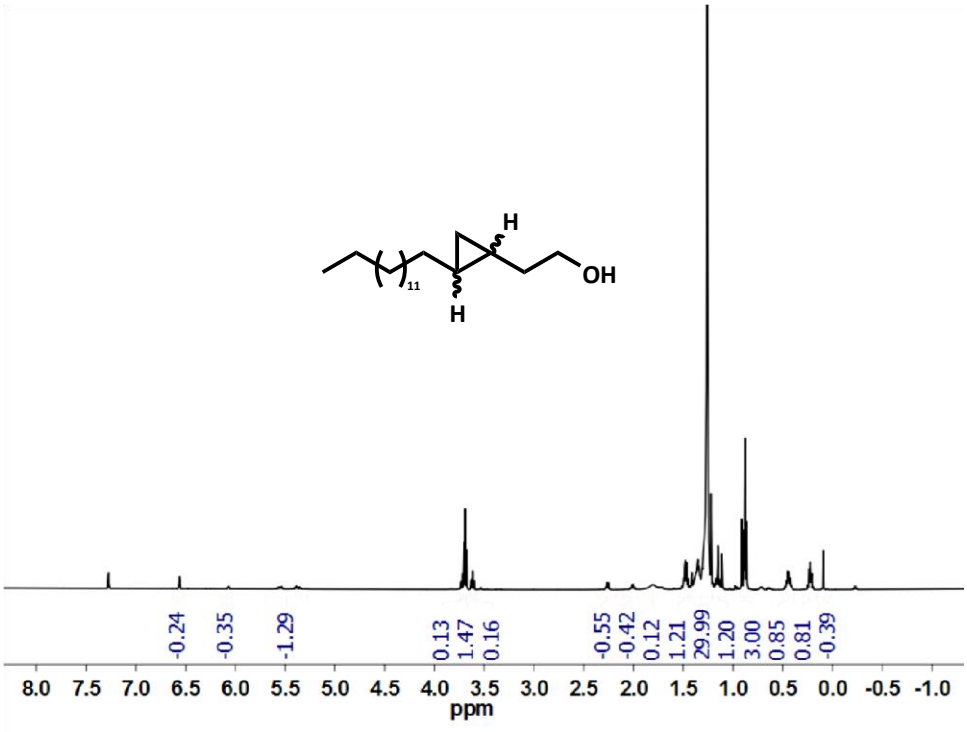

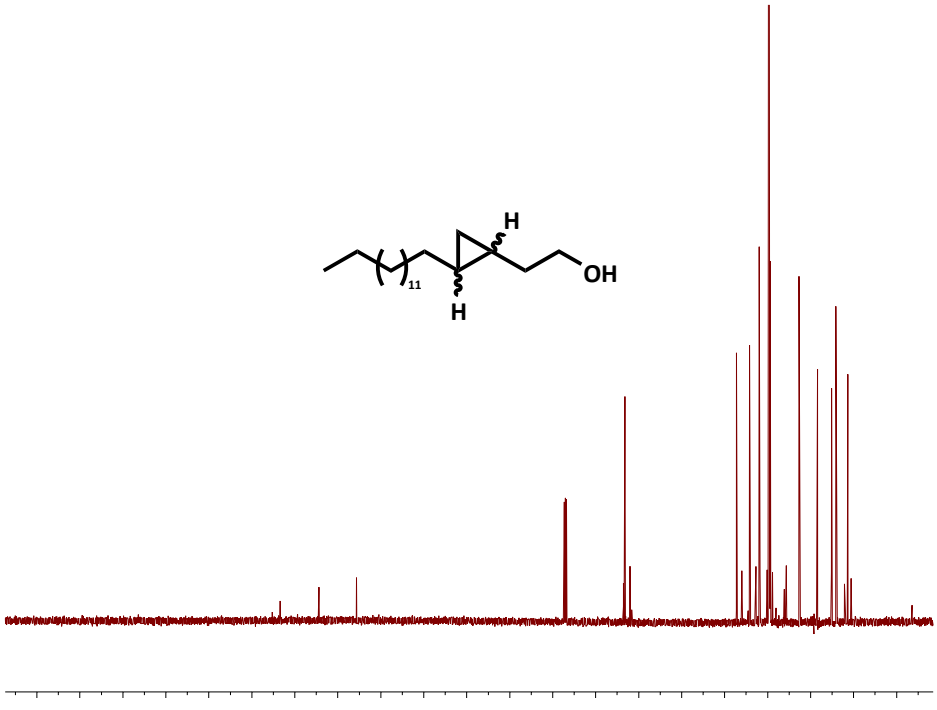

Figure A.6. ^{1}H and ^{13}C NMR spectrum of compound **5** in CDCl3

Synthesis of 2-(2-tetradecylcyclopropyl)acetaldehyde (6)

To a solution of **5** (100 mg, 0.34 mmol) in dichloromethane at room temperature were added TEMPO (5 mg, 0.034 mol) and BAIB (120 g, 0.37 mmol). The reaction was stirred at room temperature for 3 hours under nitrogen. After completion, the crude reaction mixture was concentrated using a rotatory evaporator and subjected to silica-gel column chromatography in nhexane/ethylacetate in which the gradient of the solvent was gradually increased from neat n-hexane to 0.5 % ethylacetate/n-hexane to obtain **6** (60 mg, 65%). The compound was pure as judged by NMR (Figure A.7) and TLC. The identity of the compound was confirmed by high resolution electron-impact MS (*m/z*): calculated 280.2760; observed 280.2766. GC-MS analysis of **6** indicated that the compound was a mixture of ~ 70:30 *trans*- to *cis*-stereoisomers. ^{1}H NMR (400 MHz, $CDCl_3$) of **6** (major stereoisomer) δ 9.76 (t, *J* = 7 Hz, 1H), 2.30-2.26 (m, 2H), 1.39-1.24 (m, 22H), 0.86 (t, *J* = 6.8 Hz, 3H), 0.700.66 (m, 1H), 0.55-0.50 (m, 1H), 0.41-0.30 (m, 2H); ^{13}C NMR (100 MHz, $CDCl_3$) δ 202.52, 48.20, 47.30, 43.22, 33.87, 32.69, 31.89, 29.80, 29.67, 29.65, 29.63, 29.53, 29.45, 29.39, 29.33, 29.13, 28.95, 22.66, 18.54, 15.04, 14.09, 11.70, 11.51, 10.74, 8.95.

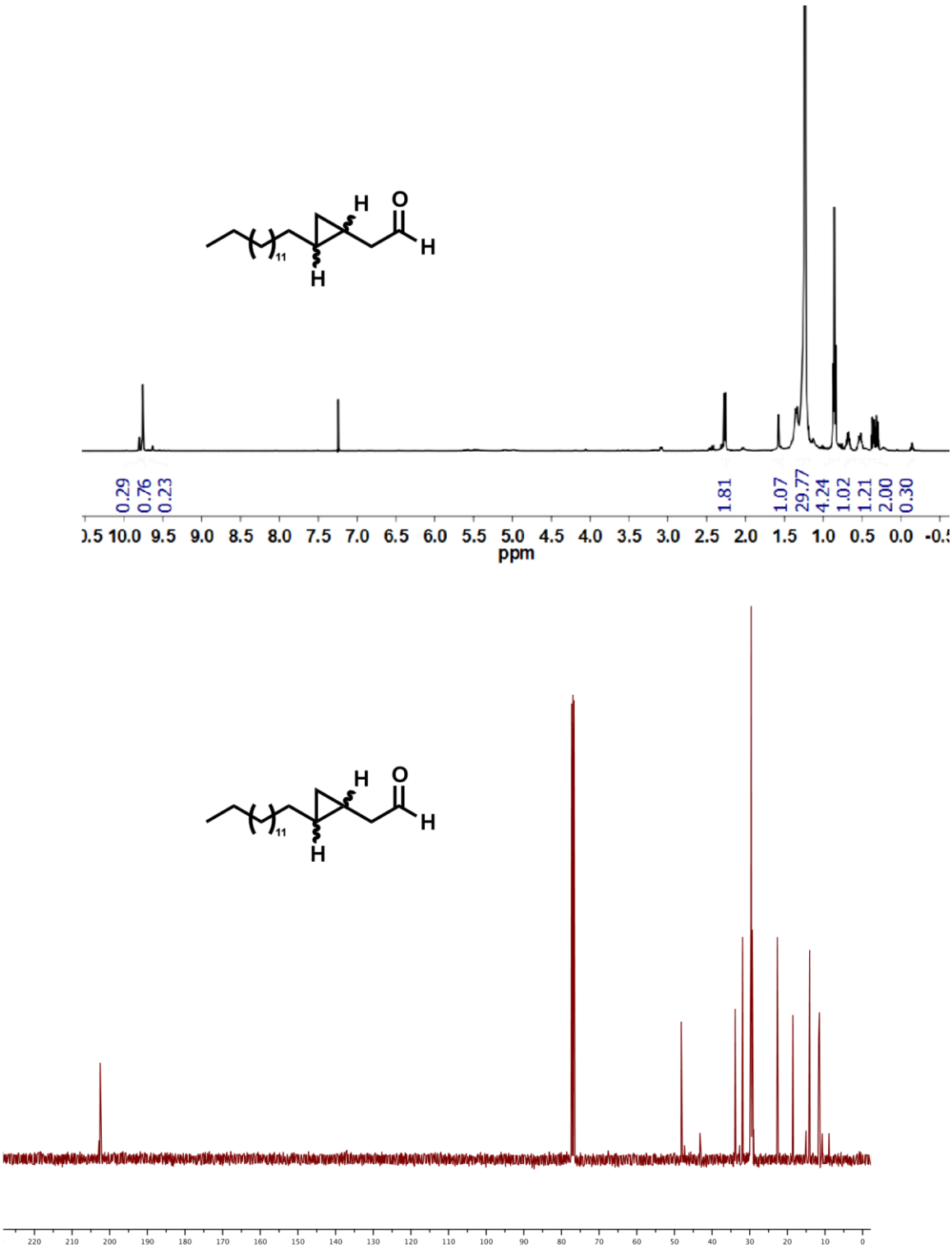

Figure A.7. ^{1}H and ^{13}C-NMR of cyclopropyl compound **6**.

References

1. De Mico, A.; Margarita, R.; Parlanti, L.; Vescovi, A.; Piancatelli, G. *J. Org. Chem.* **1997**, *62*, 6974.
2. Schlosser, M.; Christmann, K.F. *Angew. Chem. Intl. Ed.* **1966**, *5,* 126.
3. Rajesh, M.; Sen, J.; Srujan, M.; Mukherjee, K.; Sreedhar, B.; Chaudhuri, A. *J. Am. Chem. Soc.* **2007**, *129*, 11408.
4. Furukawa, J.; Kawabata, N.; Nishimura, J. *Tetrahedron* **1968**, *24,* 53.
5. Lebel, H. L.; Marcoux, J.-F.; Molinaro, C.; Charette, A. B. *Chem. Rev*. **2003**, *103*, 977.

Appendix B

Syntheses for Chapter 3

Synthesis and characterization of 3-nonyloxirane-2-carbaldehyde (1):

The synthesis of 3-nonyloxirane-2-carbaldehyde (**1**) was carried out in two steps as outlined in Figure B.1 below by Dr. Bishwajit Paul.

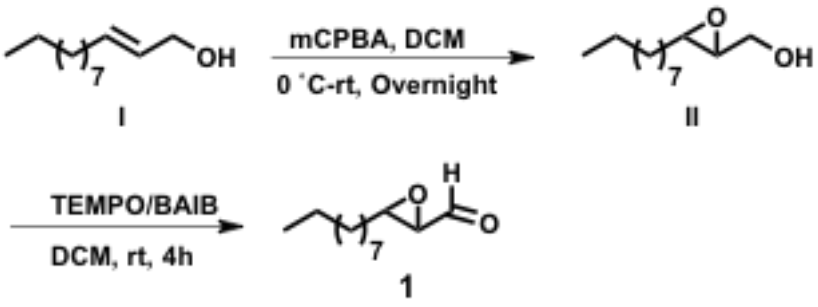

Figure B.1. Synthesis of 3-nonyloxirane-2-carbaldehyde (**1**)

Synthesis of (3-nonyloxiran-2-yl)methanol (II)

The oxidation of (*E*)-dodec-2-en-1-ol **(I)** to (3-nonyloxiran-2-yl)methanol **(II)** was performed using standard perbenzoic acid strategy.[1] To a solution of (*E*)-dodec-2-en-1-ol (**I**, 200 mg, 1.1 mmol) were added metachloroperbenzoic acid (mCPBA, 200 mg, 1.16 mmol) and in dichloromethane at ice-cold condition. The reaction was stirred at room temperature for overnight. The solvent was removed under reduced pressure using a rotatory evaporator and the crude mixture was subjected to a silica-gel column equilibrated in n-hexane. The column was eluted by slowly increasing the polarity of the solvent using a gradient of 0 to 1 % ether in hexane to obtain **II** (190 mg, 85%). The compound was pure as judged by NMR (Figure B.2). ^{1}H NMR (400 MHz, $CDCl_3$) δ 3.82-3.79 (dd, 1H), 3.52-3.48 (dd, 1H), 2.87-2.83 (m, 2H), 1.49-1.46 (m, 2H), 1.36-1.34 (m,

2H), 1.24-1.19 (m, 12H), 0.82-0.78 (t, 3H) ^{13}C NMR(400 MHz, $CDCl_3$), δ 61.81, 58.71, 56.08, 53.37, 31.80, 31.50, 29.46, 29.43, 29.39, 29.33, 29.22, 29.14, 25.86, 22.58, 22.56, 13.99.

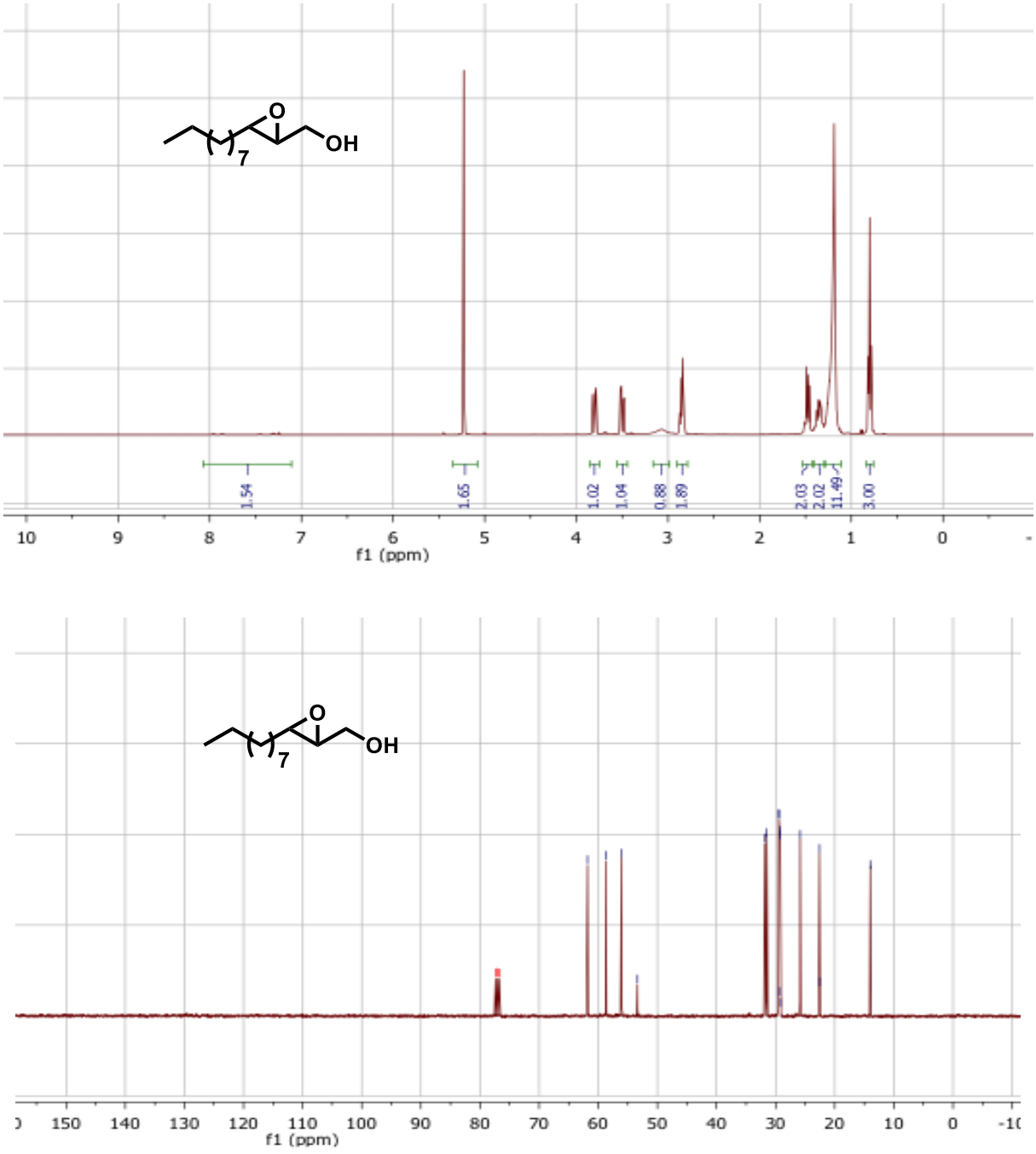

Figure B.2. ^{1}H and ^{13}C-NMR spectra of compound **II**.

Synthesis of 3-nonyloxiran-2-carbaldehyde (1)

To a solution of **II** (150 mg, 0.75 mmol) in dichloromethane at room temperature were added TEMPO (10 mg, 0.064 mol) and BAIB (250 mg, 0.77 mmol).[2] The reaction was stirred at room temperature for 6 hours under nitrogen. After completion, the crude reaction mixture was concentrated using a rotatory evaporator and subjected to silica-gel column chromatography in n-hexane/ethylacetate in which the gradient of the solvent was gradually increased from neat n-hexane to 0.5 % ethylacetate/n-hexane to obtain **1** (50 mg, 35 %). The compound was pure as judged by NMR (Figure B.3) and TLC. The identity of the compound was confirmed by high resolution electron-impact MS (*m/z*): calculated 198.1620; observed 198.1617. GC-MS analysis of **1** indicated that the compound was a mixture of ~ 98:2 *trans*- to *cis*-stereoisomers. ^{1}H NMR (400 MHz, $CDCl_3$), 8.97-8.95 (d, 1H), 3.20-3.16 (m, 1H), 3.09-3.07 (m, H), 1.65-1.56 (m, 2H), 1.47-1.40 (m, 2H), 1.39-1.22 (m, 12H), 0.85-0.81 (t, 3H), ^{13}C NMR (100 MHz, $CDCl_3$) δ 198.4, 59.09, 56.71, 31.79, 31.15, 29.38, 29.37, 29.34, 29.20, 29.16, 28.08, 25.71, 22.60, 14.03

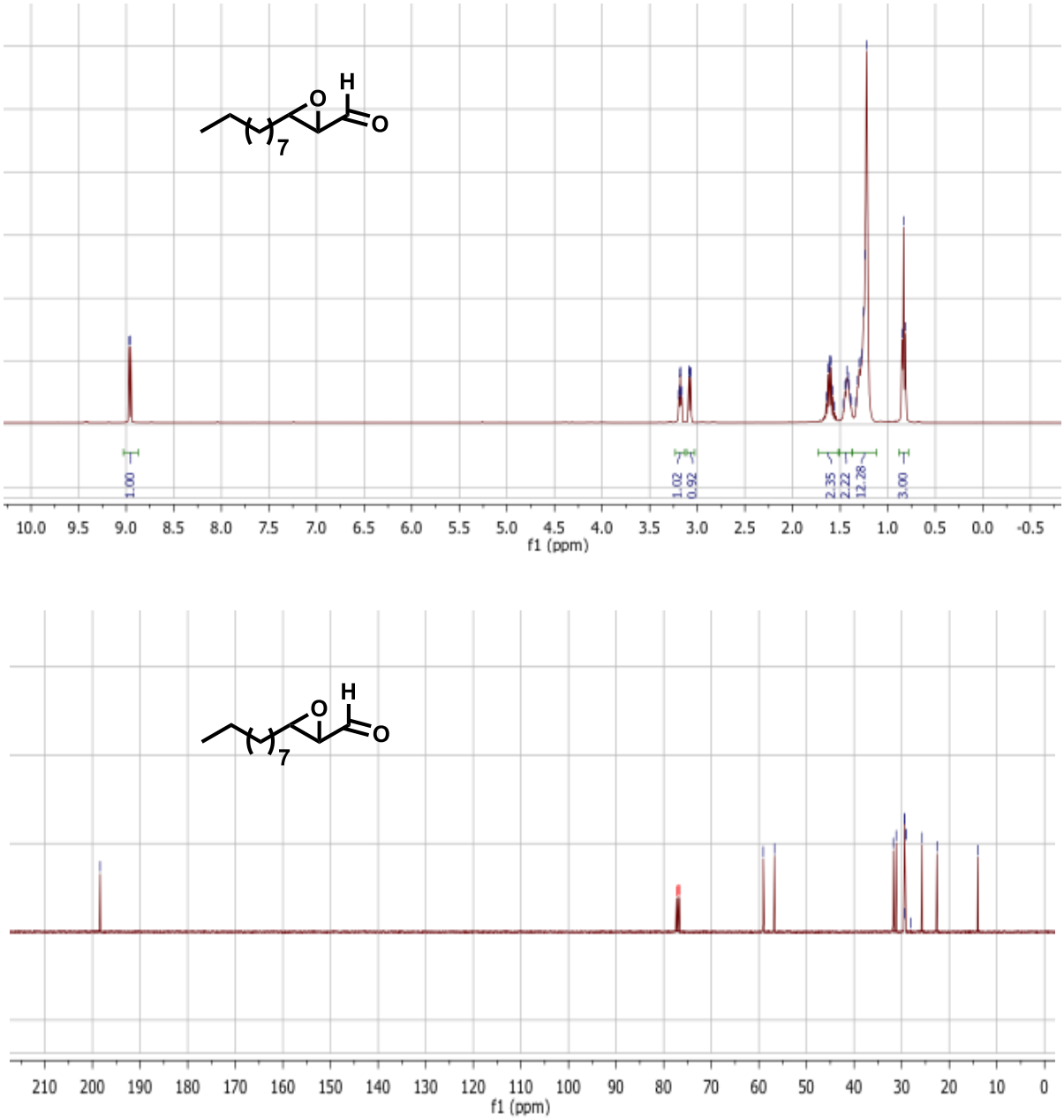

Figure B.3. ^{1}H and ^{13}C NMR spectra of compound **1**.

Synthesis and characterization of 2-nonyloxirane (IV):

The synthesis of 2-nonyloxirane **(IV)** was carried out in one-step using standard perbenzoic acid strategy[1] as outlined in Figure B.4 below.

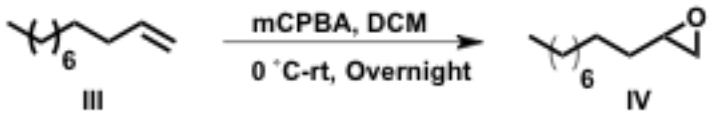

Figure B.4. Synthesis of 2-nonyloxirane **(IV)**

Synthesis of 2-nonyloxirane (IV)

To a solution of undec-1-ene (**III**, 154mg, 1 mmol) were added metachloroperbenzoic acid (mCPBA, 189 mg, 1.1 mmol) and in dichloromethane at ice-cold condition. The reaction was stirred at room temperature for overnight. The solvent was removed under reduced pressure using a rotatory evaporator and the crude mixture was applied to a silica-gel column equilibrated in n-hexane. The column was developed by slowly increasing the polarity of the solvent using a gradient of 0 to 1 % ether in hexane to obtain **IV** (60 mg, 35%). The compound was pure as judged by NMR (Figure B.4). ^{1}H NMR (400 MHz, $CDCl_3$) δ 2.91-2.85 (m, 1H), 2.75-2.73 (t, 1H), 2.46-2.43 (dd, 1H), 1.55-1.50 (m, 2H), 1.48-1.43 (m, 2H), 1.35-1.27 (m, 12H), 0.89-0.86 (t, 3H). ^{13}C NMR (100 MHz, $CDCl_3$), δ 52.29, 47.10, 32.50, 31.88, 29.56, 29.51, 29.45, 29.30, 25.98, 22.67, 14.09.

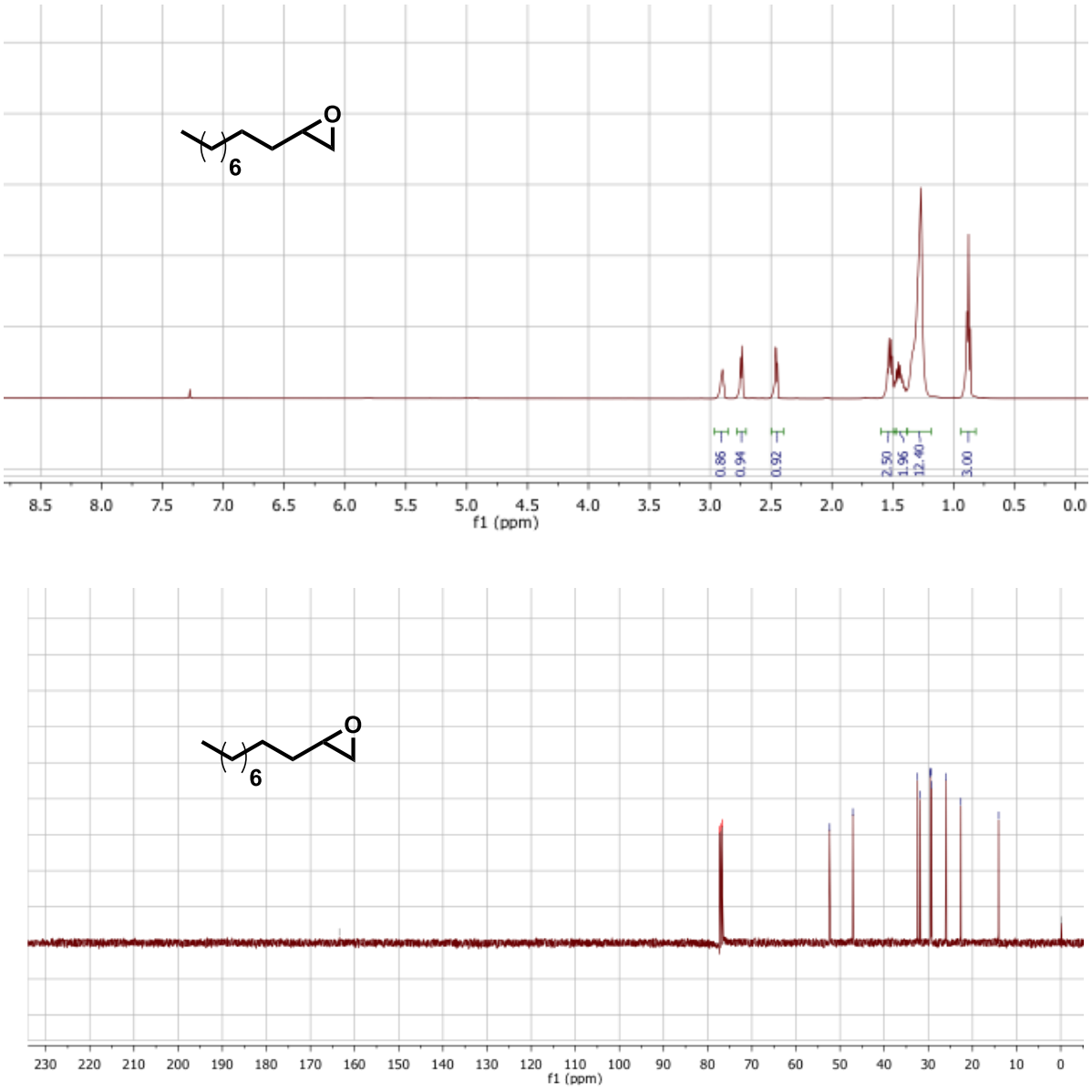

Figure B.5. ^{1}H and ^{13}C NMR spectra of 2-nonyloxirane (**IV)**

Synthesis and characterization of 3-pentadecyloxirane-2-carbaldehyde (2):

The synthesis of 3-pentadecyloxirane-2-carbaldehyde **(2)** was carried out in three steps as outlined in Figure B.6 below. The synthesis of compounds V, VI, VII and 2, and the corresponding product standard, are detailed below.

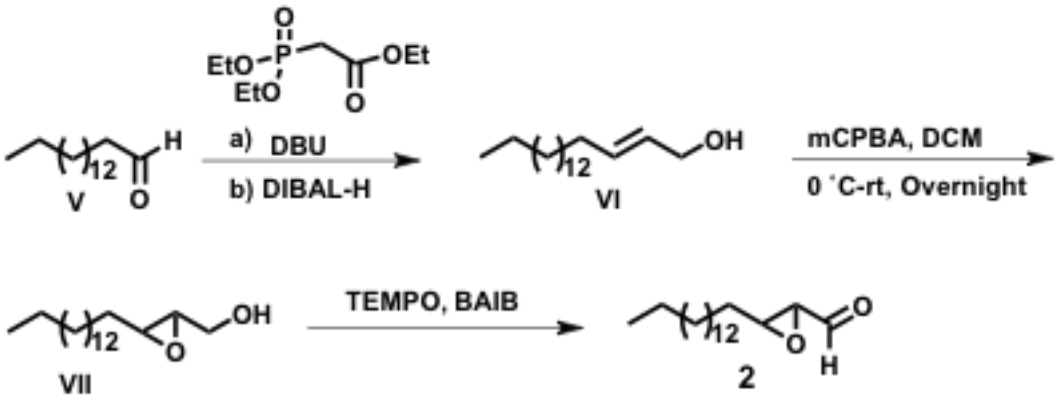

Figure B.6. Synthesis of 3-pentadecyloxirane-2-carbaldehyde **(2)**

Synthesis of (E)-Octadec-2-en-1-ol (VI)

The Horner-Wittig reaction of hexadecanal (**V)** with ethyl-2-(diethoxylphosphoryl) acetate was performed according to a literature procedure.[1] To a solution of 1,8-diazabicyclo[5.4.0]undec-7-ene (DBU) (470 mg, 3.08 mmol) in tetrahydrofuran (THF), 2-(diethoxylphosphoryl) acetate (734 mg, 3.28mmol) was added dropwise at 0 °C. The mixture was warmed to room temperature and stirred for 1 hr. The solution was then cooled to -78 °C in a dry ice/acetone mixture bath for 15 min, followed by dropwise addition of hexadecanal (503 mg, 2.1 mmol) (**V**) (dissolved in minimum volume of THF). The mixture was warmed to room temperature and stirred for overnight. The resulting mixture was diluted with diethyl ether, washed with water and then dried over sodium sulphate. After evaporation of the solvent, pure ethyl-2-octadec-2-enoate was obtained as judged by TLC (450 mg, 75% yield). The next step of the reaction was carried out without further characterization.

To a solution of ethyl-2-octadec-2-enoate (450 mg, 1.45 mmol), in diethyl ether at 0 °C, DIBAL-H (515 mg, 3.62 mmol) was added dropwise. The solution was warmed to

room temperature and stirred for 1 hr. The resulting mixture was cooled to 0 °C and quenched with MeOH and warmed to room temperature. The solution was washed with dichloromethane for several times, washed with brine and dried over sodium sulphate and concentrated under reduced pressure by rotatory evaporator. The crude mixture was subjected to silica gel column chromatography in n-hexane/diethyl ether mixture in which the gradient of the solvent was gradually increased from neat n-hexane to 30% Ether/n-hexane to obtain **VI** (270 mg, 68 %) as a predominant *trans* isomer. The compound was pure as judged by NMR (Figure B.7) ^{1}H NMR (400 MHz, $CDCl_3$) δ 5.66-5.63 (m, 2H), 4.07-4.06 (q, 2H), 2.04-2.01 (m, 2H), 1.37-1.24 (m, 26H), 0.86-0.84 (t, 3H); ^{13}C NMR (100 MHz, $CDCl_3$) δ 133.60, 128.73, 63.84, 32.19, 31.90, 29.67, 29.63, 29.59, 29.48, 29.34, 29.17, 29.11, 22.67, 14.10.

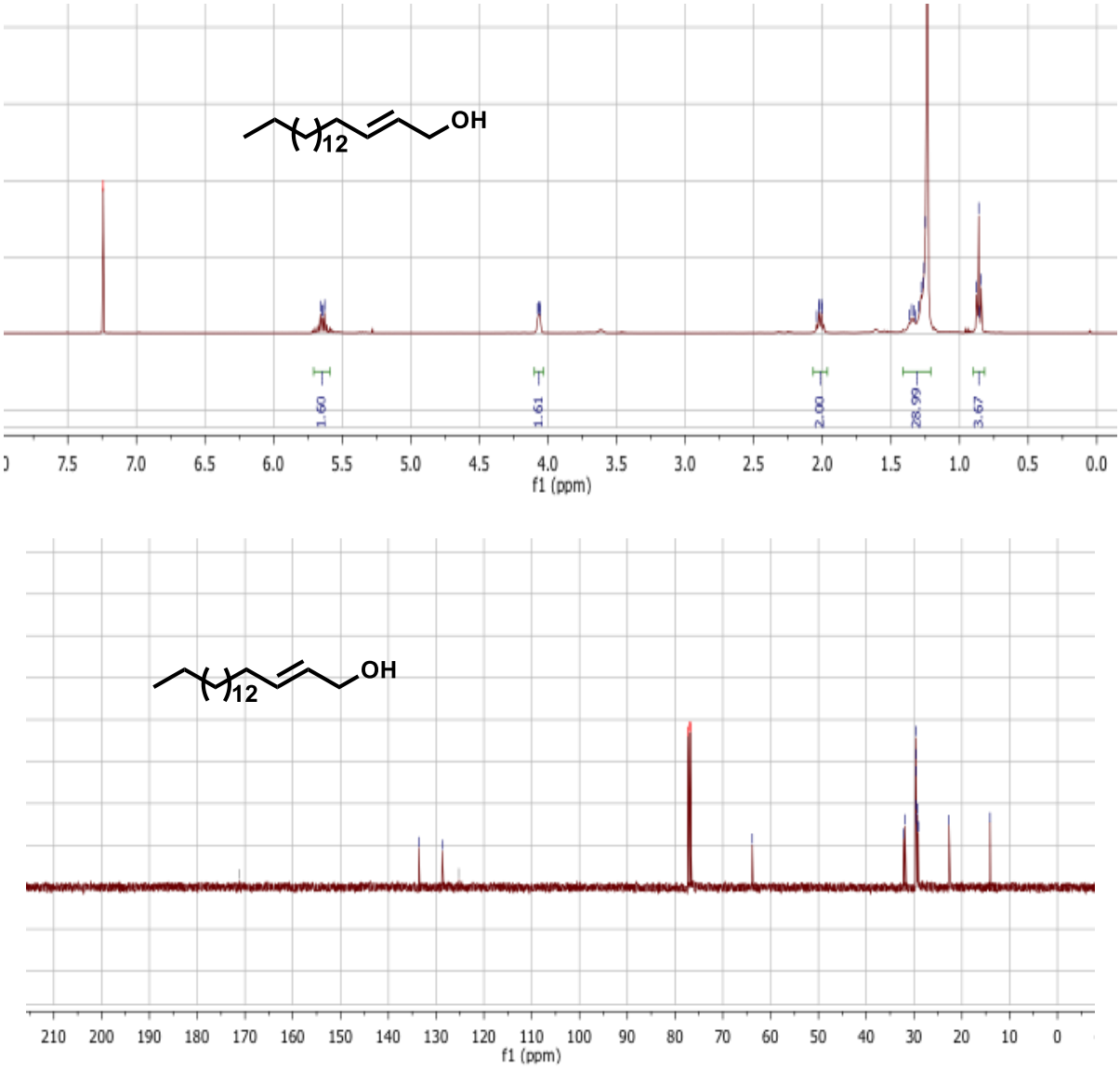

Figure B.7. ^{1}H and ^{13}C NMR spectra of (*E*)-Octadec-2-en-1-ol **(VI)**

Synthesis of (3-pentadecyloxiran-2-yl)methanol (VII)

The oxidation of (*E*)-Octadec-2-ene-1-ol (**VI**) to (3-pentadecyloxiran-2-yl)methanol **(VII)** was performed using standard perbenzoic acid strategy.[1] To a solution of (*E*)-octadec-2-en-1-ol (**VI**, 200 mg, 0.75 mmol) were added metachloroperbenzoic acid

(mCPBA, 150 mg, 0.87 mmol) and in dichloromethane at ice-cold condition. After 30 min, the reaction was warmed to room temperature allowed to stir for overnight. The solvent was removed under reduced pressure using a rotatory evaporator and the crude mixture was applied to a silica-gel column equilibrated in n-hexane. The column was developed by slowly increasing the polarity of the solvent using a gradient of 0 to 1 % ether in hexane to obtain **VII** (200 mg, 90%). The compound was pure as judged by NMR (Figure B.8). ^{1}H NMR (400 MHz, $CDCl_3$) δ 3.92-3.88 (m, 1H), 3.63-3.59 (m, 1H), 2.96-2.89 (m, 2H), 1.54-1.53 (m, 3H), 1.45-1.39 (m, 2H), 1.37-1.24 (m, 21H), 0.86-0.84 (t, 3H) ^{13}C NMR (100 MHz, $CDCl_3$), δ 61.64, 58.34, 55.96, 31.90, 31.53, 29.67, 29.63, 29.61, 29.52, 29.50, 29.37, 29.34, 25.92, 22.67, 14.10.

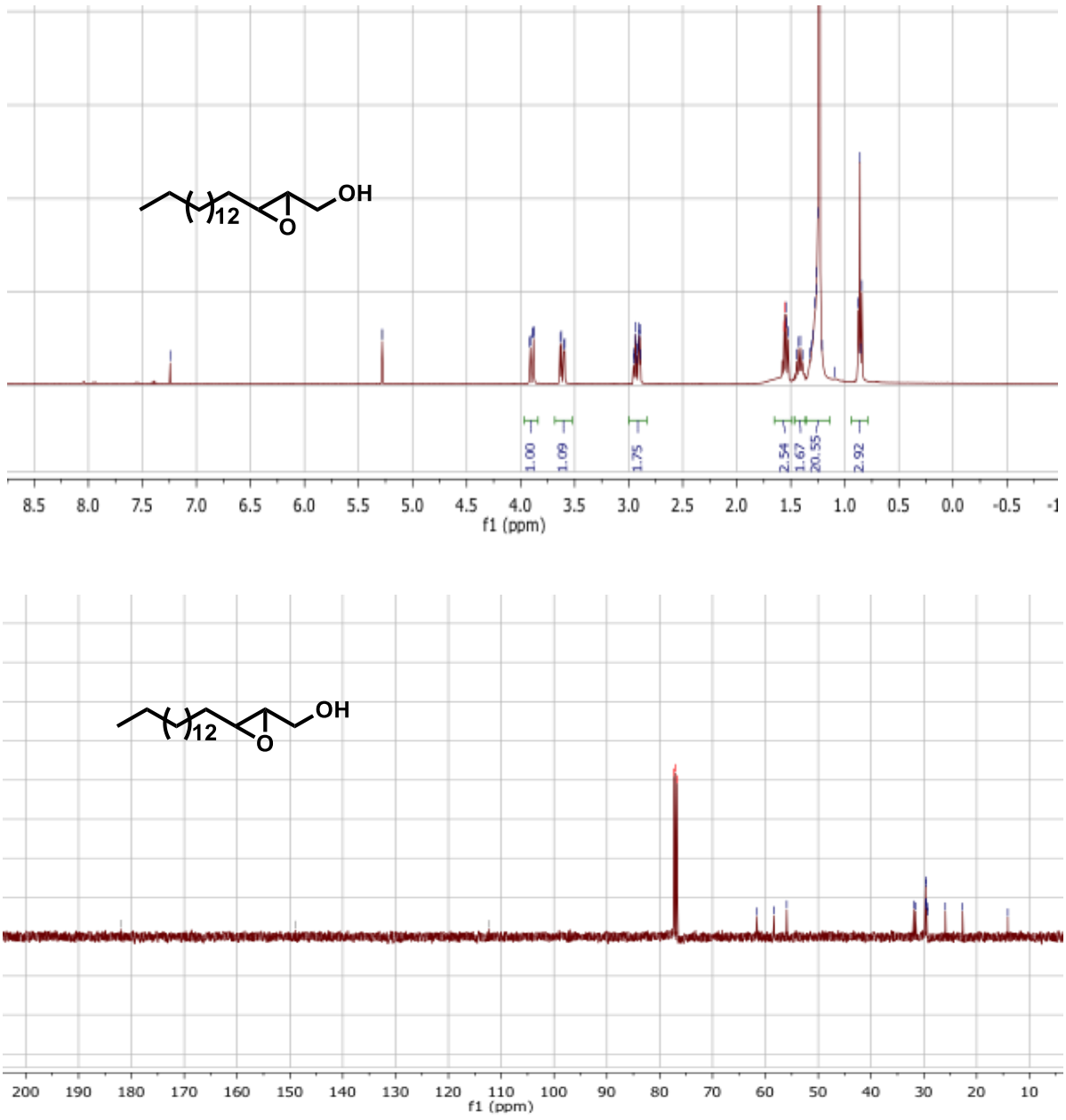

Figure B.8. ^{1}H and ^{13}C-NMR spectra of (3-pentadecyloxiran-2-yl)methanol **(VII)**

Synthesis of 3-pentadecyloxiran-2-carbaldehyde (2)

To a solution of **VII** (100 mg, 0.354 mmol) in dichloromethane at room temperature were added TEMPO (6 mg, 0.038 mol) and BAIB (120 g, 0.37 mmol).[2] The reaction was

stirred at room temperature for 3 hours under nitrogen. After completion, the crude reaction mixture was concentrated using a rotatory evaporator and subjected to silica-gel column chromatography in n-hexane/ether in which the gradient of the solvent was gradually increased from neat n-hexane to 0.5 % ether/n-hexane to obtain **2** (40 mg, 40%). The compound was pure as judged by NMR (Figure B.9) and TLC. The identity of the compound was confirmed by high resolution electron-impact MS (*m/z*): calculated 282.2559; observed 282.2561. GC-MS analysis of **2** indicated that the compound was a mixture of ~ 90:10 *trans*- to *cis*-stereoisomers. ^{1}H NMR (400 MHz, $CDCl_3$) of **2** (major stereoisomer) δ 9.01-8.99 (d, 1H), 3.23-3.19 (m, 1H), 3.13-3.10 (m, 1H), 1.66-1.62 (m, 2H), 1.46-1.44 (m, 2H), 1.34-1.24 (m, 24H) 0.88-0.86 (t, 3H),^{13}C NMR (100 MHz, $CDCl_3$) δ198.49, 59.15, 56.78, 31.90, 31.18, 29.67, 29.66, 29.64, 29.63, 29.61, 29.57, 29.46, 29.40, 29.33, 29.20, 25.75, 22.67, 14.10.

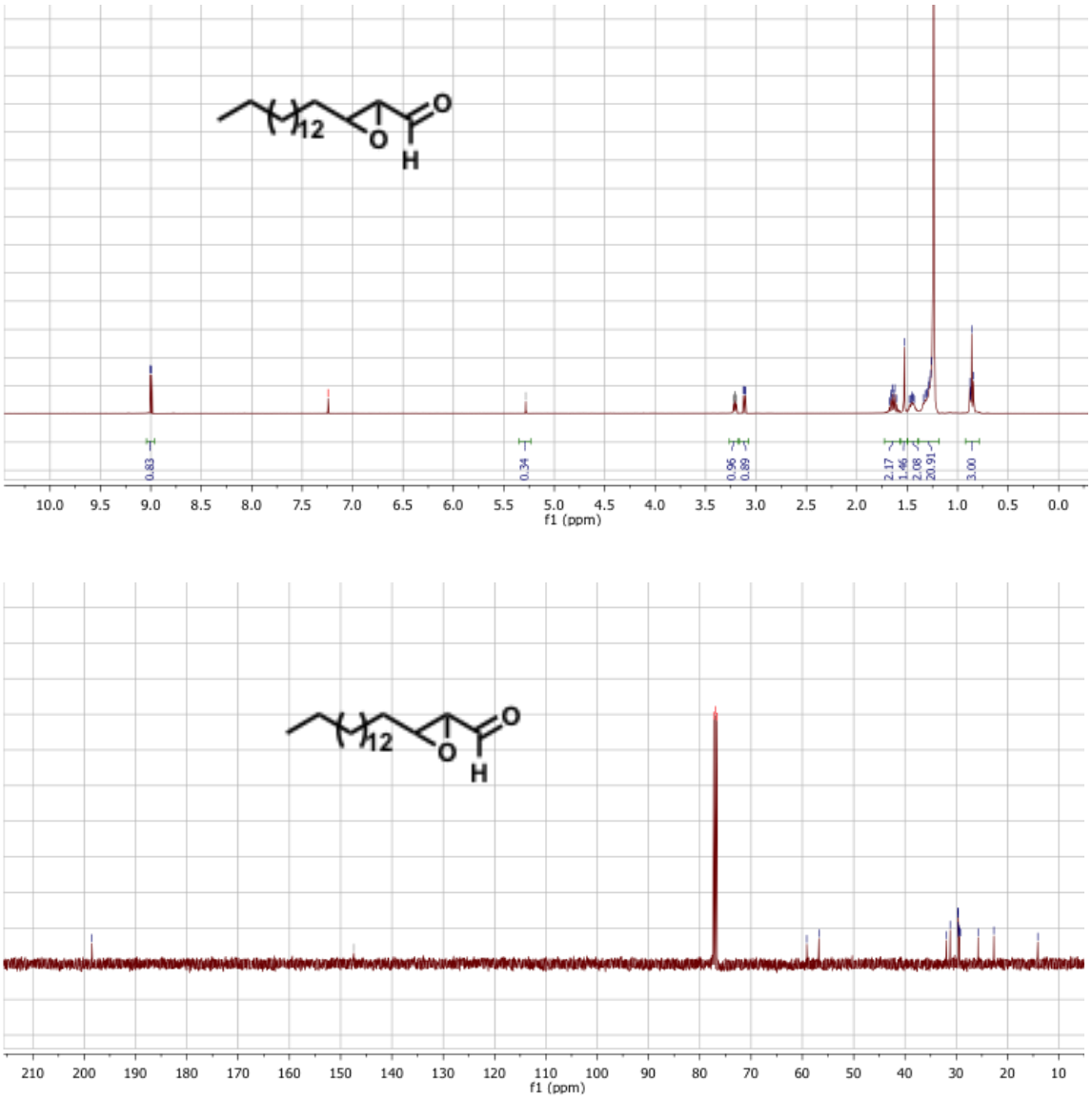

Figure B.9. ^{1}H and ^{13}C-NMR spectra of 3-pentadecyloxiran-2-carbaldehyde **(2)**

Synthesis and characterization of 2-pentadecyloxirane (IX)

The synthesis of 2-pentadecyloxirane **(IX)** was carried out in a one-step reaction using standard perbenzoic acid strategy[1] as outlined in Figure B.10.

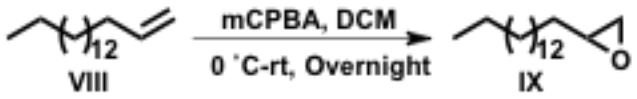

Figure B.10. Synthesis of 2-pentadecyloxirane **(IX)**

Synthesis of 2-pentadecyloxirane (IX)

The oxidation of heptadec-1-ene (**VIII**) to 2-pentadecyloxirane **(IX)** was performed using standard perbenzoic acid strategy.[1] To a solution of -heptadec-1-ene (120 mg, 0.5 mmol) were added metachloroperbenzoic acid (mCPBA, 100 mg, 0.58 mmol) and in dichloromethane at ice-cold condition. The reaction was stirred at room temperature for overnight. The solvent was removed under reduced pressure using a rotatory evaporator and the crude mixture was applied to a silica-gel column equilibrated in n-hexane. The column was developed by slowly increasing the polarity of the solvent using a gradient of 0 to 1 % ether in hexane to obtain **IX** (100 mg, 75%). The compound was pure as judged by NMR (Figure B.11). ^{1}H NMR (400 MHz, $CDCl_3$) δ 2.91-2.89 (m, 1H), 2.76-2.73 (t, 1H), 2.47-2.45 (m, 1H) 1.53-1.50 (m, 2H), 1.47-1.41 (m, 2H), 1.33-1.25 (m, 24H), 0.89-0.86 (t, 3H). ^{13}C NMR (100 MHz, $CDCl_3$), 52.42, 47.15,32.49, 31.92, 29.69, 29.66, 29.63, 29.55, 29.45, 29.36, 25.97, 22.69, 14.13.

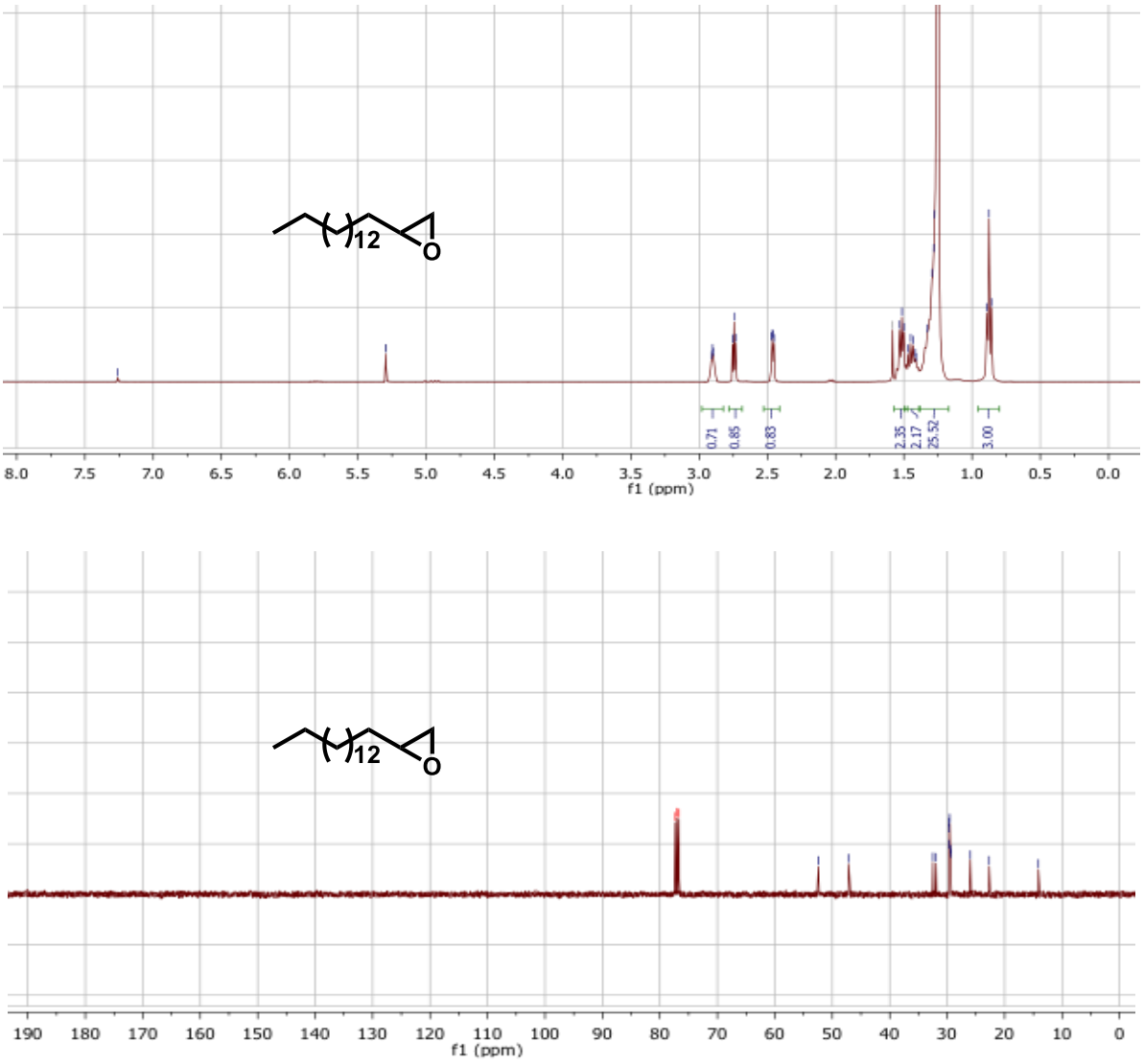

Figure B.11. ^{1}H and ^{13}C-NMR spectra of 2-pentadecyloxirane **(IX)**

References

1. Barrett, A.G.M.; Head, J.; Smith M. L.; Stock, N.S.; White, A.J.P. and Williams, D.J. *J. Org. Chem.* **1999**, *64*, 6005.
2. Paul, B.; Das, D.; Ellington, B.; Marsh, E. N. G. *J. Am. Chem. Soc.* **2013**, *135*, 5234.

Appendix C

Syntheses for Chapter 4

Synthesis of 3-nonylcyclopropane-2-carbaldehyde

The synthesis of 3-nonylcyclopropane-2-carbaldehyde (**1, 1A, 1B**) and 3-nonylcyclopropane (**2, 2A**) (compounds shown in Figure C.1) is summarized in Figure C.2 and Figure C.3 below, and was performed by Dr. Bishwajit Paul.

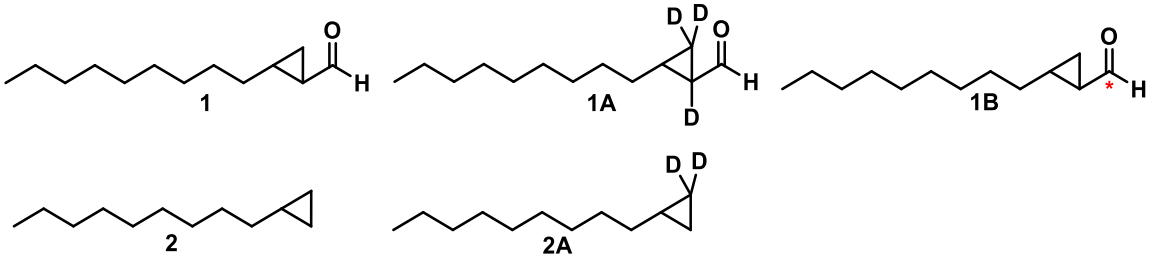

Figure C.1. Chemical structures of synthesized substrate and product standard, as well as isotopic labels thereof.

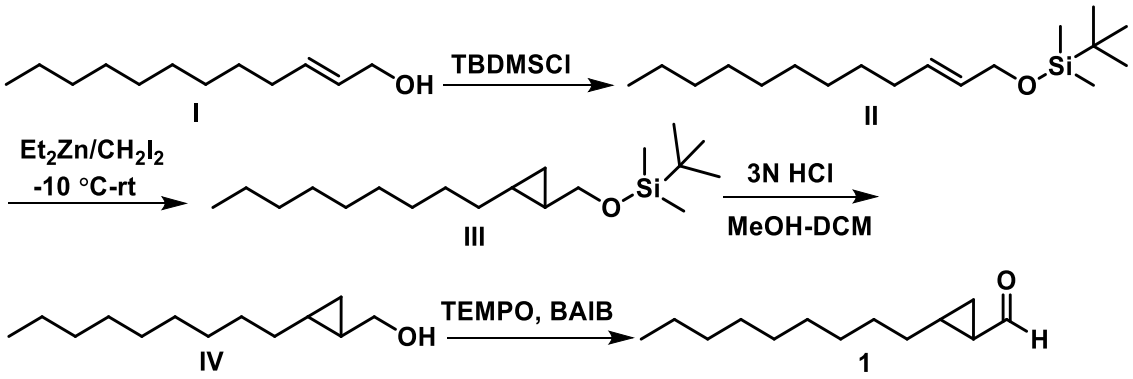

Figure C.2. Synthetic scheme of compound **1**

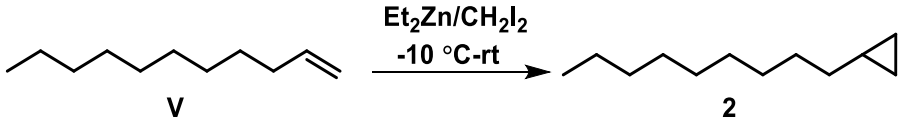

Figure C.3. Synthetic Scheme of compound **2**

Synthesis of (*E*)-*tert*-butyl(dodec-2-en-1-yloxy)dimethylsilane (II)

The alcohol functional group in **I** was protected by *tert*-Butyl-dimethylsilyl group (TBDMS).[1] To a solution of **I** (500 mg, 2.7 mmol) in anhydrous dicholoromethane (DCM) at 0 °C were added imidazole (125 mg, 1.84 mmol), and catalytic amount of DMAP. TBDMS chloride (500 mg, 3.3 mmol) was added to the reaction mixture resulting in the formation of white suspension. The reaction mixture was gradually warmed to room temperature and stirred overnight. The reaction mixture was diluted with DCM (50 ml) and washed with water (2 X 5 ml). The organic layer was separated, dried over anhydrous sodium sulphate and concentrated on a rotatory evaporator. The crude mixture was purified by silica-gel chromatography using 1 % ethylacetate/n-hexane as the eluting solvent to yield **II** (700 mg, 86%). The compound was pure as judged by NMR (Figure C.4) and TLC. ^{1}H NMR (500 MHz, Chloroform-*d*) δ 5.65–5.54 (m, 2H), 4.16–4.12 (m, 2H), 2.07-2.03 (m, 2H), 1.45-1.20 (m, 12H), 0.97-0.83 (m, 15H), 0.08 (s, 6H). ^{13}C NMR (126 MHz, Chloroform-*d*) δ 131.57, 129.05, 64.11, 32.21, 31.92, 29.61, 29.53, 29.35, 29.22, 25.99, 22.69, 18.43, 14.12, -5.10.

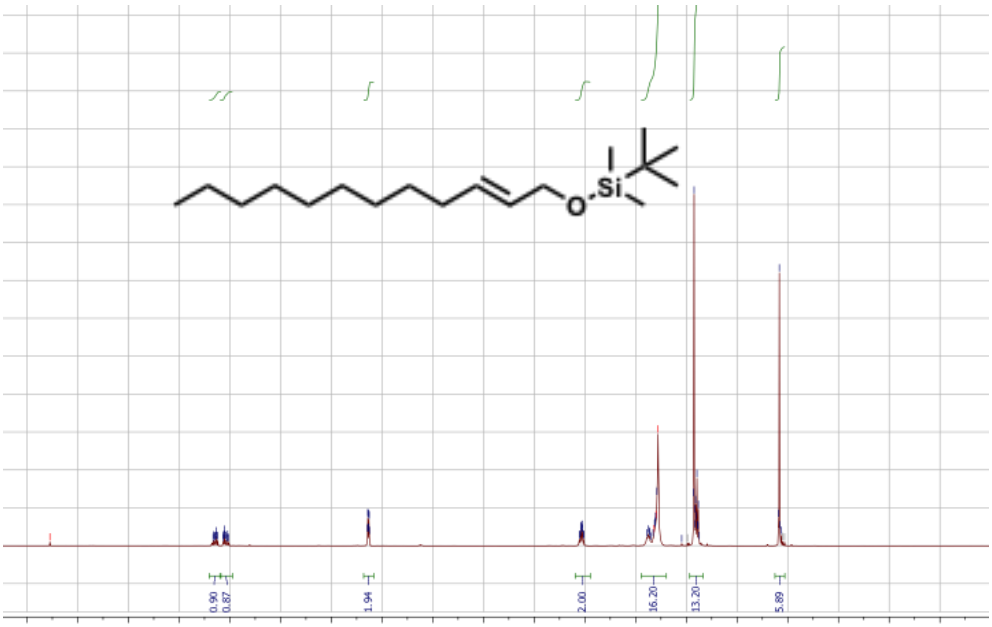

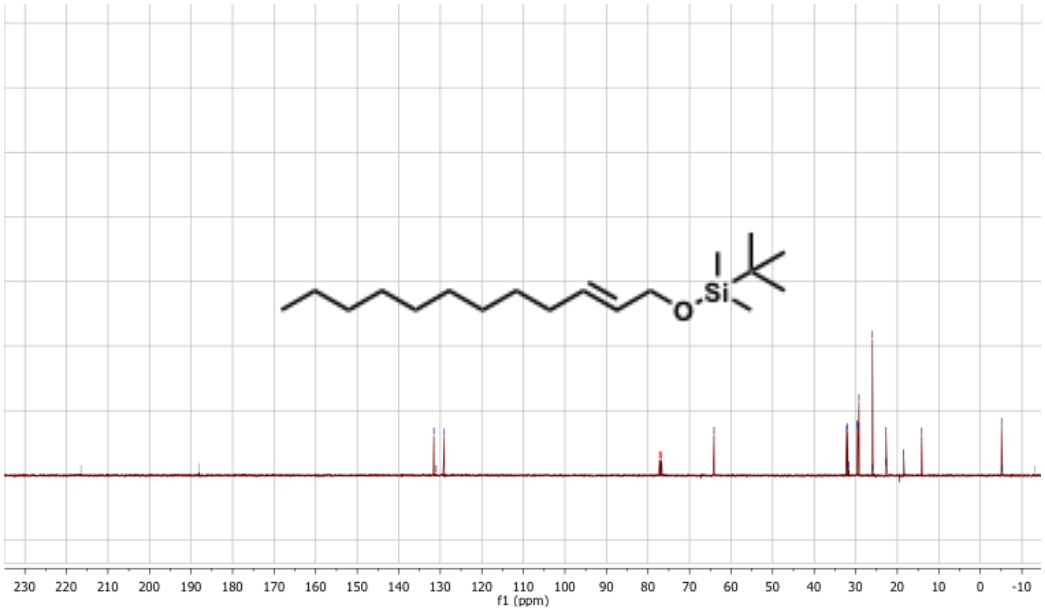

Figure C.4. ^{1}H and 13C-NMR of Compound II

Synthesis of tert-butyldimethyl((2-noncyclopropyl)methoxy)silane (III)

II was converted to **III** based on literature procedures.[2] To a solution of **II** (100 mg, 0.33 mmol) in anhydrous dichloromethane at 0 °C were added diethyl zinc (80 μl, 0.78 mmol) and diiodomethane (100 μl, 1.24 mmol). The reaction mixture was warmed to 40 °C and stirred for overnight. Upon completion of the reaction as judged by TLC, the crude mixture was concentrated on a rotatory evaporator. **III** was purified by silica-gel column chromatography using 1% ethylacetate/n-hexane as the eluting solvent and was obtained as predominant the *trans*-stereoisomer (62 mg, 60 %). The compound **III** was > 90% pure as judged by NMR (Figure C.5) and TLC. ^{1}H NMR (401 MHz, Chloroform-*d*) δ 3.53-3.40 (m, 2H), 1.39-1.16 (m, 16H), 0.91-0.77 (m, 15H), 0.78-0.68 (m, 1H), 0.59-0.49 (m, 1H), 0.36-0.28 (m, 1H), 0.26-0.19 (m, 1H), 0.05 (d, *J* = 2.1 Hz, 6H). ^{13}C NMR (101 MHz, Chloroform-*d*) δ 67.06, 34.63, 33.75, 31.91, 31.58, 29.70, 29.62, 29.59, 29.52, 29.49, 29.42, 29.36, 29.33, 29.28, 29.13, 25.95, 25.24, 22.67, 22.64, 21.01, 18.36, 16.95, 14.07, 9.78, -5.16, -5.19.

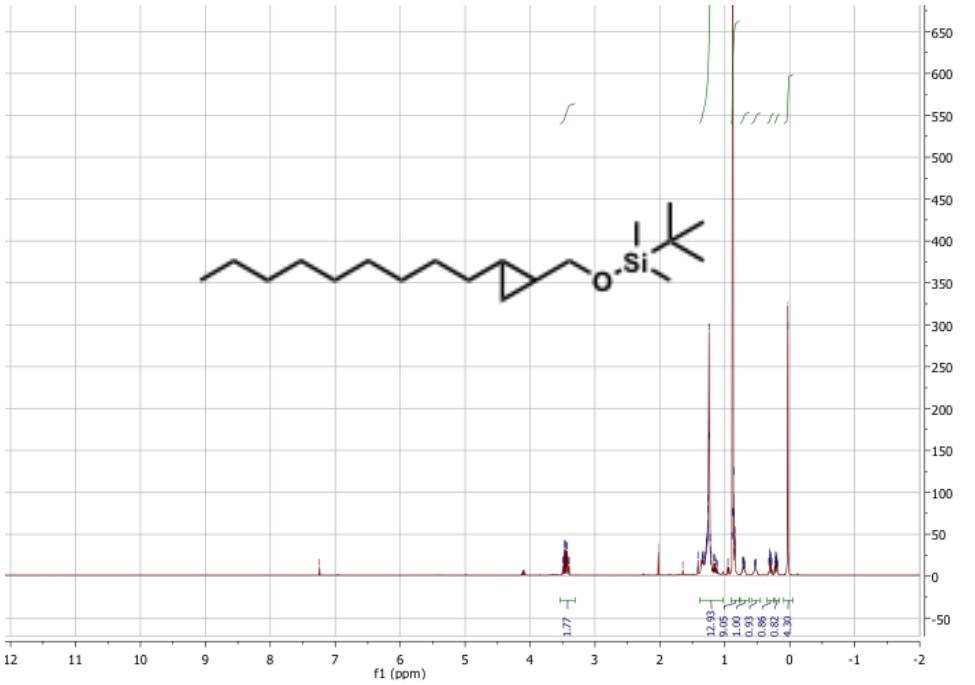

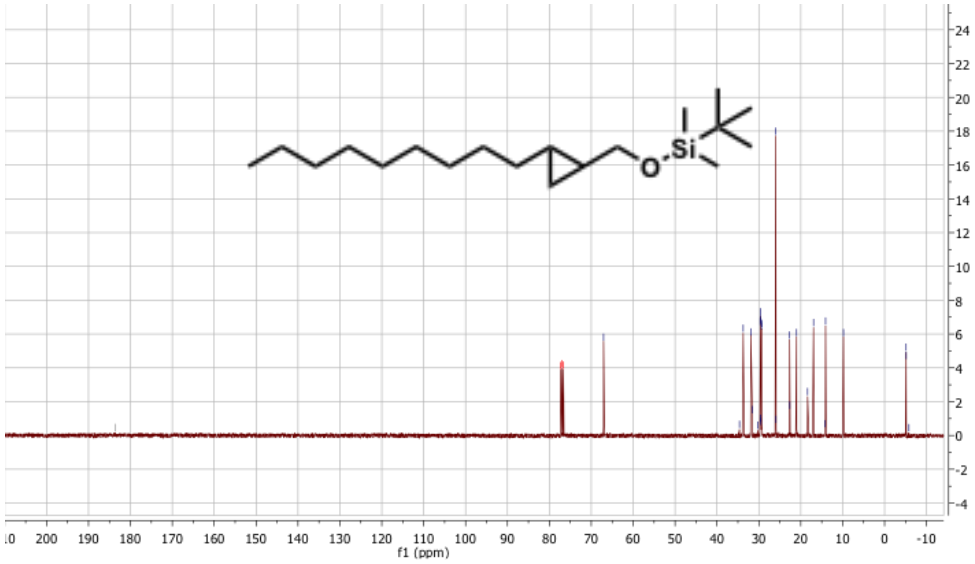

Figure C.5. ^{1}H and ^{13}C-NMR of Compound III

Synthesis of (2-nonylcyclopropyl)methanol (IV)

1 ml of 3N methanolic hydrochloric acid was added to a solution of **III** (100 mg, 0.32 mmol) in dichloromethane at 0°C for 4 hours. The reaction mixture was diluted with 50 ml dichloromethane and washed with water (2 x 5 ml) and brine (2 x 2 ml). The organic layer was dried over sodium sulphate and concentrated by rotatory evaporation to afford the crude product as yellow oil that was further subjected to silica-gel chromatography using 10% ethylacetate/n-hexane as the eluting solvent and yielded **IV** as yellow liquid (50 mg, 80%). The compound **IV** was pure as judged by NMR (Figure C.6) and TLC. ^{1}H NMR (400 MHz, Chloroform-*d*) δ 3.52-3.25 (m, 2H), 1.47-1.09 (m, 16H), 0.92-0.71 (m, 4H), 0.62-0.47 (m, 1H), 0.39-0.25 (m, 2H). ^{13}C NMR (100 MHz, Chloroform-*d*) δ 67.21, 33.56, 31.87, 29.64, 29.58, 29.41, 29.31, 22.65, 21.16, 17.17, 14.08, 9.89.

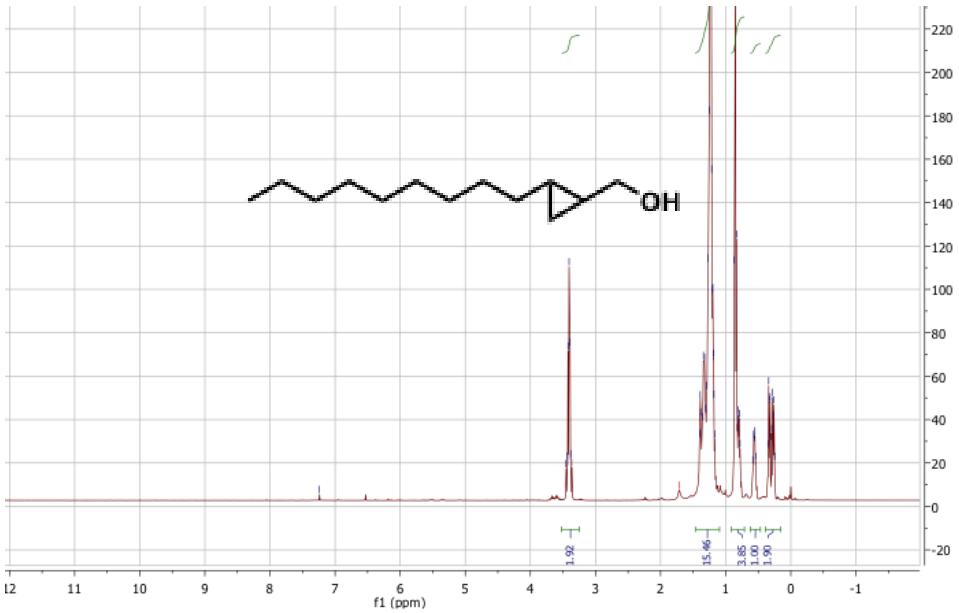

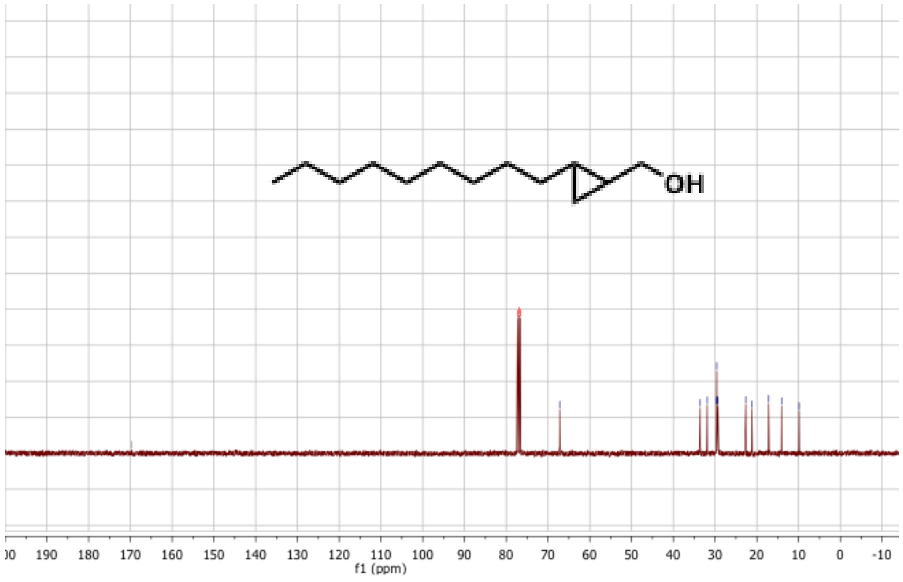

Figure C.6. ^{1}H and ^{13}C-NMR of Compound IV

Synthesis of 2-nonylcyclopropane-1-carbaldehyde (1)

To a solution of **IV** (50 mg, 0.25 mmol) in dichloromethane at room temperature were added TEMPO (4 mg, 0.2 mmol) and BAIB (75 mg, 0.23 mmol).[3] The reaction was stirred at room temperature for 3 hours under nitrogen. After completion, the crude reaction mixture was concentrated using a rotatory evaporator and subjected to silica-gel column chromatography in n-hexane/diethylether in which the gradient of the solvent was gradually increased from neat n-hexane to 5% diethylether/n-hexane to obtain **1** (30 mg, 40%). The compound was pure as judged by NMR (Figure C.7) and TLC. The identity of the compound was confirmed by high resolution electron-impact MS (*m/z*): calculated 197.1905; observed 197.1907. ^{1}H NMR (500 MHz, Chloroform-*d*) δ 9.00 (d, *J* = 5.6 Hz, 1H), 1.66-1.60 (m, 1H), 1.51-1.45 (m, 1H), 1.42 – 1.23 (m, 18H), 0.91 – 0.87 (m, 5H). ^{13}C NMR (101 MHz, Chloroform-*d*) δ 201.02, 32.60, 31.84, 30.50, 29.51, 29.26, 29.22, 29.05, 22.68, 22.63, 14.85, 14.06.

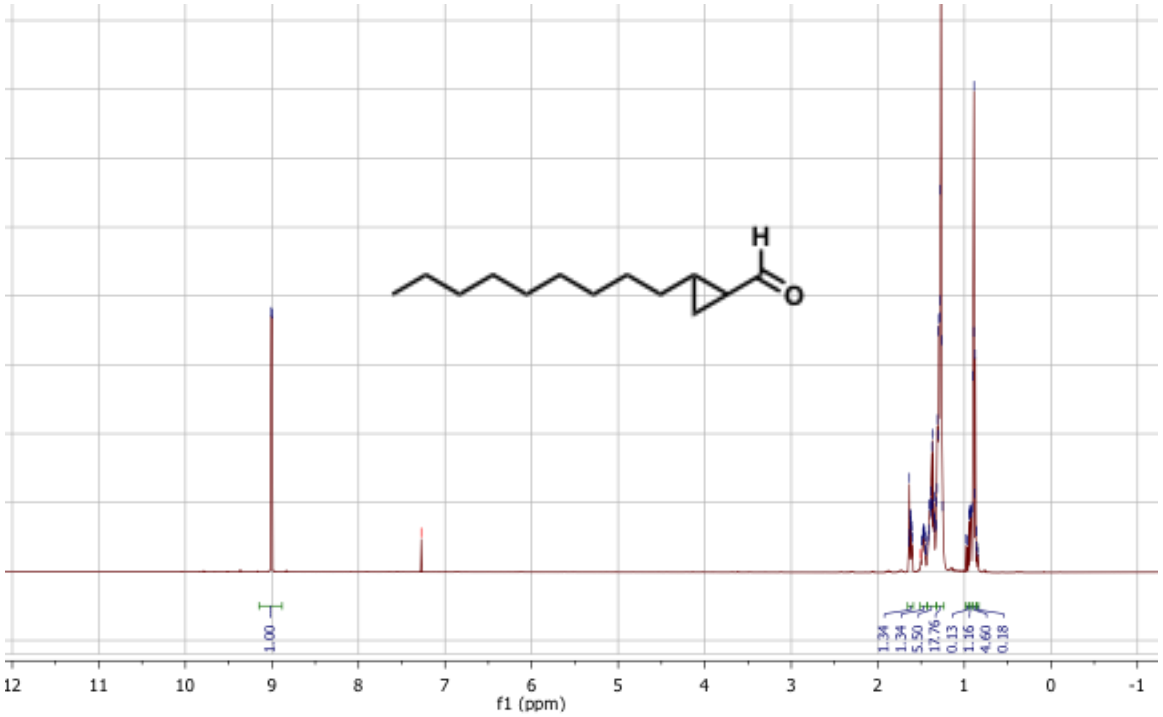

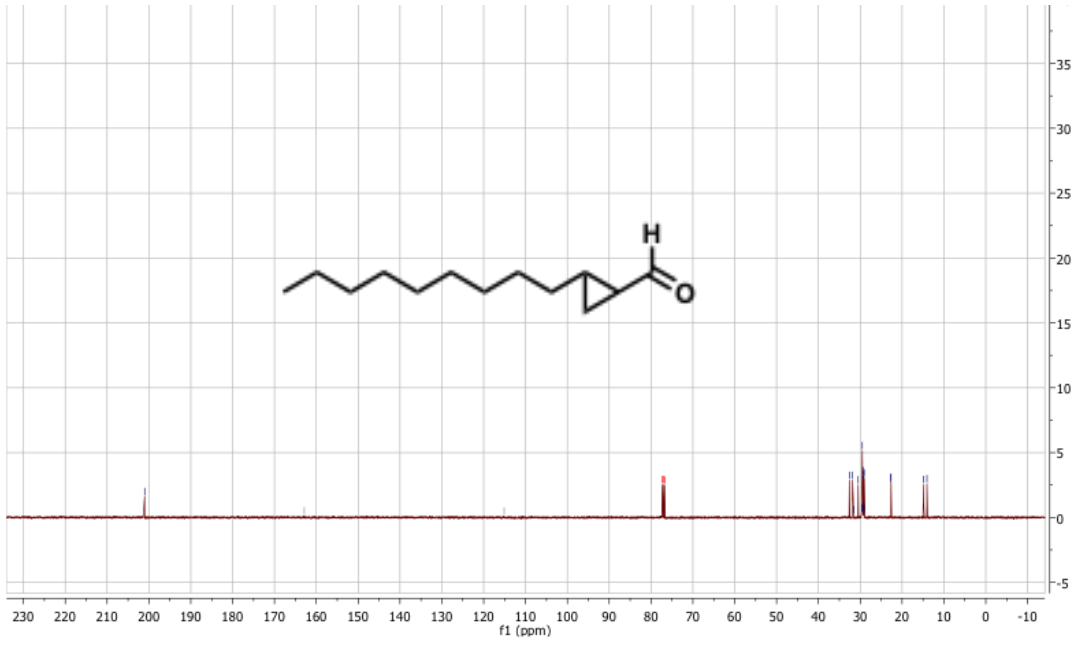

Figure C.7. ^{1}H and ^{13}C-NMR of Compound 1

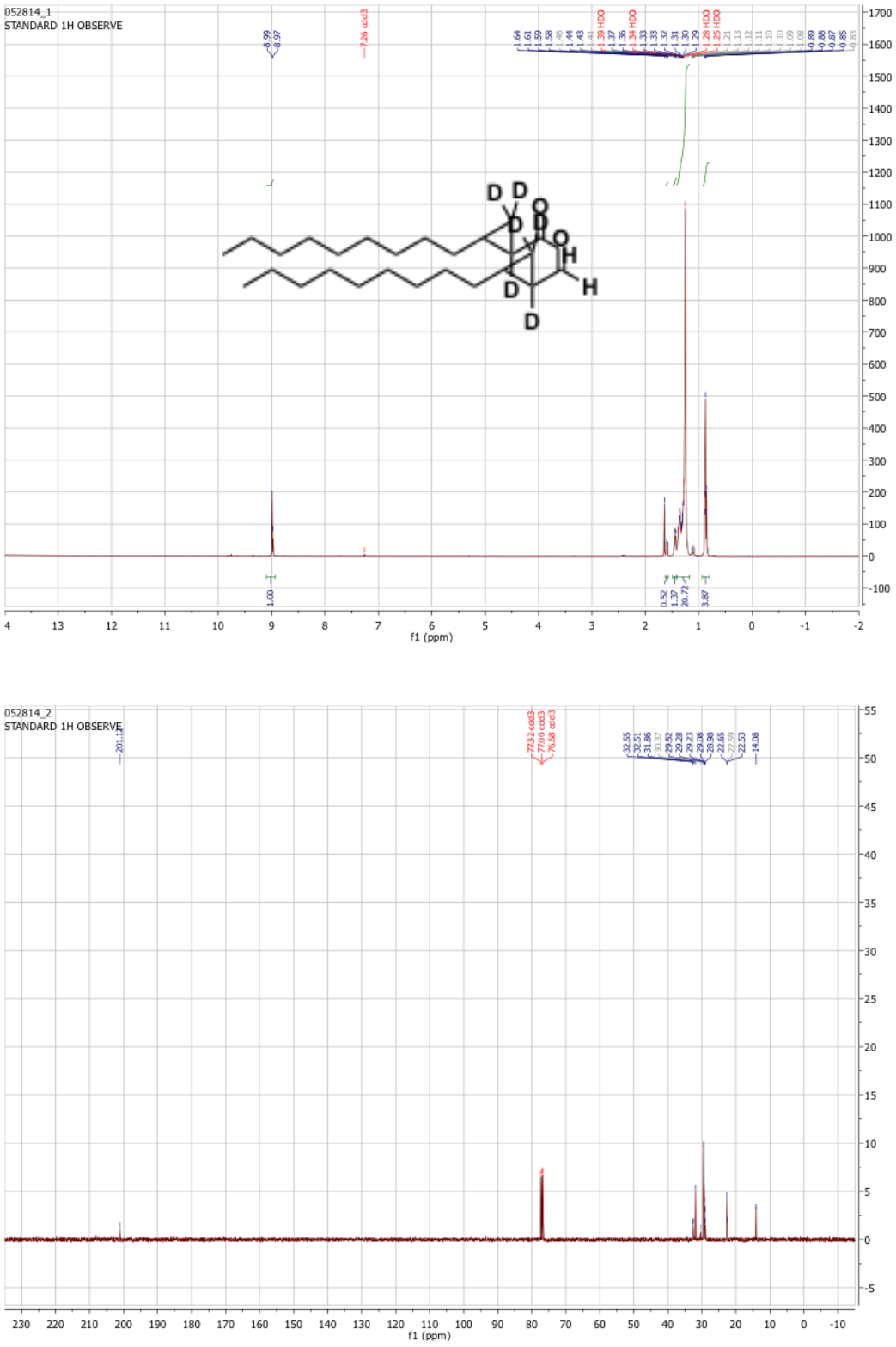

Figure C.8. ^{1}H and ^{13}C-NMR of Compound 1A

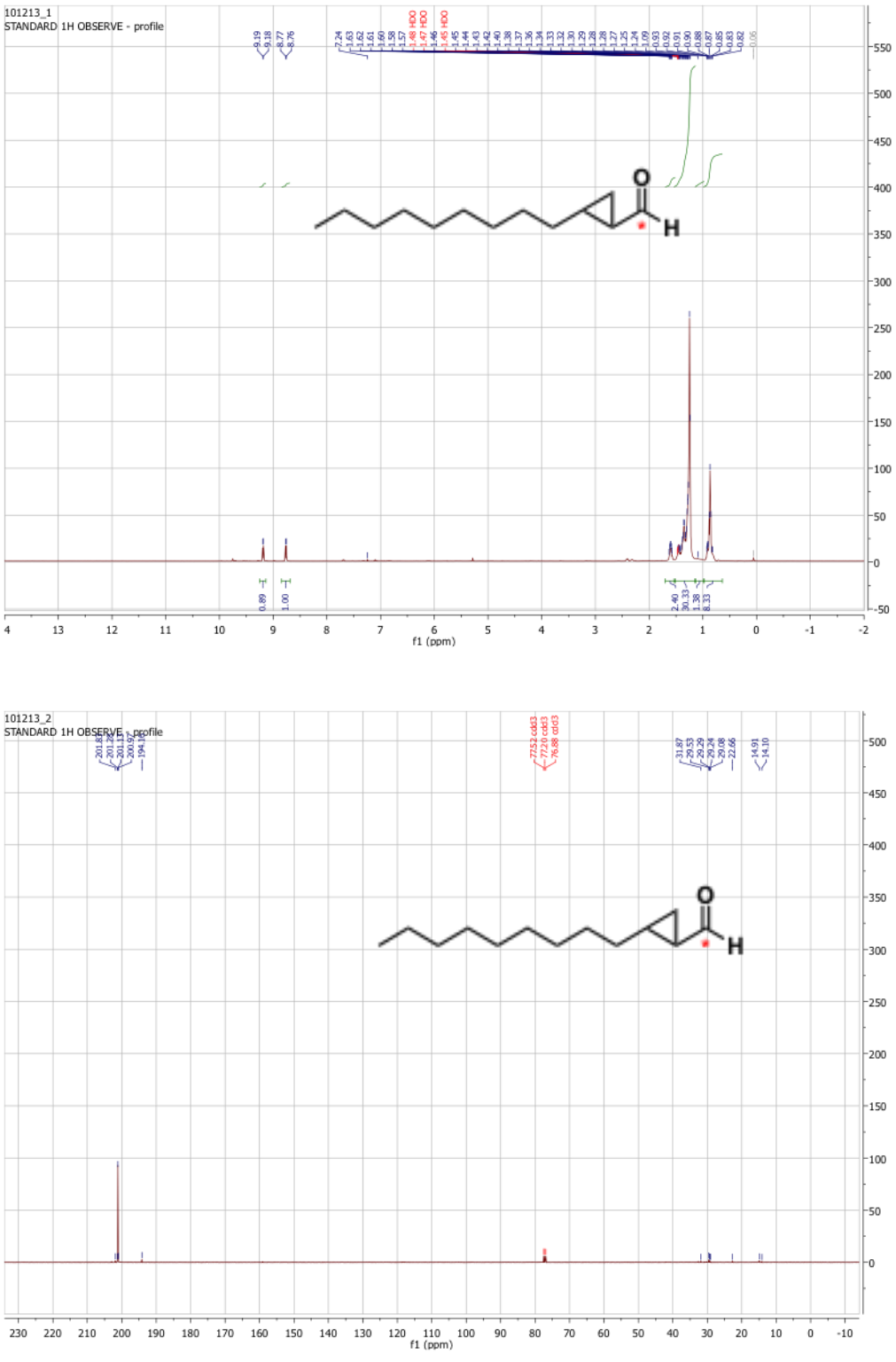

Figure C.9. ^{1}H and ^{13}C-NMR of Compound 1B

Synthesis of nonylcyclopropane (2)

1-undecene was converted to **2** based on literature procedures.[2] To a solution of 1-undecene (200 μl , 1 mmol) in anhydrous dichloromethane at -20 °C were added diethyl zinc (150 μl, 1.5 mmol) and diiodomethane (200 μl, 2.5 mmol). The reaction mixture was warmed to room temperature and stirred for 48 hours. The crude mixture was concentrated on a rotatory evaporator. **2** was purified by silica-gel column chromatography using 1% ethylacetate/n-hexane as the eluting solvent (200 μl , 60%). The compound was < 60% pure as judged by NMR (Figure C.10) and TLC and contains unreacted 1-undecene.

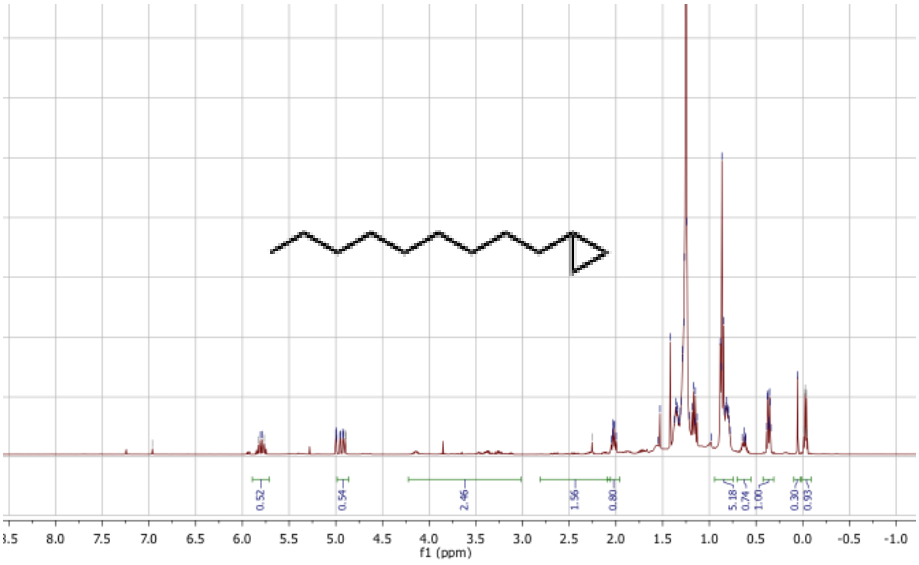

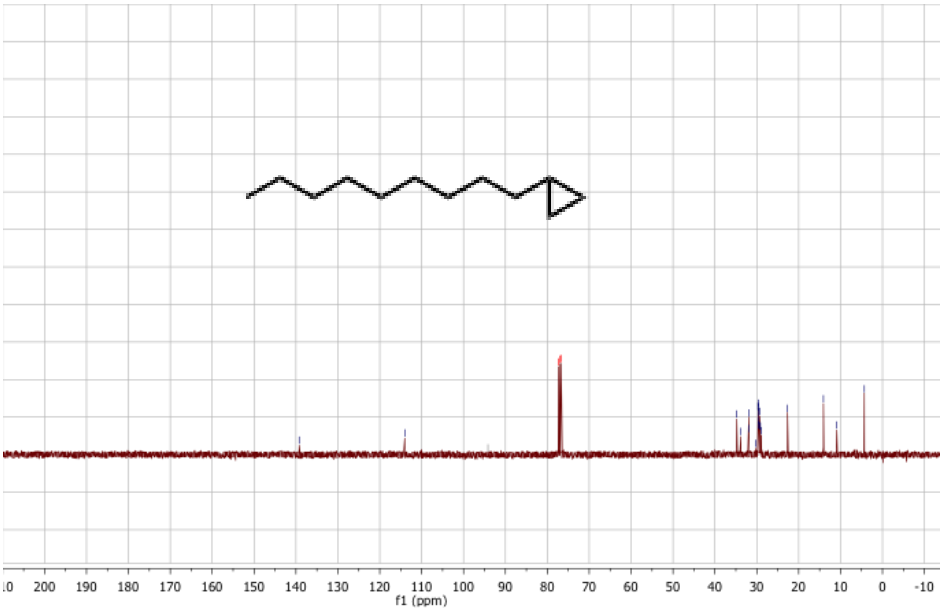

Figure C.10. ^{1}H and ^{13}C-NMR of Compound **2**

Synthesis of nonylcyclopropane-d_2 (2A)

1-undecene was converted to **2A** based on literature procedures.[2] To a solution of 1-undecene (200 μl , 1 mmol) in anhydrous dichloromethane at -20 °C were added diethyl zinc (150 μl, 1.5 mmol) and diiodomethane-d_2 (200 μl, 2.4 mmol). The reaction mixture was warmed to room temperature and stirred for 48 hours. The crude mixture was concentrated on a rotatory evaporator. **2A** was purified by silica-gel column chromatography using 1% ethylacetate/n-hexane as the eluting solvent (200 μl, 40%). The compound was < 50% pure as judged by NMR (Figure C.11) and TLC and contains unreacted 1-undecene.

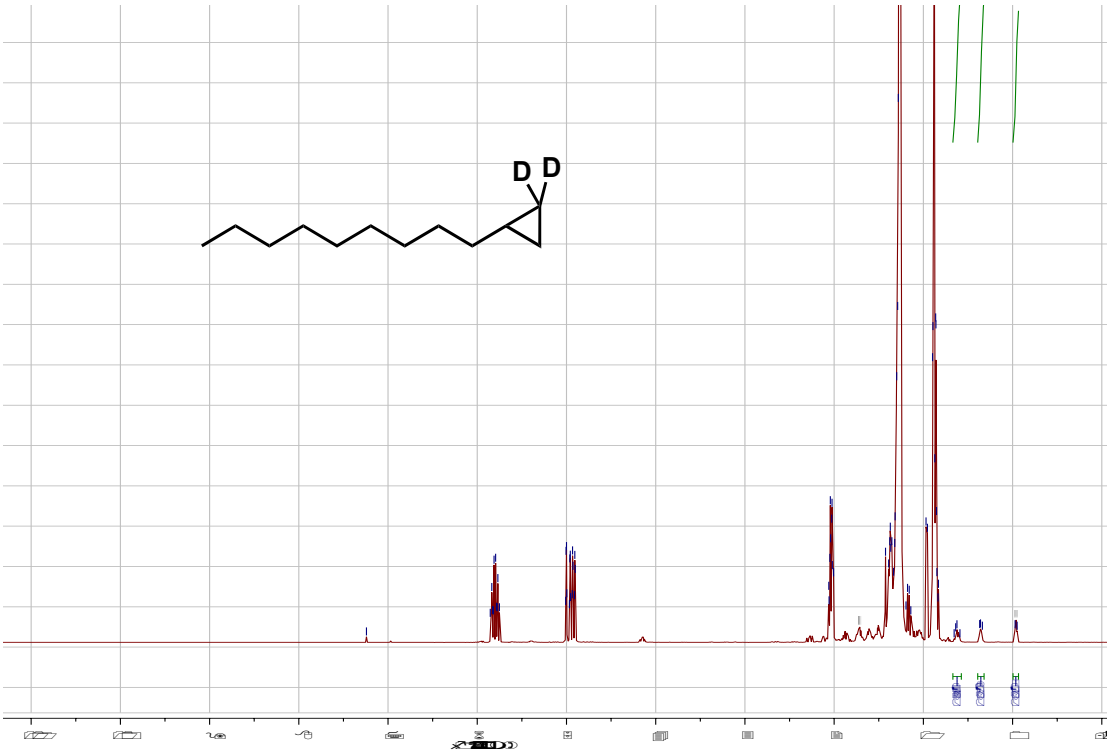

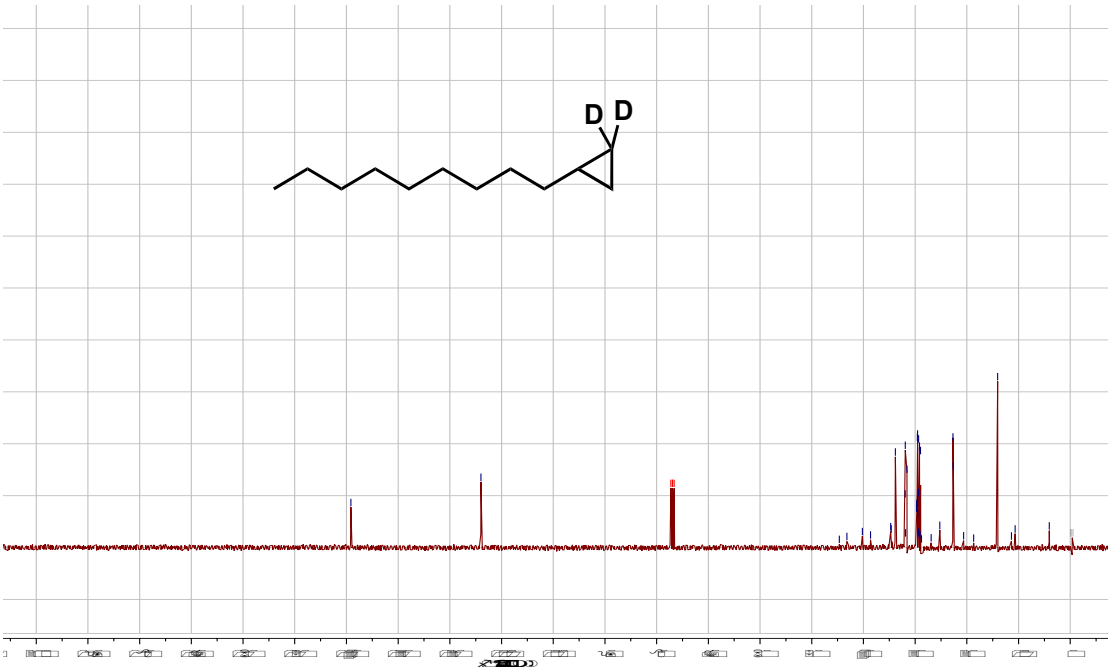

Figure C.11. ^{1}H and ^{13}C-NMR of Compound 2A

References

1. Rajesh, M.; Sen, J.; Parlanti, L.; Srujan, Mukherjee, K. Sreedhar, B., Chaudhuri, A. (2007**)** Dramatic Influence of the Orientation of Linker between Hydrophilic and Hydrophobic Lipid Moiety in Liposomal Gene Delivery, *J. Am. Chem. Soc. 129*, 11408–11420.

2. Furukawa, J., Kawabata, N., Nishimura, J. *Tetrahedron*, **1968**, *24,* 53

3. De Mico, A.; Margarita, R.; Parlanti, L.; Vescovi, A. Piancatelli, G. (1997**)** A Versatile and Highly Selective Hypervalent Iodine (III)/2,2,6,6-Tetramethyl-1-piperidinyloxyl-Mediated Oxidation of Alcohols to Carbonyl Compounds, *J. Org. Chem. 62*, 6974–6977.

Appendix D

VIPERIN

Introduction

Only recently discovered, VIPERIN (**V**irus **I**nhibitory **P**rotein; **E**ndoplasmic **R**eticulum associated, **IN**terferon inducible) is a highly conserved protein throughout such diverse species as rodents, primates and fish.[1] Induced by both type I and II Interferons, VIPERIN has been shown to inhibit infection and replication of multiple viruses, including Dengue Fever, HIV, and Influenza.[1-2] The 42 kDa membrane-bound protein is composed of an n-terminal leucine-zipper domain with an amphipathic helix, a radical SAM domain and a c-terminal domain, each of which has been implicated in its various modes of viral inhibition (Figure D.1).[3] Despite the highly interesting nature of this protein, much remains unknown about its mechanism of action. Understanding of this broad-spectrum antiviral action could greatly advance our ability to treat viral infection.

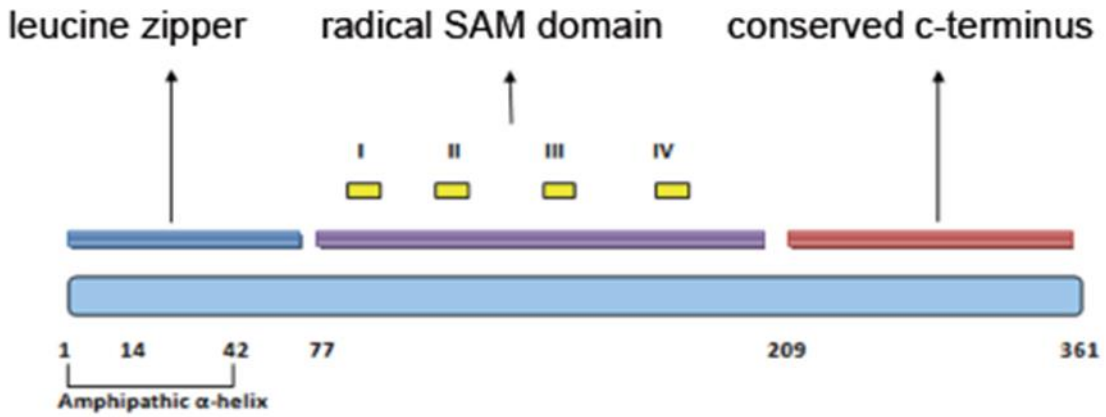

Figure D.1. VIPERIN Structure and domains.[3]

One proposed mechanism of action, discovered by Wang et al in 2007, involves disruption of cell membrane lipid rafts, inhibiting the release of budding viral capsids.[1] In addition, interaction of Farnesyl Pyrophosphate Synthase (FPPS) and VIPERIN was discovered through pull-down assays. VIPERIN expression reduced the activity of FPPS *in vivo*, and overexpression of FPPS effectively reversed the VIPERIN-mediated inhibition of Influenza replication and release.[1] Although the evidence for VIPERIN's mechanism of viral inhibition being linked to FPPS is quite strong, little mechanistic understanding of its function has yet been obtained. To this end, I worked alongside Dr. Gabriel Roman and others to elucidate the mechanistic underpinnings of VIPERIN-mediated FPPS interaction and inhibition.

Anti-Flag Pull-Down Assays

Although previous studies indicated that FPPS was pulled down by Interferon-induced VIPERIN expression, I set out to confirm the interaction of FPPS and VIPERIN using transient overexpression in HEK293T Cells. HEK293T cells were grown to 30% confluency in 10cm dishes, then either grown without transfection (control) or transfected using Fugene (don't remember number) Transfection Reagent as per standard protocol with hFPPS, VIPERIN, or both hFPPS and VIPERIN (coexpression). Cells were grown 48h, then harvested and frozen at -80C. Upon thawing in 500µL D-PBS with 0.1% TRITON-X, cells were lysed on ice by manual sonication at a power level of 4 with 3 sets of 3 2s pulses. Lysate was cooled 5m on ice between each set of pulses.

Lysate was centrifuged 10m at 12,000xg to clarify and remove precipitates (samples taken before and after clarification for Western Analysis). Clarified lysate was loaded onto 100µL packed, equilibrated (D-PBS + 0.1% TRITON-X) ANTI-FLAG® M2 Affinity Gel from Sigma-Aldrich or 50 µL packed, equilibrated Ni-NTA Resin. Resin+lysate was incubated with gentle mixing for 2h at 4C, then flowthrough removed (sample saved for Western Analysis) and resin washed 3x with 5CV D-PBS + 0.1% TRITON-X, and 2x further with 5CV D-PBS (sample saved from final wash for Western Analysis). Proteins were eluted using five 1CV solutions of 100µg/mL FLAG peptide in D-PBS (for Anti-Flag Resin) or 500 µM Imidazole (for His-Tag), run on SDS-PAGE and visualized by Western Blot Analysis.

Though no strong evidence for the VIPERIN-FPPS pull-down was obtained through the course of my studies, a consistent and significant decrease in FPPS expression levels in the presence of VIPERIN expression was noted (Figure D.2). Though we were unsuccessful in duplicating the pull-down of VIPERIN by hFPPS, the presence of an effect on FPPS was quite interesting. Control experiments were run to verify that the effect was due to VIPERIN, rather than just due to overloading of transcription machinery in the coexpression by overexpressing GAPDH and FPPS in a control, and only VIPERIN coexpression was seen to result in lowered FPPS concentrations.

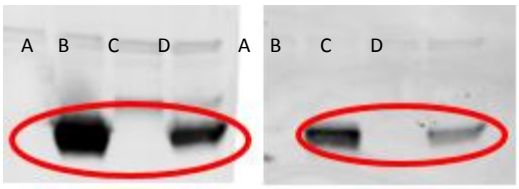

Figure D.2. VIPERIN expression results in decreased FPPS levels. Gels shown are duplicates; circled is FPPS by Western Gel Analysis. Lanes as follows; *A*, HEK293T Control; *B*, hFPPS; *C*, VIPERIN; *D*, hFPPS+VIPERIN Coexpression.

Currently, efforts are underway to further understand the mechanism by which VIPERIN actively decreases hFPPS levels in the cell, as well as the mechanism by which VIPERIN inhibits hFPPS activity.

References

1. Wang, X.; Hinson, E. R.; Cresswell, P., The Interferon-Inducible Protein Viperin Inhibits Influenza Virus Release by Perturbing Lipid Rafts. *Cell Host & Microbe* **2007,** *2* (2), 96-105.

2. (a) Chin, K.-C.; Cresswell, P., Viperin (cig5), an IFN-inducible antiviral protein directly induced by human cytomegalovirus. *Proceedings of the National Academy of Sciences of the United States of America* **2001,** *98* (26), 15125-15130; (b) Rivieccio, M. A.; Suh, H.-S.; Zhao, Y.; Zhao, M.-L.; Chin, K. C.; Lee, S. C.; Brosnan, C. F., TLR3 Ligation Activates an Antiviral Response in Human Fetal Astrocytes: A Role for Viperin/cig5. *The Journal of Immunology* **2006,** *177* (7), 4735-4741.

3. Helbig, K. J.; Carr, J. M.; Calvert, J. K.; Wati, S.; Clarke, J. N.; Eyre, N. S.; Narayana, S. K.; Fiches, G. N.; McCartney, E. M.; Beard, M. R., Viperin Is Induced following Dengue Virus Type-2 (DENV-2) Infection and Has Anti-viral Actions Requiring the C-terminal End of Viperin. *PLoS Neglected Tropical Diseases* **2013,** *7* (4), e2178.